Contract DASG60-98-M-0073

Spatial-Spectral Sensor Techniques for Detection of Atmospheric Turbulence

Phase I Final Report

Small Business Innovative Research Program

SPONSORED BY

BMDO Innovative Science and Technology Office

MANAGED BY

U.S. Army Space and Missile Command

March 3, 2000

Final Report by

Robert D. Sears
Vanguard Research, Inc.
10400 Eaton Plaace, Suite 450
Fairfax, VA 22030-2201

Dr. Lyle Broadfoot
Lunar and Planetary Laboratory
University of Arizona
Tucson, Arizona

U.S. Army Space and Missile Command
P.O. Box 1500
Huntsville, Alabama 35807-6804

Approved for public release

Exhibit A

REPORT DOCUMENTATION PAGE

Form Approved
OMB No. 0704-0188

1. AGENCY USE ONLY (Leave Blank)	2. REPORT DATE	3. REPORT TYPE AND DATES COVERED
	March 3, 2000	Final 30 Apr 98 - 30 Apr 2000

4. TITLE AND SUBTITLE
Spatial-Spectral Sensor Technologies for Detection of Atmospheric Turbulence

5. FUNDING NUMBERS
DASG-60-98-M-0073

6. AUTHOR(S)
Robert D. Sears
Lyle Broadfoot

7. PERFORMING ORGANIZATION NAME(S) AND ADDRESS(ES)
Vanguard Research, Inc. 10400 Eaton Pl., Suite 450
Fairfax, VA 22030

8. PERFROMING ORGANIZATION REPORT NUMBER
VRI-99-02

9. SPONSORING/MONITORING AGENCY NAME(S) AND ADDRESS(ES)
Sponsor: Director, BMDO, ATTN: BMDO/ST (Jeff Bond)
7100 Defense Dr., Pentagon
Washington, D.C. 20301-7100

10. SPONSORING/MONITORING AGENCY REPORT NUMBER
BMD98-01

11. SUPPLEMENTARY NOTES
Phase I SBIR Final Report. Monitored by U.S. Army Space & Missile Command (SMDC-IM-PA) Richard Rogers (256-955-4825), P.O. Box 1500, Huntsville, AL 35807-3801

12a. DISTRIBUTION/AVAILABILITY STATEMENT
Approved for public release

12b. DISTRIBUTION CODE

13. ABSTRACT (Maximum 200 words)

This report addresses the application of spatial-spectral (hyperspectral) imaging from space-borne or multi-platform sensors to detect and characterize atmospheric turbulence. Turbulence may impact performance of optical systems deployed for energy propagation, such as airborne and space-based lasers, and sensors systems used for dim target detection, such as aircraft or cruise missile surveillance and tracking. Techniques developed allow global scientific investigation of regions of atmospheric turbulence and clutter, including the study of cirrus clouds. Potential commercial applications include improved detection and understanding of clear air turbulence to improve aircraft safely. Military applications include improved understanding of the effect of the atmospheric on propagation of laser energy and the detection and tracking of dim targets such as cruise missiles.

14. SUBJECT TERMS	15. NUMBER OF PAGES	16. PRICE CODE
Atmosphere, turbulence, laser propagration, optical sensor	70	

17. SECURITY CLASSIFICATION OF REPORT	18. SECURITY CLASSIFICATION OF THIS PAGE	19. SECURITY CLASSIFICATION OF ABSTRACT	20. LIMITATION OF ABSTRACT
Unclassified	Unclassified	Unclassified	Unlimited

PREFACE

This is the final technical report on contract DASG60-98-M-0073 that was funded by Ballistic Missile Defense Organization and managed by US Army Space and Missile Defense Command. Kestrel Corporation in Albuquerque NM and Dr. Lyle Broadfoot at University of Arizona at Tucson were subcontractors and contributed substantially to the effort.

LIST OF FIGURES

LIST OF TABLES

TABLE OF CONTENTS

1. INTRODUCTION

This report addresses the problem of utilizing spatial-hyperspectral imaging capabilities of space-borne sensors to detect and characterize regions of atmospheric turbulence and cirrus cloud clutter which may impact employment and/or performance of space based laser and airborne high energy laser weapons systems.

Our concept for worldwide detection, characterization and mapping of atmospheric turbulence and cirrus clouds involves use of satellite-borne (and possibly airborne) spectral and hyperspectral imagers operated in the UV to MWIR spectral range in virtual triangulation geometry. Spectral and hyperspectral imagery allows altitude sounding of atmospheric clutter from turbulence and cirrus clouds. Triangulation geometry allows precise altitude selection by cross correlation of the backscatter signals. The combination of altitude and Fourier-space background spectral discrimination will provide an altitude resolved measurement of atmospheric clutter from clear air turbulence and from cirrus clouds, both of which may affect performance of the SBL (Space Based Laser) and the Airborne Laser (ABL) systems.

Figure 1 illustrates the virtual triangulation concept by forward-looking and backward-looking imaging sensors from a satellite.

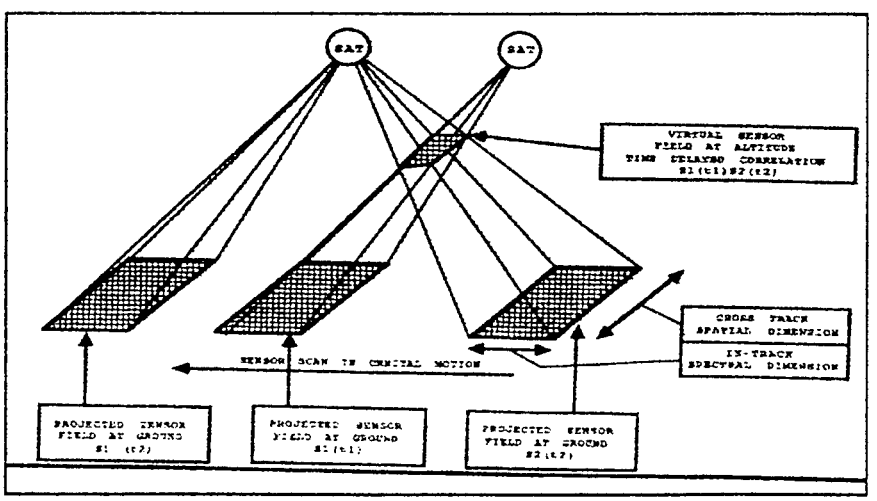

Figure 1 Conceptual Optical Triangulation Geometry to Isolate Atmospheric Turbulence, Characterize Ground-based Clutter, and Detect Weak Targets. The virtual triangulation geometry allows mapping of random atmospheric clutter and CAT vs. altitude by cross correlation of forward-viewing and backward-viewing imaging signals and assists in separating weak airborne targets from the atmospheric background clutter.

We anticipate that the conceptual satellite sensor can be tested on ground-based and airborne platforms prior to finalization of a satellite sensor design. This phase one SBIR project has initiated such conceptual tests but further work is required, especially with respect to airborne tests of the concept versus clear air turbulence (CAT).

Anticipated commercial applications of this research are automated background scene content identification and weak target recognition by small, real-time programmable space-borne sensors and remote sensing of atmospheric structure which leads to a capability for mapping CAT (clear air turbulence) from airborne or space-borne detectors.

2. STATEMENT OF PROBLEM AND MEASUREMENT CONCEPT

2.1.1 Technical Problem Summary

The technical problem addressed by this SBIR program is to devise unique spatial-spectral satellite-based observation techniques to detect weak targets in the presence of background clutter. The weak targets that we address are in order of observability:

- small, low observable airborne vehicles,
- thin atmospheric cirrus clouds,
- atmospheric clear air turbulence, and
- turbulent structure in the troposphere, stratosphere, and lower thermosphere.

This report concentrates on the more difficult "targets", atmospheric turbulence and clear air turbulence (CAT) layers. The rationale for measurement of the atmospheric quantities is that this class of backgrounds forms the limiting cases of background clutter, which if measurable by a satellite passive sensor ensures that other airborne targets, will be detectable.

2.1.2 Technical Approach

We validated the virtual triangulation – spectral – spatial weak target detection and characterization technique by analytical simulation techniques and by experimental simulation using ground-based spectral-spatial structure sensors and by using the GLO sensors carried on the Space Shuttle[1].

Validation by Simulation

We used the NSS (Non-stationary Stochastic Structure) Model[2] and LAMSS[3] (Low Altitude Mesoscale Stochastic Structure) models to simulate structure in the mesopause region (~90 km) and in the troposphere (< 20 km) respectively. These simulations were generated using an geometrical driver for the sensor LOS to generate an artificial data stream appropriate to the experimental validation geometries.

Validation by Experiment

Two experiments were conducted to validate the satellite sensor cross-beam concept: a low altitude experiment measured turbulent structure and winds in the boundary layer between about 50 and 300 feet altitude. We intended that the daytime measurements would be coordinated with meteorological tower measurements of winds and turbulence but this experiment could not be consummated under the resources of the project. A high altitude set of measurements was conducted at nighttime used the airglow emission in the 80 to 130 km altitude range to provide the signal. Daytime experiments used the Kestrel AIRCAM sensors. operating in the 450 to 950 nm spectral range. The nighttime high altitude structure experiments used the Fourier Transform Hyperspectral Imager FTHSI and supporting imaging instrumentation from LANL and University of Arizona.

2.1.3 Results Summary

The Phase I simulations and ground-based experiments validated to a certain extent the ability of a satellite-borne passive atmospheric structure sensor to provide worldwide measurements of atmospheric turbulence and wind structure especially thin cirrus clouds and clear air turbulence. Validation experiment results may be applied to further experiments to determine atmospheric structure phenomenology and clutter maps for the Airborne Laser System (ABL), the Space-based Laser System (SBL), CAT maps for the civilian sector, and detection weak targets through efficient mitigation of of atmospheric background structure-induced clutter.

3. CONCEPT VALIDATION

The atmospheric structure sounding concept was validated by two techniques. Simulation of atmospheric structure and synthesis of atmospheric backscatter signals for low altitude structure and atmospheric airglow signals for high altitude structure was carried out for a limited number of cases and scenarios. Experiments designed to simulate possible satellite and/or airborne sensor environments and their respective signals generated by structure were conducted to investigate the utility of Hyperspectral Imagery. Data from the GLO sensor that has been repeatedly flown on the Space Shuttle also contributed to our experimental database.

3.1 VALIDATION BY SIMULATION

3.1.1 Simulation of Winds and Turbulence

Atmospheric turbulence was simulated in two dimensions by the technique demonstrated by Strugala and Sears, et. al. (See reference). Two different two-dimensional spectra were adopted: a $k^{-5/3}$ power law approximates the turbulence spectrum for an optically thick medium, and a $k^{-8/3}$ power law spectrum approximates an optically thin turbulent medium. Both spectra are of the modified Kolmogorov type with a correlation length of 10 cm, about the value expected for the lower atmosphere.

Equation 1 illustrates the functional form of the spectra for a two dimensional scene:

$$P(k_x, k_y) = [\Gamma(p)\,\Gamma(p)\,L_{cx}\,L_{cy}]/\{kx/L_{cx}\}^2 + \{ky/L_{cy}\}^2]\}^p \qquad (1)$$

Where,

$p =$ 5/6 or 8/6 for $k^{-5/3}$ or $k^{-8/3}$ spectral forms respectively,

$n = (p-1)/p$,

$k_{y,y}$ is the spatial frequency in either x or y dimension

$\Gamma(n)$ is the gamma function with argument determined by the spectral index

The background spatial scenes were implemented using the method of Strugala and Sears wherein a random Gaussian number field is created, then convolved with the desired 2-D spectral function (equation 1) to achieve a correlated random background intensity field. Figure 2 illustrates the two dimensional scenes generated by the simulation routine. Here, we used the same random number set in two dimensions to generate the arrays and vary only the power spectral density slope. A 64x64 pixel sample was cut from each 256x256 scene to show that the higher slope (k-8/3) has much more high frequency structure as indicated by the density of the contour lines. Each picture was digitized to a six-level contour interval.

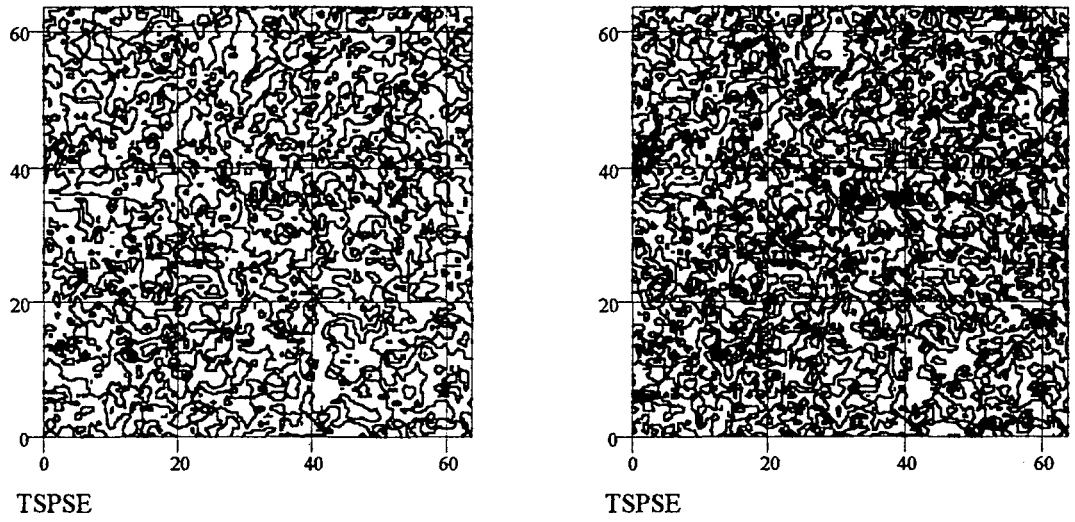

Figure 2 Contour maps of 2-D scenes generated from the same Gaussian random number field, but with spectral indices of $k^{-5/3}$ (left) and $k^{-8/3}$ (right) which physically corresponds to Kolmogorov turbulence in an optical thick and optically thin medium.

In order to simulate the effects of winds on the turbulence observations, we cut subimages from the 256x256 images and displaced them spatially by a constant number of pixels in the x and y dimensions. The analysis algorithms then were applied to compute the complex cross power spectral densities of the spectral images.

The basic algorithms used for the triangulation geometry as well as the successive frame analysis in the vertical direction is the cross power spectral density algorithm group first applied to geophysical phenomena by Gossard et. al.[4] The Cross Power Spectra for either a set

of one dimensional vector quantities V1, V2, or a sequence of two dimensional images I1, I2 may be generically expressed as:

$$XP\ (V1_{i,},\ V2_{i,}\ \text{or}\ I1_{i,j},\ I2_{i,j}) = \mathbf{CFT}(V1 + iV2,\ \text{or}\ I1 + iI2) \qquad (2)$$

Where the data vectors or image fields have indices i, and i,j respectively

CFT is the complex Fourier Transform with the vector or image quantities combined as a complex argument.

Whereas Gossard et al described the process in terms of the cross correlation functions of a data series, modern algorithms such as the Fast Fourier Transform allow direct computation of the data set. This analytical procedure was implemented by using standard complex Fourier Transform Algorithms contained in Mathcad.[5]

3.1.2 Simulation of Triangulation Geometry

We simulated the triangulation geometry in two dimensions corresponding to the right angled intersection of the low altitude structure and wind experiment described later.

3.1.3 Signal Analysis of Simulations

We analyzed the simulation experiments for two cases. The 2-D single beam, vertical looking geometry that corresponds to the low altitude experiments measures MWIR scattered sunlight as a signal as the turbulent scattering irregularities are convected through the field of view of the sensors. The 2-D low altitude triangulation geometry corresponds to the scattered sunlight signal in the region of intersection of the sensor fields of view.

In the case of the vertical viewing sensor simulation, we computed the complex cross spectral information in both real and imaginary regime and using standard signal processing techniques (see reference 4) derived the AS (Amplitude spectra), PSD (power spectral densities), IPSD (imaginary components of PSD), and the PHSD (Phase Spectra) for each pair of images. Then we looked for peaks in the phase spectra (PHSD) which might correspond to the motion of the turbulent scattered scenes across the sensor field of view.

The two dimensional PSD's and Phase Spectra (PHSD) for an image array A are defined by the standard expressions involving the periodogram PA of the array A which is derived from the "cfft" complex Fourier Transform of the array A. In the simulation case, the image arrays A are the computed Gaussian matrices GM.

$$PA = \text{cfft}(A),\ PSD = |PA|^2 \tag{3}$$

$$PHSD = -\arctan\ (\text{Im}(PA)/(\text{Re}(PA)) \tag{4}$$

As a diagnostic we compare in Figure 3 the ideal Kolmogorov $k^{-5/3}$ PSD input to the program, the computed periodogram for the convolution of the GM, Gaussian correlated noise matrix, and the raw periodogram of the array GM itself. The periodograms will be converted to power spectral densities (PSD's) later in the analysis

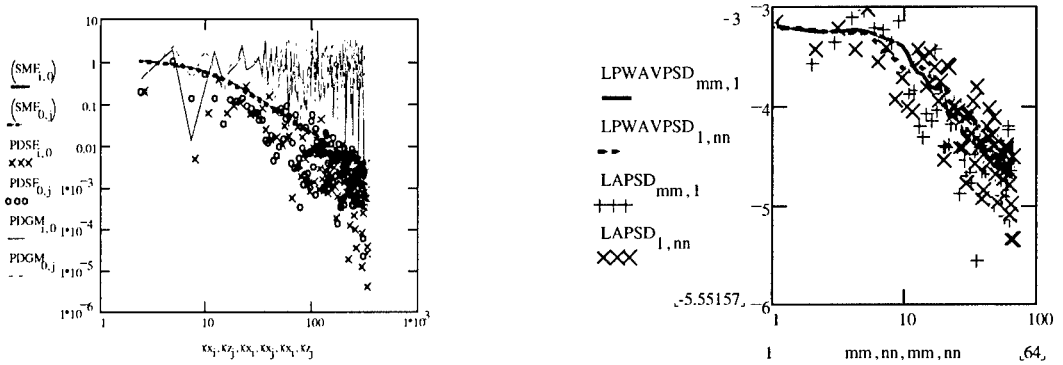

Figure 3 Left Image Compares the Correlated Gaussian Noise Matrix 1-Dimensional Periodograms and the input data (smooth line). SME is the input PSD, PDSE is the Periodogram of the Noised Gaussian Matrix, and PDGM is the Periodogram of the Gaussian Noise Matrix before convolution with SME. Values of PDSE and SME are normalized to their maximum values. The right image shows the 1-D PSD's (lines) after a Parzen filter is applied. The data points correspond to the noisey periodogram in the left image. The x axes correspond to spatial frequency in units of inverse pixels.

This exercise confirms that the PSD of the simulated random turbulence field reproduces the input spectrum.

Also it is necessary to validate that phase spectra can be produced, using the Gaussian random structure simulation. Figure 4 illustrates the phase spectrum over the range of zero to

1/64 pixel spatial frequency range. Histograms indicate that the phase spectral field is a correlated Gaussian distribution as expected.

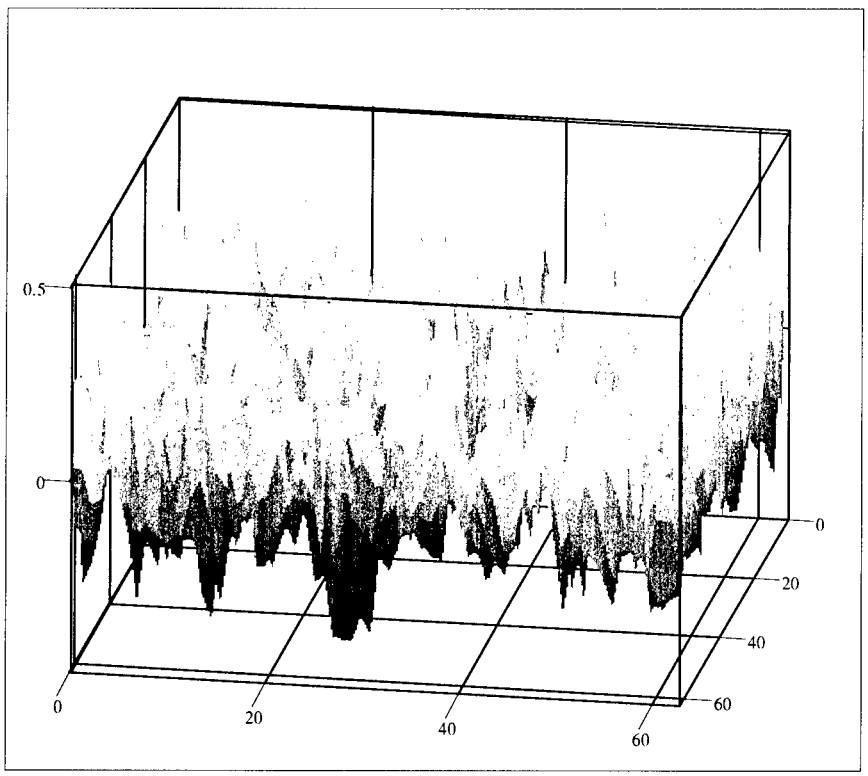

Figure 4 Phase Spectrum for Gaussian Correlated Simulation Scene. The spectrum extends from zero to 1/64 pixel spatial frequency in both spatial dimensions and from -1 to 1 radian in phase.

The Cross Power Spectral Density and Cross-Phase spectra are used to estimate the spatial displacement of the images and the vector velocity of the passage through the simulated two fields of view, from successive analyses of the sub-image pairs that are separated by 20 pixels.

The 2-D Cross PSD is smoothed by the Parzen window technique and then converted to a 2-D correlation function my means of a complex FFT. Figures 5A and 5B illustrate the 2-D PSD as a 2-D plot, and as a pair of 1-D cuts along the axes.

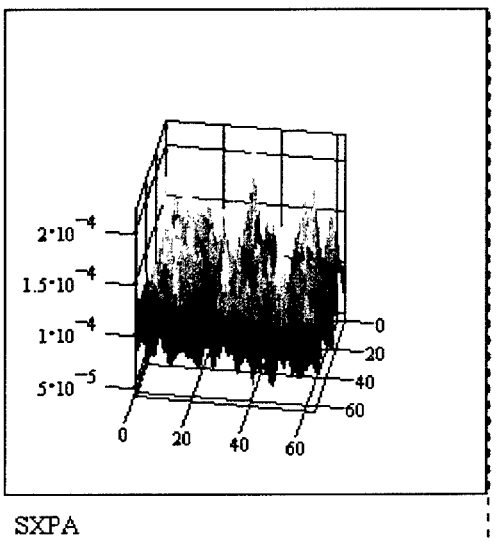

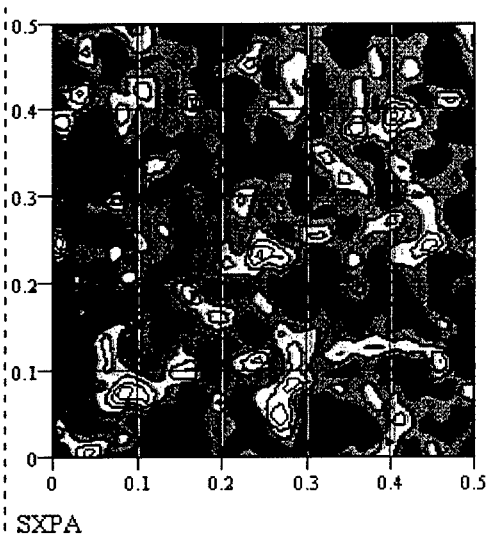

Figure 5A Smoothed Cross PSD as a surface plot. Note the occurrence of several spectral peaks

Figure 5B Smoothed Cross PSD shows spectral peaks on the frequency x-y diagonal as anticipated. The other peaks appear to be extraneous features.

The coordinates of Figure 5A are in units of spatial frequency divided by the pixel dimension of the image (ie 128 pixels with 2 pixels being the Nyquist frequency). Units of 5B are in inverse pixels such that 0.5 is equivalent to the Nyquist frequency of 1/(2 pixels).

After conversion of the 2-D Cross PSD's to cross correlation plots, it is necessary to threshold the data to bring out the pertinent features on the desired scale. Figures 6A and 6B show respectively the un-thresholded 2-D cross correlation plot and the thresholded image. The threshold chosen for this case was 7 times the standard deviation of the cross correlation scene after removal of the random energy component at zero delay.

The axes are in units if 1/pixels, hence the value 0.5 is equivalent to 2 pixel displacement and 0.1 is equivalent to 10 pixels displacement. The length of the thresholded correlation value in Figure 6B shows that the width of the correlation results equals about 20 pixels and is in the diagonal dimension as specified by the original image pairs.

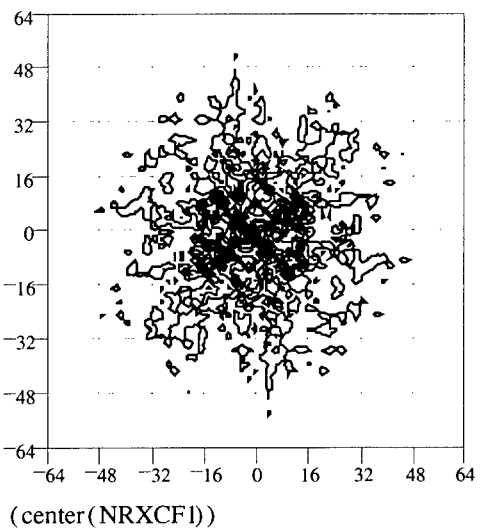

Figure 6A 2D Cross Correlation Plot Unthresholded

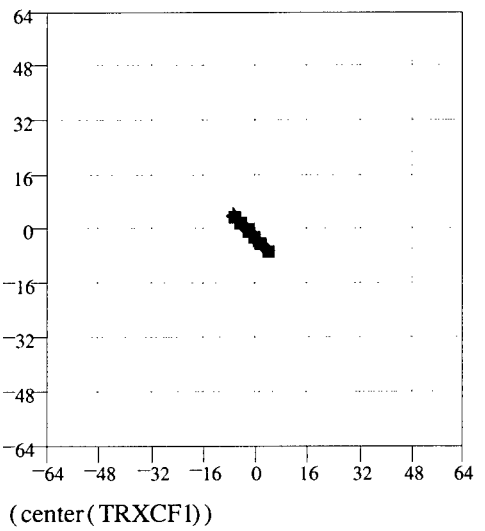

Figure 6B 2-D Correlation Plot Thresholded at 7 Sigma

Figures 7A and 7B show the phase spectrum thresholded at two levels, guided by the histogram of phase (not shown here). Spatial frequencies are in units of inverse pixels.

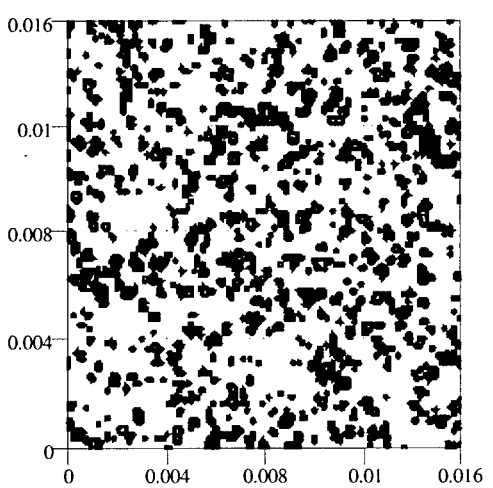

Figure 7A Exceedance Map for 1 sigma Thresholded Phase Difference Spectrum.

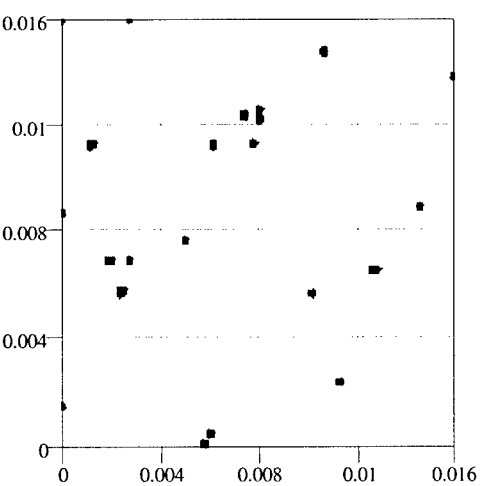

Figure 7B Exceedance Map for 3 sigma Thresholded Phase Difference Spectrum.

VALIDATION BY EXPERIMENT

3.1.4 Low Altitude Wind and Turbulence Experiments

Low altitude wind and turbulence experiments were conducted at Kestrel Corporation using a set of filtered CCD cameras. These cameras are normally operated as an airborne remote sensing system by Kestrel Corporation and provide digital images with 8 bit resolution and a 252 x 252 image pixel frame size. The goal of these experiments was to measure solar backscatter from aerosols and Rayleigh scatter in the lower troposphere, in the near vicinity (a few hundred meters) of the sensors. Appendix 1 summarizes the sky-scatter structure experiments conducted by Kestrel Corporation. In summary, we obtained individual green and blue images with unpolarized, horizontally, and vertically polarized images, plus dark response on each focal plane (cover on), and uniformity of the focal plane responsivity by use of a sunlit diffusion source.

Figures 8A to 8C illustrate luminance images (combined green and blue filters) used to determine the focal plane background dark noise (8A), the focal plane response to a diffuse illumination source (8B), and the response to the sunlit sky. In the case of the sunlit sky figure 8C illustrates the solar scatter symmetry very well in both green and blue. Unfortunately black and white reproduction is unable to show these features clearly.

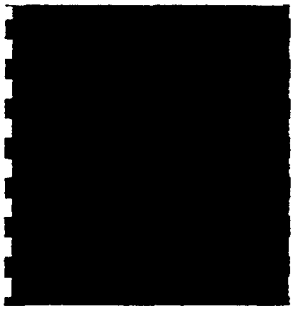

Figure 8A Dark Focal Plane

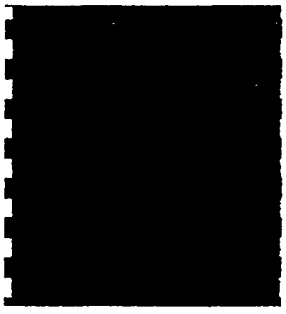

Figure 8B Diffusely Illuminated Image

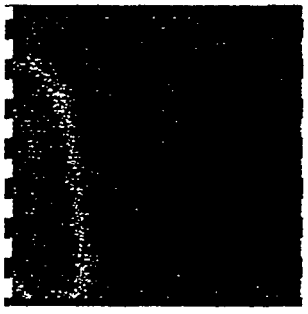

Figure 8C Luminance image of sky showing green and blue scatter from the sun.

Figures 9A and 9B show the solar scatter pattern observed by camera V2 observed in green and blue channels respectively. Image analysis can be accomplished using the composite G+B to enhance signal to noise ratio or the separated G and B channels.

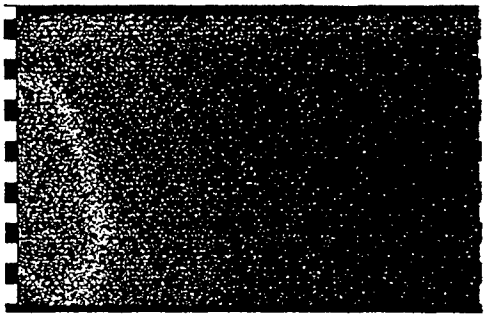

Figure 9A Solar Scatter Observed in Green Band, Sensor V2

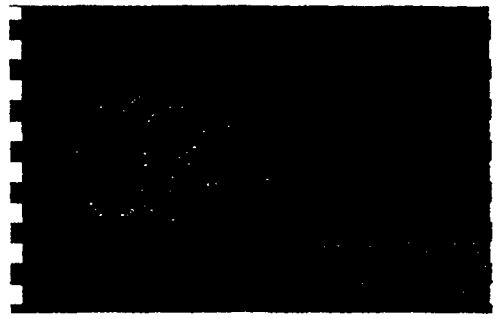

Figure 9B Solar Scatter Observed Blue Band, Horizontally Polarized

Several diagnostic configurations were explored for this experiment. The dark current statistical noise characteristics for the cameras were measured by covering the instruments and recording data. The focal plane structure noise was measured by putting an (almost) uniform diffusive surface over the lenses and recording data. Finally measurements were made in several wavebands, and in two polarization modes for vertically viewing sensors and for the virtual triangulation geometry with the sensors separated by 66.5 feet and the altitude of intersection about 100 feet. Table 1 summarizes the focal plane and objective-space characteristics of the visible and NIR cameras. For more details of this experiment refer to the Kestrel data summary report in Appendix 1.

Table 1

Camera Characteristics and Projected Objective Space Quantities

Camera	Band	Pixel IFOV mrad	FOV mrad	Pixel Footprint At 100 ft	Image Dimension – pixels
V2	Green,Blue (Polarized)	.91	442 x 1075	~2.8 cm	768x486
V4	Green,Blue (Polarized)	.91	442 x 1075	~2.8 cm	768x486
IR	MWIR 3-5 mm	1.4	680 x 680	~4.7 cm	486 x 486

In addition to the visible G-B data sets an Amber near infrared (3-5 μm) camera was operated to view zenith in the vicinity of the visible beam intersection. This camera was used primarily to see if the signal to noise ratio on a cooled MWIR system could detect structure in the lower atmosphere. Because of the 8-bit digitization level (i.e. 256 intensity levels) we believed that this sensor might be marginal for detecting atmospheric structure but the presence of water vapor and nearly subvisual clouds may have enhanced our ability to detect turbulence and winds. Figures 10A – 10C compares one data frame obtained by the IR camera with the focal plane response to both cold and hot plates placed over the objective lens. It is apparent that a strong asymmetry in focal plane response exists.

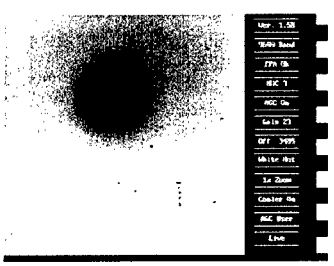

Figure 10A IR Data Image

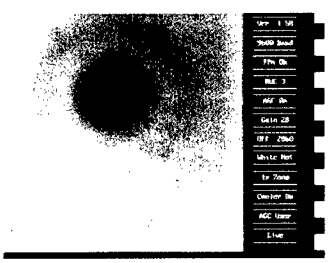

Figure 10B IR Hot Plate Image

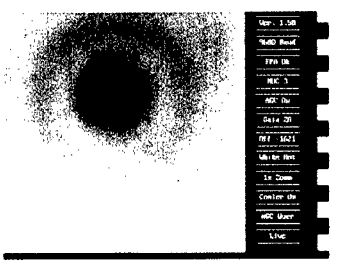

Figure 10C IR Cold Plate

The 2-dimensional spatial PSD's (Power Spectral Density estimates) of truncated images (128x128) pixels and 2-d correlation functions were computed. The images were truncated to ensure that radial variation in focal plane noise and responsivity could be minimized. This procedure also (nearly) eliminates the requirement for flat-fielding the data frames.

The PSD's computed for the Kestrel AIRCAM imager in measurement mode, dark current mode, and diffuse scatter mode are compared in Figure 11A and 11B. Figure 11A compares the measured sky background spectrum with example spectral slopes, $k^{-5/3}$, k^{-2} and $k^{-8/3}$. The experiment spectrum drops into the noise level at a spatial wavelength about 30 pixels. Figure 11B shows that the focal plane pattern and dark current noise (symmetric in k-space) and the readout noise (1/f or (k^{-2}) spectrum in the readout direction may be a significant deterrent to measurement of very small-scale structure inasmuch as the structure spatial frequency may lie beyond the noise cutoff frequency.

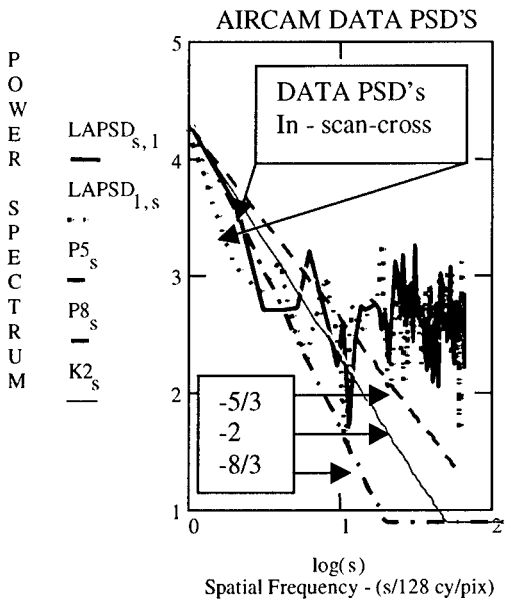

Figure 11A AIRCAM sky data 1-D PSD compared to slopes, -5/3, -2, –8/3. Note that this camera was uncooled.

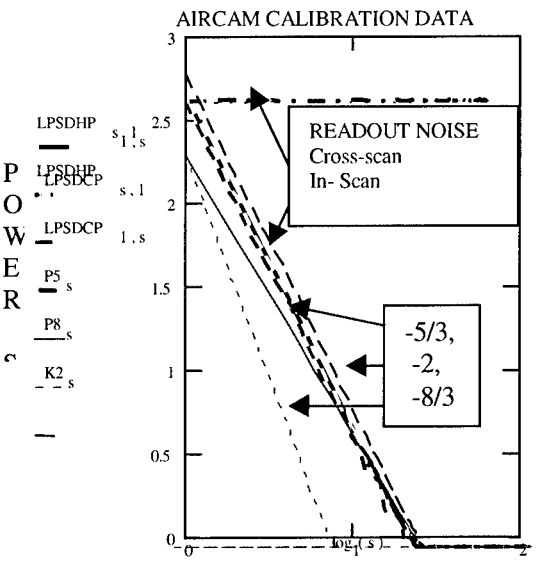

Figure 11B AIRCAM Calibration PSD's for dark counts and uniform illumination The readout noise is the k-2 slope

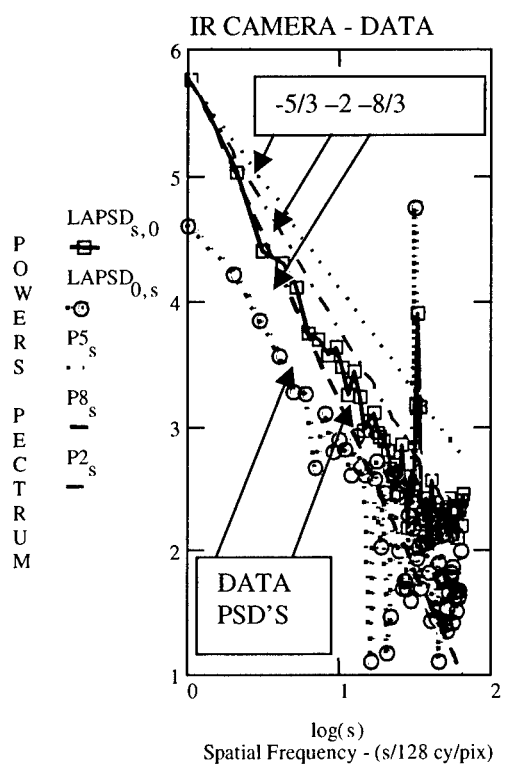

Figure 12A IR Camera Data PSD's Compared to model PSD slopes.

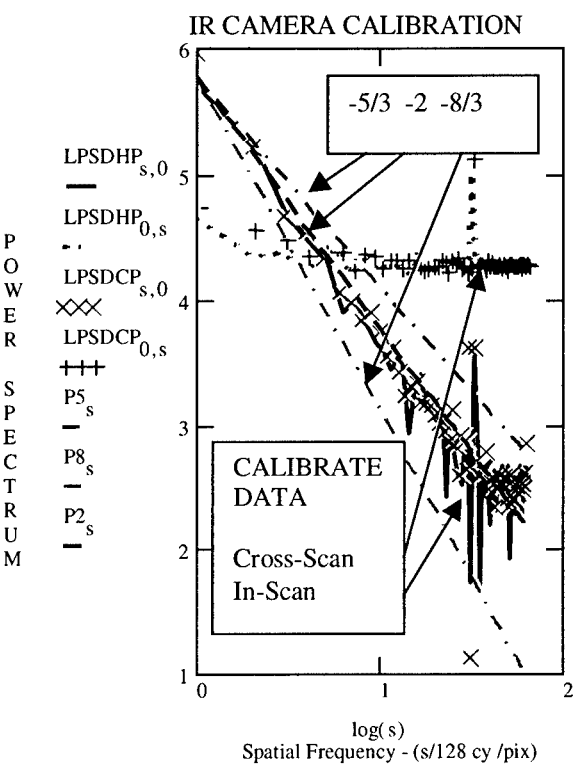

Figure 12B IR Camera PSD's on Calibration Plates compared to models

Figures 11 and 12 clearly show the role of focal plane noise and readout noise in the AIRCAM and IR sensors. The readout noise is clearly 1/f (in amplitude) and is approximately the same magnitude for the IR sensor sky data as for the hot plate and cold plate calibration frames. In fact, the mean value of sky background in the IR band was lower than either the hot or cold calibration frame values, indicating that the sky was colder than either calibration temperature. For these reasons we do not attempt to correct the IR camera data for noise and cannot pursue analysis in terms of structure motion and correlation length.

We pursued estimation of the phase drift and the correlation function parameters for the AIRCAM data based upon the nearly 2 order of magnitude signal to noise ratio (accounting for focal plane plus readout noise spectra). Figure 13 illustrates the average autocorrelation function for the five frames of data. Figure 14 presents the "auto-Phase spectrum for the same set of AIRCAM data frames.

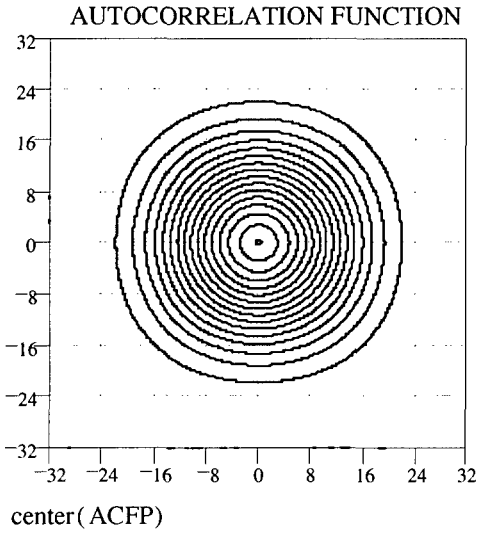

Figure 13 Autocorrelation Function for 5 successive AIRCAM Image Frames

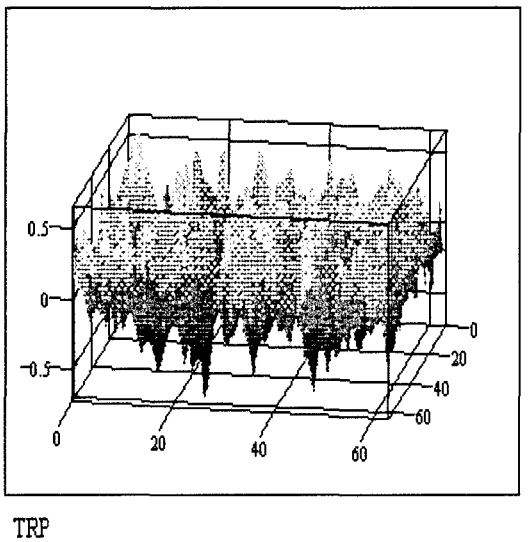

Figure 14 Average Phase Spectrum for Same set of AIRCAM Images

The autocorrelation data clearly shows a symmetric pattern characteristic of the Gaussian (presumably) characteristic of atmospheric low altitude turbulence as averaged over 5 successive image frames. The phase data are ambiguous, but seem to indicate definite phase peaks at selected spatial frequencies which may be emphasized by our thresholding method.

The Parzen- windowed power spectra illustrated in Figure 15A are used to compute the cross correlation functions for successive image frame delay times as illustrated in Figure 15B.

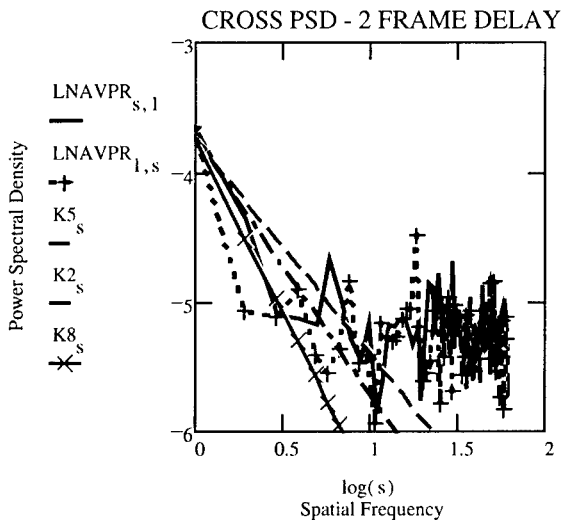

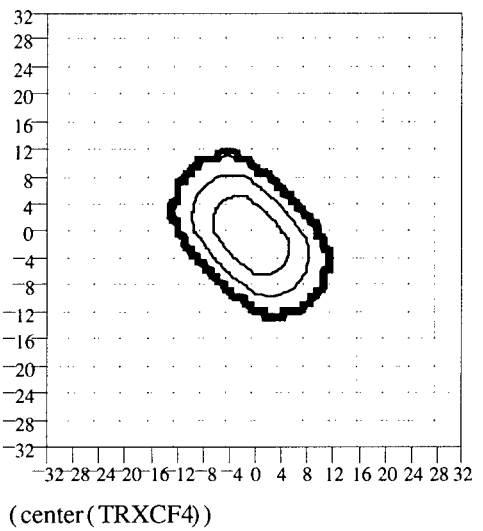

Figure 15A Cross PSD for Successive AIRCAM IMAGE Frames. Straight Lines are K-5/3, k-2, and k-8/3 slopes.

Figure 15B Cross Correlation Function For Same Image Frames. Displacement From center indicates a 2 pixel lag in Diagonal direction (=2 mrad).

The results shown in Figure 15A and B show that valid cross PSD and correlation functions can be computed for atmospheric turbulence on a small scale despite the high noise levels in the sensor and backgrounds. The 2 pixel offset in the correlation function center corresponds to a horizontal "wind" displacement of the turbulent structure of about 40 cm corresponding to a wind velocity of about 5 to 10 mph. This is consistent with local observations.

3.1.5 High Altitude Experiments

Two types of high altitude simulation experiments were conducted. We analyzed the GLO spectrometric data from the University of Arizona instruments flown on Shuttle Flight STS-85. The GLO instruments were flown in the look-forward, look-back configuration with a $\pm$ 65 degree azimuth with respect to the perpendicular to the spacecraft velocity vector to provide virtual triangulation geometry. The instrument lines of sight intersected the limb at about 58 km.

The second experiment was observation of the airglow emissions in the visible to Near-IR spectral range using the Kestrel Fourier Transform Hyperspectral Imager (FTHSI). In both experiments, the atmospheric airglow emission was the target signal. The goals of these experiments were first, to determine if the virtual triangulation geometry actually could be implemented by space-borne detectors and second, to determine if an FTHSI instrument could produce useable atmospheric data with sufficient spatial and spectral resolution to identify well known atmospheric airglow features.

3.1.5.1 GLO Airglow Data Analysis

Dr. Lyle Broadfoot of University of Arizona, Lunar and Planetary Institute has conducted GLO experiments on several STS flights. A selection of data from STS - 85 were provided to this project under subcontract. The geometry of the STS - 85 experiment is similar to that shown in figure 1 except that the two sensors, GLO 5 and GLO 6 are oriented to intersect the limb with a line-of-sight tangent altitude of 59 km. Appendix 2 contains selected details of the STS - 85 GLO experiments. Table 2 summarizes the spacecraft parameters and camera details relevant to this experiment

Table 2
Spacecraft Parameters and Camera Characteristics

Spacecraft:	**STS – 85**
Altitude:	**400 km**
Orientation:	**Pitch = 180 degrees, Yaw = 270**
Velocity	**~ 7 km/sec**
Hyperspectral Cameras:	**GLO 5 & GLO 6**
Camera Spectral Range:	
Camera Orientation:	**Elevation Angle (depression) 22 degrees, azimuth = ± 65 degrees**
LOS Tangent Altitude (center)	**59 km (drifts with time)**
Range to Tangent:	**2120 km**
LOS Velocity at tangent	**~ 5 km/sec**
Geometrical Time Lag of 5-6 LOS	**~420 sec. (= 2120 km/5 km/sec)**
Spatial footprint	**5 km at earthlimb**

Figure 16 summarizes the GLO airglow data for one satellite pass. Figures 17- 21 show the detailed GLO measurements of four airglow species emissions where the time variability between GLO 5 (forward-looking) and GLO 6 (backward-looking) and the time delay

between the data sets is established by matching intensity features. Each plot shows a delay from the forward to backward-pointing sensors appropriate to the airglow enhancements at their emission altitude. The thin airglow emitting layers are intercepted by the sensors operating at 59 km tangent altitude at two positions, a near field between the tangent point and the sensors and a far field intercept point on the far side of the 59 km tangent point. The emission "onion skin" characteristic leads to two possible lag times, corresponding to features in the near and far fields. It is unlikely that the sensor vertical resolution is sufficient to spatially resolve the far-field component so we will concentrate on near field results.

We computed the delay times for a number of emission altitudes: 85, 95, 130 and 240 km to compare with the GLO5-6 delay observations. Table 3 summarizes the airglow characteristics and near- and far-field ranges for the sensor to intercept the emitting layer. The corresponding delay times compared with the GLO values. We adopted an LOS velocity of 6 km/sec.

Table 3
Airglow Delay Predictions and Observations

Emitter Species	Band nm	Altitude km	Range km –Near	Range km – Far	Delay min. –near	Delay min.-far	GLO Observation-min.
OH	762	85	670	6100	1.9	17	7.2
Na	589.3	95	470	6300	1.3	18	4.8
O2	762	95	470	6300	1.3	18	2.8
OI	557.7	~130	340	6400	1.	18	2.8
OI	630	~240	320	7000	0.9	19	2

Comparison of the computed estimates of delay time vs. GLO measurements shows that most of the observed delay times are about a factor of 2 greater than the predicted estimates. Some of the factors creating this discrepancy may be due to airglow horizontal structure, and the exact altitude of the layer as the two sensors scan the same region. There also is a trend in the GLO observations to much higher values of delay time in the OH and Na emissions. Both of these emissions are highly structured spatially and temporally so may not indeed be statistically stationary over the period of the measurement, about 30 minutes.

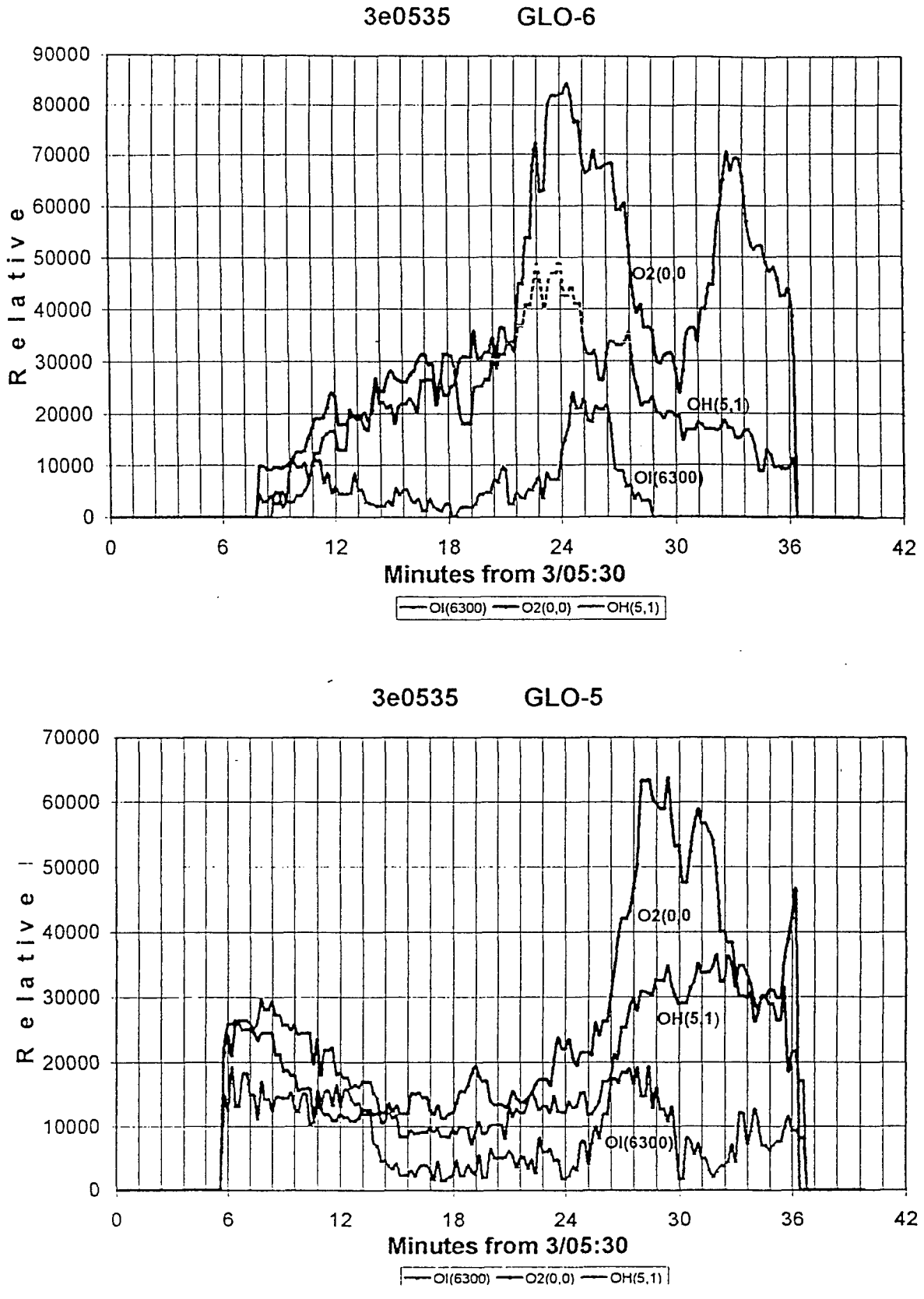

Figure 16 Summary of Airglow Intensity vs. Time for GLO-5 and GLO-6

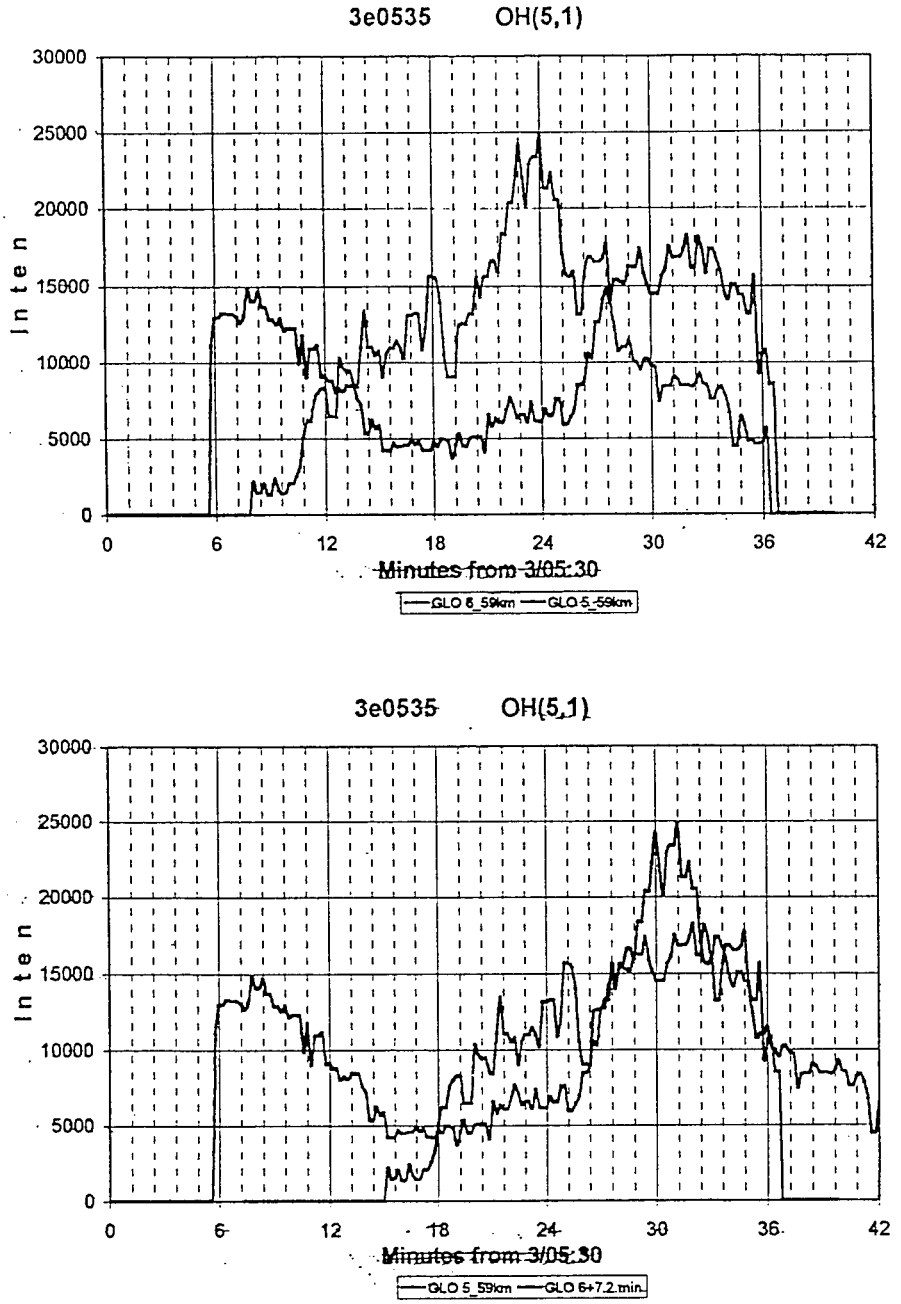

Figure 17 OH (5-1) Meinel Band Intensity vs. time from GLO-5 and GLO-6. The top panel shows the data at the time of acquisition. The bottom panel shows the same data with the trailing sensor plot time offset for a best fit of the intensity features

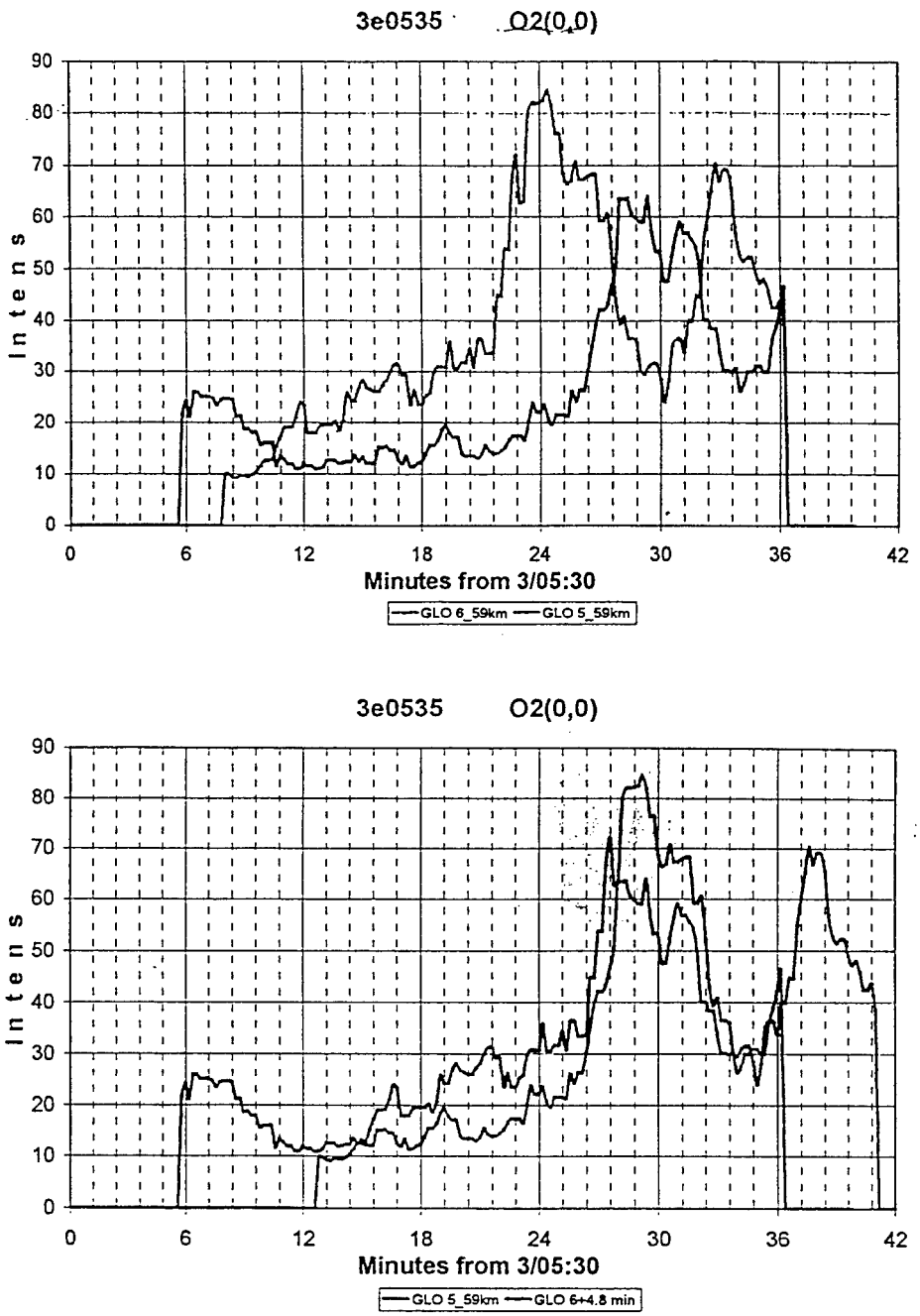

Figure 18 O2 Atmospheric Band Intensity vs. time from GLO-5 and GLO-6. The top panel shows the data at the time of acquisition. The bottom panel shows the same data with the trailing sensor plot time offset for a best fit of the intensity features

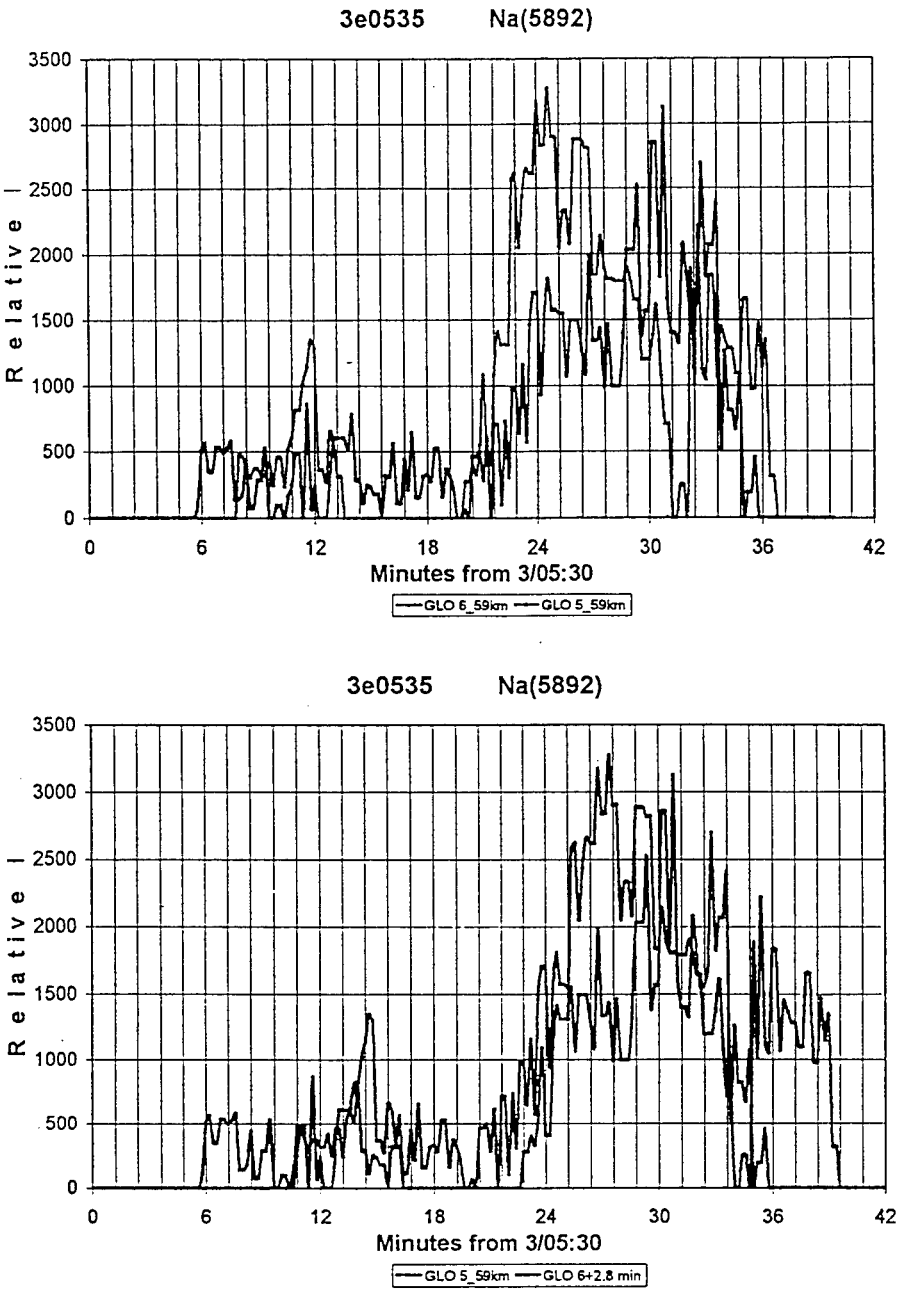

Figure 19 Na 589 & 589.6 nm Intensity vs. time from GLO-5 and GLO-6. The top panel shows the data at the time of acquisition. The bottom panel shows the same data with the trailing sensor plot time offset for a best fit of the intensity features

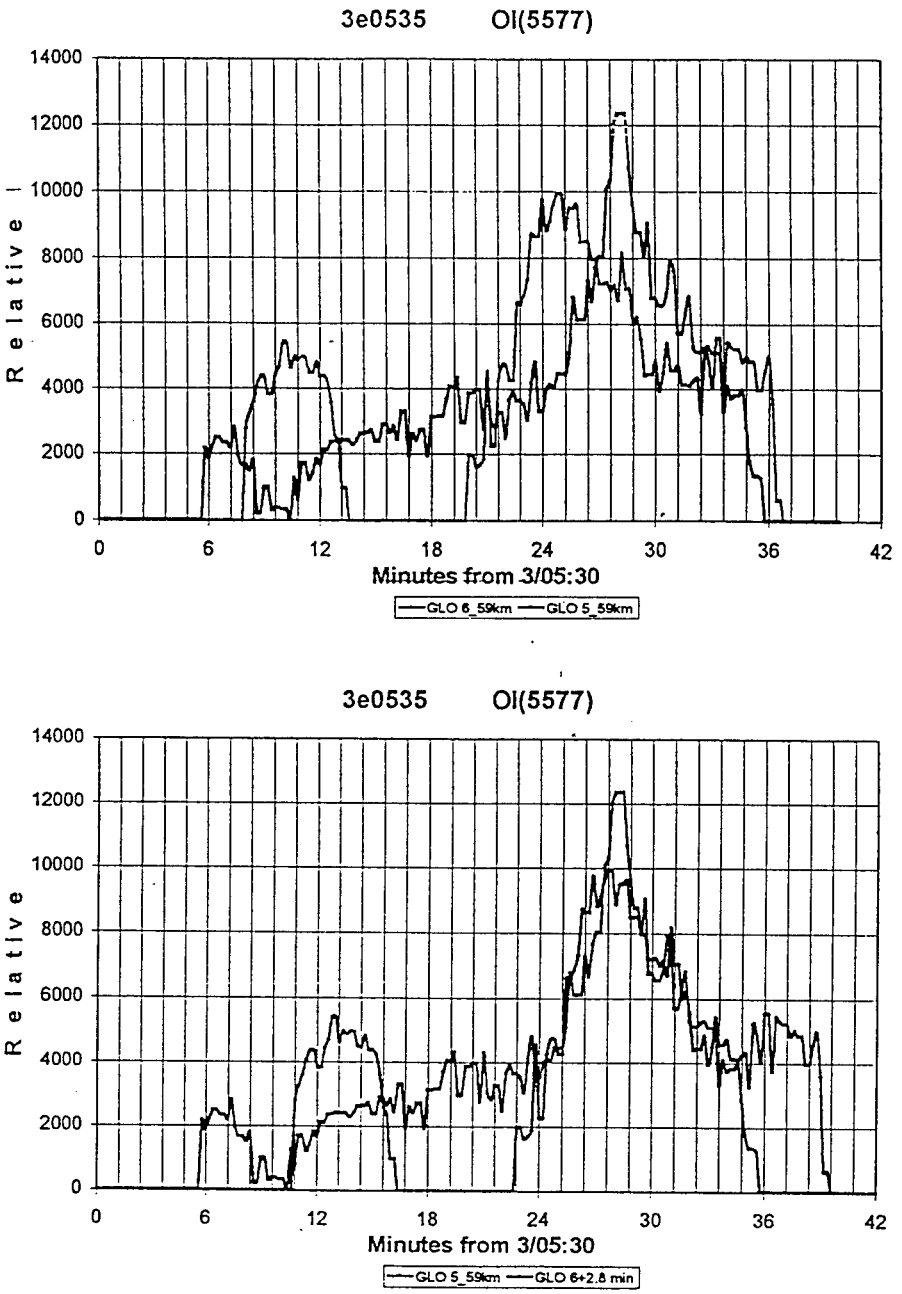

Figure 20 OI (557.7 nm) line Intensity vs. time from GLO-5 and GLO-6. The top panel shows the data at the time of acquisition. The bottom panel shows the same data with the trailing sensor plot time offset for a best fit of the intensity features

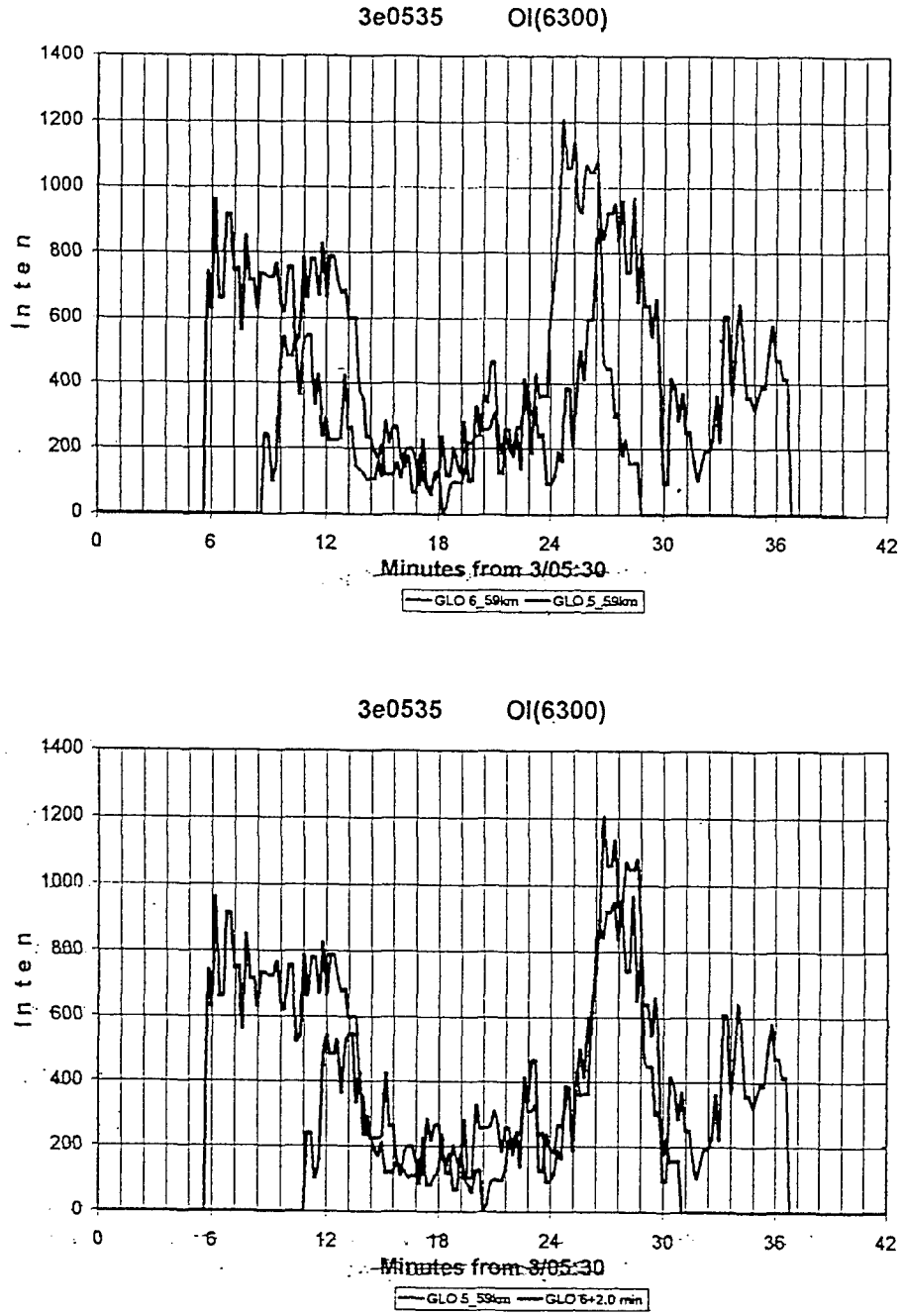

Figure 21 OI (630 nm) line Intensity vs. time from GLO-5 and GLO-6. The top panel shows the data at the time of acquisition. The bottom panel shows the same data with the trailing sensor plot time offset for a best fit of the intensity features

3.1.5.2 Hyperspectral Imager Analysis of Airglow Spectra

The Kestrel Fourier Transform Hyperspectral Imager (FTHSI) was used to estimate the capabilities of this instrument to measure high altitude airglow spectra in the 400 to 900 nm range from the ground. This instrument was not designed to perform this measurement mission, but we decided to attempt the measurement and to test the focal plane cooling requirement required to detect airglow.

Figure 22 illustrates the night airglow data obtained by the FTHSI operating in an out-of-design dry-ice cooling mode. The cross track data were integrated to obtain a higher signal to noise ratio to suppliment the cooling effect. We found that the streetlight and other urban signals such as Na and Hg lines were observed, but also we could identify most of the emission features as airglow features. Figure 22 also identifies the airglow features including Na and Hg emissions from streetlights. Only a few radiance enhancements were not identified, but this is common in an urban background environment. The integration time for these measurements was order 1 second or less, (down to TV 30 Hz sample rate).

Figure 23 shows night airglow features measured many years ago as published in Chamberlin[6]

We conclude that the FTHSI and similar imaging spectrographic instruments have the sensitivity to detect airglow emissions in the visible-near IR bands and that useful space-borne measurements can be obtained provided that the focal planes are cooled sufficiently.

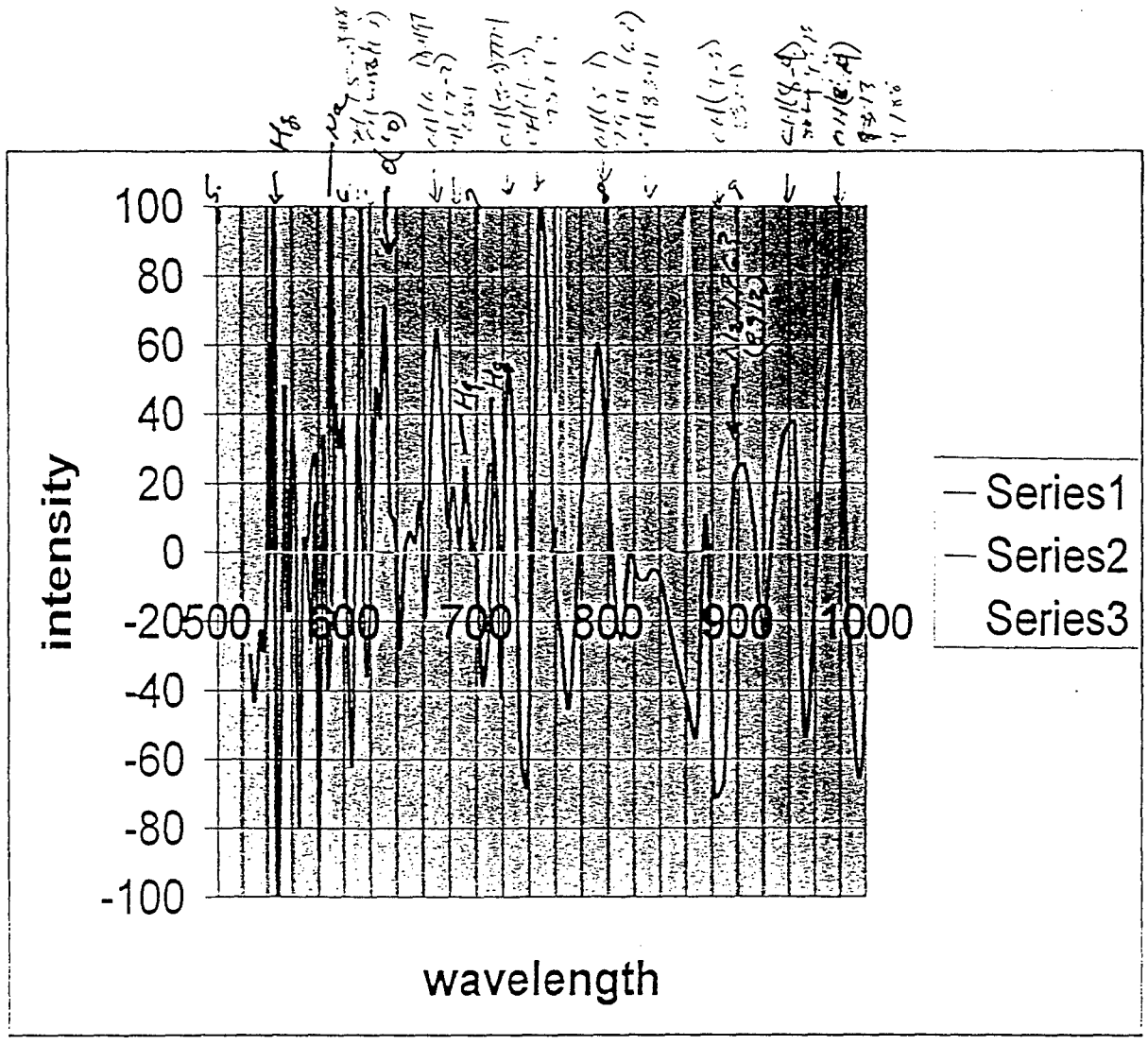

Figure 22 Airglow Spectrum Measured by FTHSI instrument. The emission features are identified by comparison with streetlight (Na and Hg) emissions which also serve as wavelength calibrations and by comparison to well known airglow features.

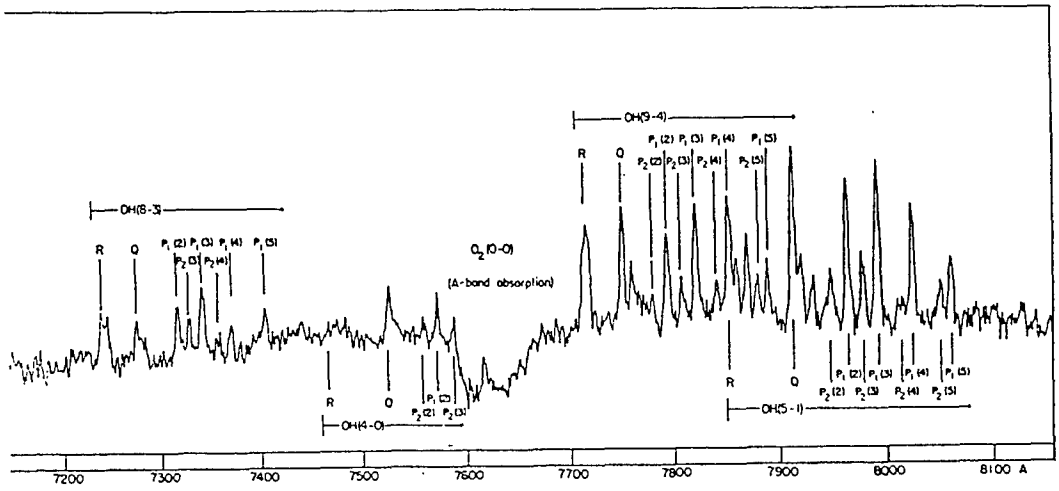

FIG. 9.11. Microphotometer tracing of nightglow spectrum, 7100-9000 A. Plate dispersion, 70 A/mm.

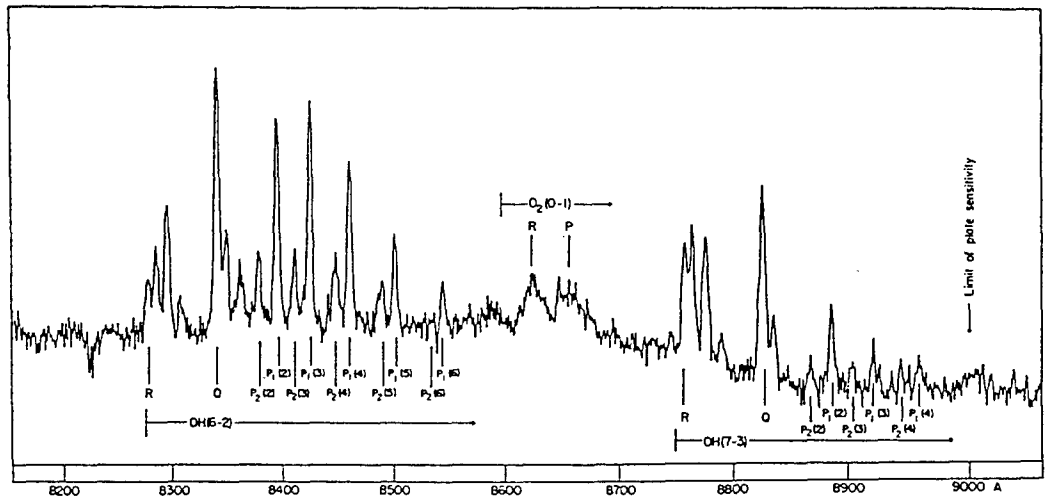

FIG. 9.11 (*cont.*)

After Chamberlain and Roesler [1955*a*]; courtesy University of Chicago Press.

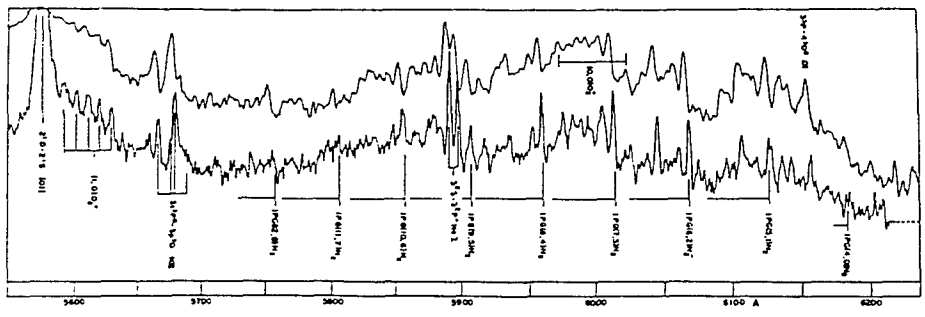

FIG. 5.16. Microphotometer tracings, 5550-6240 A, of spectrum in Fig. 5.4. After Chamberlain and Meinel [1954*a*]; courtesy University of Chicago Press.

Figure 23 Airglow Spectra published by Chamberlain for the visible, near-IR range.

4. SENSOR AND SPACECRAFT CONCEPT DEVELOPMENT

In order to provide an initial feasibility check regarding incorporating this instrument concept into a small satellite bus, we initiated a simple satellite design concept based upon the dimensions of the MightySat II bus. The purpose of this design effort was to ascertain whether off the shelf CCD cameras and hyperspectral imagers could be coupled with a MightySat II class buss and preserve the telescope resolution, instrument placement, and other parameters required for the virtual triangulation, hyperspectral measurement requirements. Figures 24 and 25 illustrate the design concept drawings.

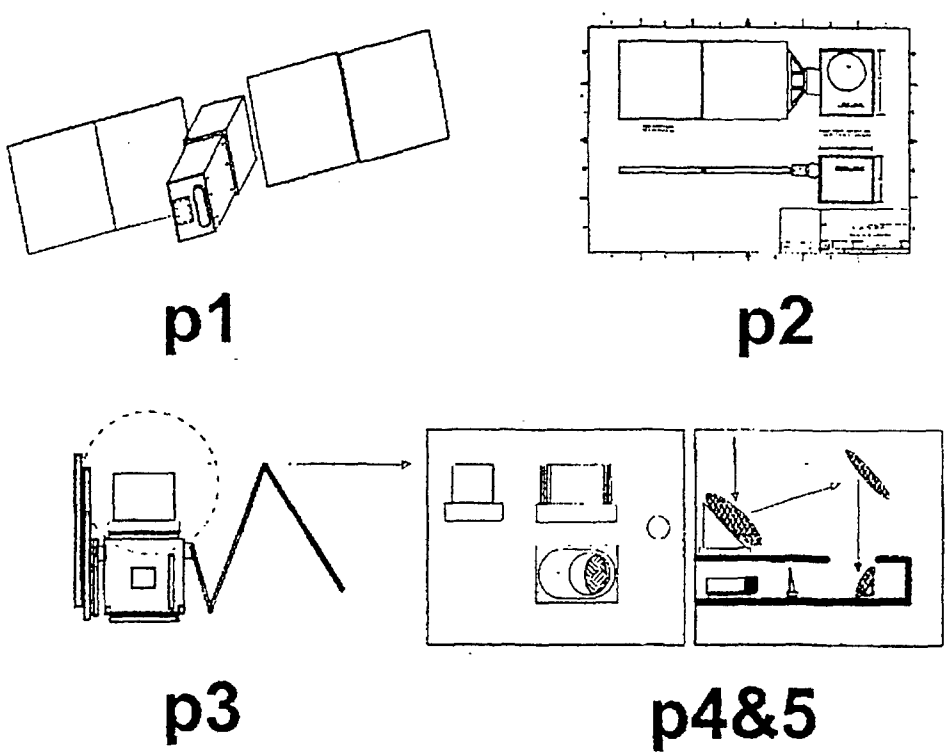

Figure 24 Overall line drawing of conceptual sensor and satellite bus based upon MightySat-II bus dimensions. The instrument dimensions are semi-scale, based upon commonly available cooled CCD focal plane detectors for UV and visible spectral range. An MWIR instrument may be somewhat larger and will require a second beam splitter.

Panel P1 shows an overall view of the MightySat II bus, solar panels, and attached optical system. P2 shows orthogonal views of the concept satellite MightySat II bus. P3 shows the third orthogonal view with the solar panels partly folded. The optical system is designed to fit within the envelope of the folded solar panels, with the exception of the heat exchanger on the space-viewing side of the satellite. P4 shows the overall envelope of the proposed optical system the configuration for which is shown in P5. We plan to use dielectric layered beamsplitters to separate UV, visible and IR optical signals.

Figure 25 shows the optical layout of a two camera (UV and IR) sensor. The dimensions of the components are approximately to the scale of commercially available visible and UV cameras. A cooled MWIR camera such as those made by AMBER would be considerably larger, but the height of the optical module would fit would be scaled to accommodate the specific unit selected.

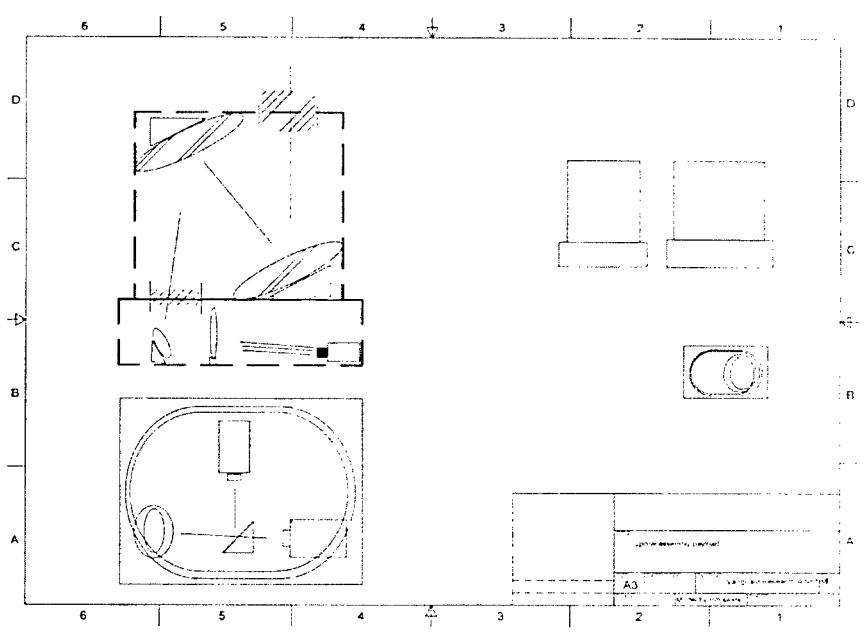

Figure 25 Telescope mirror layout for conceptual instrument design. The instrument uses an off-axis telescope in order to maximize cross track field of view.

We also assembled a very semi-scale model of a satellite to show that commonly available cooled CCD detectors would fit on a MightySat-II bus. Figures 26A and 26B show a rendition of the satellite concept as a third-scale model.

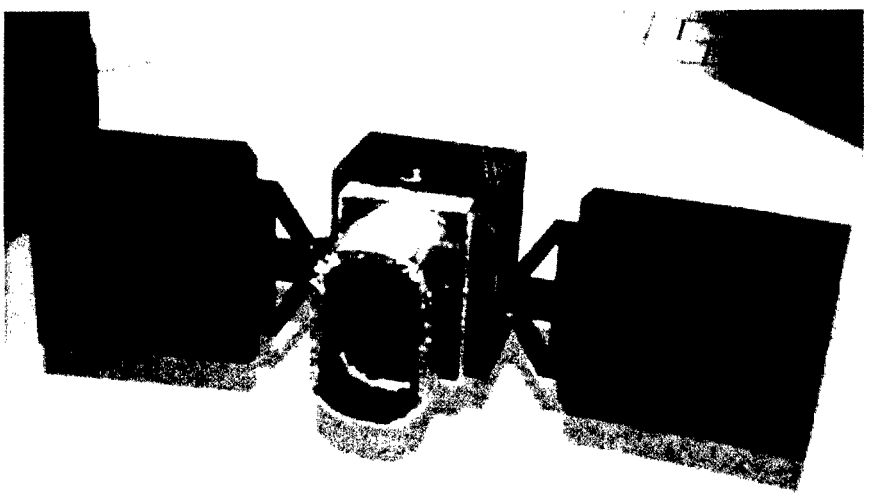

Figure 26A Front view of concept satellite model based upon MightySat II dimensions. The optical sensor unit is a small module between the telescope and the satellite bus.

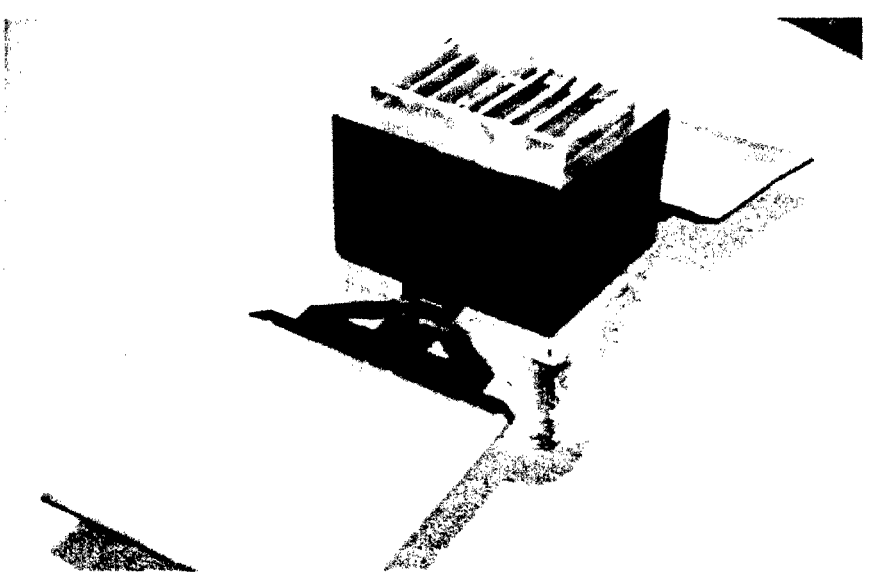

Figure 26B Rear view of concept satellite model as above. The focal plane and telescope-cooling grid is attached to the space-directed black surface of the MightySat-II bus. The present concept involves using heat pipes to cool the telescope and focal planes.

5. COMMERCIAL APPLICATIONS

Commercial and military applications for the multispectral, virtual triangulation remote sensing technique lie in the following areas:

- Airborne sensing of atmospheric clear air turbulence (CAT) and small scale turbulence as applied to airborne and space-borne laser weapons systems,
- Satellite-borne mapping of atmospheric turbulence, waves, and winds as applied to transmission of energy by means of waves and turbulence from the troposphere through the stratosphere into the mesosphere,
- Satellite-borne sensing of atmospheric turbulence regions which would affect airborne and space-borne laser weapons systems.

Our commercialization plan incorporates the following elements which will be implemented in the Phase II program:

- Modification of the existing space-qualified GLO sensor system developed by University of Arizona, by improving the field of view, pixel resolution, and inclusion of a Fourier Transform Hyperspectral imager in place of the dispersive imaging spectrometer. We also will incorporate the quad C-40 processor. Both the FTHSI and the Quad C-40 will be tested on the MightySat II.1 satellite testbed. This instrument will operate in the UV through NIR spectral range (300 to 900 nm). This instrument will be space qualified for Shuttle flight. We will seek a Shuttle manifest slot in collaboration with our subcontractors at University of Arizona.

- Development of a GLO and FTHSI-based instrument which will be compatible with the MightySat II spacecraft platform. We will seek a MightySat II satellite development and launch slot in collaboration with the USAF Research Laboratory Spacecraft Division.
- Exercise of the developmental prototype instruments on an airborne platform to investigate their capabilities for detection of CAT.

6. CONCLUSIONS

We summarize the work performed and the accomplishments on this SBIR contract as follows:

- Partial simulations of the background Gaussian correlated random noise structure allowed measurement of the PSD and Phase Spectra and velocity for the virtual triangulation geometry concept. High signal to noise ratio in these simulations and subsequent measurements is required to accomplish very high spatial resolution atmospheric structure measurements from satellite altitudes.
- More detailed simulations, involving a true 3-D correlated random background drifting through the triangulation sensors' fields of view are required and could not be performed in this phase because of computer memory limitations.
- Ground-based CCD camera measurements made to simulate tropospheric-stratospheric structure measurements show the importance of careful control of focal plane noise and pattern noise. Focal plane cooling will certainly be required for visible, UV, and MWIR atmospheric structure sounding using the techniques investigated in this project.
- The feasibility of using Fourier Transform spectrometers to detect airglow and (by inference) atmospheric backscatter structure was demonstrated by the Kestrel FTHSI instrument operated against an airglow background. Again, the importance of focal plane and instrument cooling to minimize background noise was demonstrated.
- Measurements of airglow structure from the Shuttle using the GLO instruments shows that the virtual triangulation technique is feasible. Instrument line-of-sight ambiguities and spacecraft attitude changes limited our ability to obtain detailed pixel by pixel correlation, but the overall data (integrated over the focal plane width) verifies that the virtual triangulation technique works.
- The results of this limited effort are promising but not definitive. Therefore, more detailed simulations followed by ground-based experimental measurements using the airglow layers as the signal source are recommended before proceeding to a formal instrument design phase.

7. REFERENCES

1 L. Broadfoot, B.R Sandel, D. Knecht, R. Viereck and E. Murad, "A Panchromatic Spectrograph with Supporting Monochromatic Imagers," App. Opt., 31 (16), 3083-3096, 1992. and A. L. Broadfoot, "Remote Sensing from the Space Shuttle and Space Stations," Adv. Space Res. 19, 623-626, 1997.

2 L. A. Strugala, R. D. Sears, et. al. Optical Engineering, 32 (5), 992-11001 May 1993.

3 R. D. Sears, "Simulation of Low Altitude Structure Using Multi-Component Stochastic Perturbation Models," 33rd Aerospace Sciences Meeting, AIAA Paper No. 95-0058, 10 January, 1995.

4 E. E. Gossard, D. B. Sailors, V. R. Noonkester, Guide to Computation and Use of Cross Spectra in Geophysics and Radio Physics, NELC Technical Document 136, 22 July, 1971

5 see Mathcad Users Guide, versions 6 and 7, published by Mathsoft Inc, Cambridge MA.

6 J. W. Chamberlin, "Physics of the Aurora and Airglow," Academic Press, New York, 1961, pp 167-169.

8. APPENDIX 1 Kestrel Corporation Experiment Report

This report summarizes the ground-based AIRCAM and FTHSI experiment operating parameters as conducted by the Kestrel Corporation.

KESTREL CORPORATION
6624 Gulton Court NE
Albuquerque, NM 87109
(505) 345-2327

TEST PLANNING SHEET

PROJECT: Vanguard Phase 1 SBIR
DATE: 15 September, 1998

TEST DESCRIPTION:
AirCam BACKSCATTER MEASUREMENTS.

TEST LOCATION:
Kestrel Corporation Facility parking lot.

TESTS TO BE CONDUCTED:
- Low Altitude Atmospheric Structure and Wind Experiments per BMDO-SBIRP1- 980508.doc/09/10/98 section 2.1.1

SPECIAL HANDLING REQUIREMENTS:
- Modify camera control software to allow for control of camera range and offset.

TESTING ASSIGNED TO: Al Jones DATE: 9/15/98

TESTING AUTHORIZED BY: John Otten DATE: 9/15/98

RESULTS RECIEVED BY: Robert D Sears DATE: 9/16/98

(PLEASE ATTACH ALL DOCUMENTATION TO THIS SHEET)

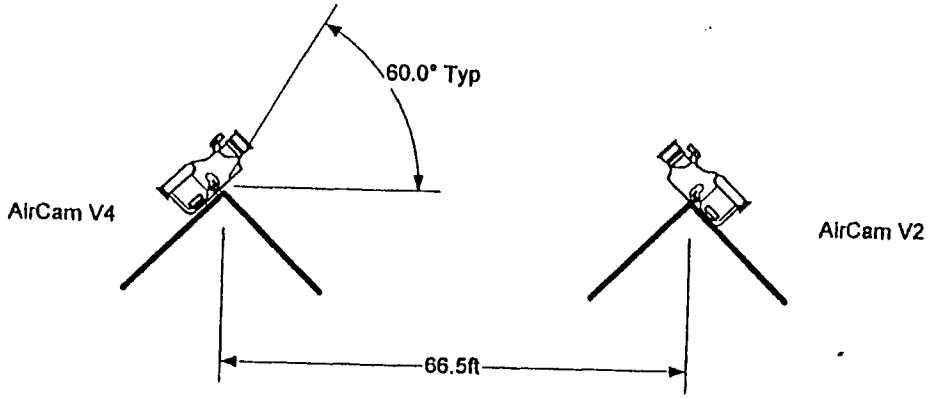

AirCam Backscatter Experiment
Separations

BACKSCATTER TEST #2A

LOCATION:	KESTREL PARKING LOT			
TIME:	14:36			
DATE:	15-Sep-98			
ITEM	V4-B	V4-G	V2-B	V2-G
TYPE	9701	9701	9701	9701
LENS TYPE:	12-0302	12-0302	12-0302	12-0302
FILTER NO.:	4	1	4	1
POLARIZER:	NONE	NONE	NONE	NONE
DIFFUSER:	NONE	NONE	NONE	NONE
F-STOP:	1.4	2.4	1.4	2.4
GATING:	7	8	7	8
RANGE:	90	90	90	90
OFFSET:	60	60	60	60
ORIENTATION:	60 DeG	60 DeG	60 DeG	60 DeG
IMAGE #S (V2)	0-100			
IMAGE #S (V4)	101-200			

BACKSCATTER TEST #2B

LOCATION:	KESTREL PARKING LOT			
TIME:	14:36			
DATE:	15-Sep-98			
ITEM	V4-B	V4-G	V2-B	V2-G
TYPE	9701	9701	9701	9701
LENS TYPE:	12-0302	12-0302	12-0302	12-0302
FILTER NO.:	1	4	1	4
POLARIZER:	VERTICAL	VERTICAL	VERTICAL	VERTICAL
DIFFUSER:	NONE	NONE	NONE	NONE
F-STOP:	1.4	2.4	1.4	2.4
GATING:	7	8	7	8
RANGE:	90	90	90	90
OFFSET:	60	60	60	60
ORIENTATION:	60 DeG	60 DeG	60 DeG	60 DeG
IMAGE #S (V2-B)	101-200	POLARIZER ON BLUE		
IMAGE #S (V4-B)	201-300	POLARIZER ON BLUE		
IMAGE #S (V2-G)	301-400	POLARIZER ON GREEN	TIME 14:53	
IMAGE #S (V4-G)	401-500	POLARIZER ON GREEN	TIME 14:53	

BACKSCATTER TEST #2C

LOCATION:	KESTREL PARKING LOT				
TIME:	14:47				
DATE:	15-Sep-98				
ITEM	V4-B	V4-G	V2-B	V2-G	
TYPE	9701	9701	9701	9701	
LENS TYPE:	12-0302	12-0302	12-0302	12-0302	
FILTER NO.:	1	4	1	4	
POLARIZER:	HORIZ	HORIZ	HORIZ	HORIZ	
DIFFUSER:	NONE	NONE	NONE	NONE	
F-STOP:	1.4	2.4	1.4	2.4	
GATING:	7	8	7	8	
RANGE:	90	90	90	90	
OFFSET:	60	60	60	60	
ORIENTATION:	60 DeG	60 DeG	60 DeG	60 DeG	
IMAGE #S (V2-B)	201-300	POLARIZER ON BLUE			
IMAGE #S (V4-B)	301-400	POLARIZER ON BLUE			
IMAGE #S (V2-G)	401-500	POLARIZER ON GREEN	TIME 15:09	DELAY FOR CLO	
IMAGE #S (V4-G)	501-600	POLARIZER ON GREEN	TIME 15:09		

BACKSCATTER TEST #2D

LOCATION:	KESTREL PARKING LOT			
TIME:	15:15			
DATE:	15-Sep-98			
ITEM	V4-B	V4-G	V2-B	V2-G
TYPE	9701	9701	9701	9701
LENS TYPE:	12-0302	12-0302	12-0302	12-0302
FILTER NO.:	1	4	1	4
POLARIZER:	NONE	NONE	NONE	NONE
DIFFUSER:	YES	YES	YES	YES
F-STOP:	1.4	2.4	1.4	2.4
GATING:	7	8	7	8
RANGE:	90	90	90	90
OFFSET:	60	60	60	60
ORIENTATION:	60 DeG	60 DeG	60 DeG	60 DeG
IMAGE #S (V2)	501-530			
IMAGE #S (V4)	601-630			

BACKSCATTER TEST #2E

LOCATION:	KESTREL PARKING LOT			
TIME:	15:19			
DATE:	15-Sep-98			
ITEM	V4-B	V4-G	V2-B	V2-G
TYPE	9701	9701	9701	9701
LENS TYPE:	12-0302	12-0302	12-0302	12-0302
FILTER NO.:	1	4	1	4
POLARIZER:	NONE	NONE	NONE	NONE
DIFFUSER:	COVER	COVER	COVER	COVER
F-STOP:	1.4	2.4	1.4	2.4
GATING:	7	8	7	8
RANGE:	90	90	90	90
OFFSET:	60	60	60	60
ORIENTATION:	60 DeG	60 DeG	60 DeG	60 DeG
IMAGE #S (V2)	531-560			
IMAGE #S (V4)	631-660			

BACKSCATTER TEST #2F

LOCATION:	KESTREL PARKING LOT
TIME:	15:24
DATE:	15-Sep-98
ITEM	IR
TYPE	amber
LENS TYPE:	25mm
FILTER NO.:	3-5um
POLARIZER:	NONE
DIFFUSER:	NONE
F-STOP:	N/A
GATING:	AUTO
RANGE:	N/A
OFFSET:	AUTO
ORIENTATION:	ZENITH
IMAGE #S	1-100

BACKSCATTER TEST #2G

LOCATION:	KESTREL PARKING LOT
TIME:	15:30
DATE:	15-Sep-98
ITEM	IR
TYPE	amber
LENS TYPE:	25mm
FILTER NO.:	3-5um
POLARIZER:	NONE
DIFFUSER:	WARM PLATE
F-STOP:	N/A
GATING:	AUTO
RANGE:	N/A
OFFSET:	AUTO
ORIENTATION:	ZENITH
IMAGE #S	101-130

BACKSCATTER TEST #2H

LOCATION:	KESTREL PARKING LOT
TIME:	15:37
DATE:	15-Sep-98
ITEM	IR
TYPE	amber
LENS TYPE:	25mm
FILTER NO.:	3-5um
POLARIZER:	NONE
DIFFUSER:	COLD PLATE
F-STOP:	N/A
GATING:	AUTO
RANGE:	N/A
OFFSET:	AUTO
ORIENTATION:	ZENITH
IMAGE #S	131-160

```
     9/15/1998          < Mission Flight Date                              >
Van_Parkinglot1         < Mission Name <80 Char with Underscores           >
    C:\VANPK1           < ACSYS Data File Storage Directory                >
             4          < Red Camera Filter Reference Number               >
             1          < Green Camera Filter Reference Number             >
             4          < Blue Camera Filter Reference Number              >
             1          < Yellow Camera Filter Reference Number            >
           100          < Number of Images to be read Sequentially         >
 35 46.00000            < Latitude Data Collection Point                   >
-106 17.00000           < Longitude Data Collection Point                  >

       780-900          < Red Camera Filter 780,900                        >
        001024          < Red Camera Serial Number                         >
      24060149          < Red Camera Lens Serial Number                    >
                        < Blue Channel V4                                  >

   412-525,455          < Green Camera Filter 412-525,hp-455               >
        001022          < Green Camera Serial Number                       >
      24061149          < Green Camera Lens Serial Number                  >
                        < Green Channel V4                                 >

       780-900          < Blue Camera Filter 780,900                       >
        001021          < Blue Camera Serial Number                        >
      24010078          < Blue Camera Lens Serial Number                   >
                        < Blue Channel V2                                  >

   412-525,455          < Yellow Camera Filter 412-525,hp-455              >
        002817          < Yellow Camera Serial Number                      >
      24009078          < Yellow Camera Lens Serial Number                 >
                        < Green Channel V2                                 >

         3-5um          < IR Camera Filter 3-5um                           >
          0010          < IR Camera Serial Number                          >
    22240-084           < IR Camera Lens Serial Number                     >
```

9. APPENDIX 2 University of Arizona Data

This is the final report from Dr. Lyle Broadfoot, University of Arizona on GLO experiment data analysis.

GLO 5 and GLO 6 Data
Notes on Data in following pages

Page 1 – GLOVIEW – see description in "Home Page"
"www.glo.lpl.arizona.edu/glo"
Page 2 – see notes on page

Files are named by the MET time of their recording

3053530A is 3/05:35:30 MET

The alpha character represents the CCD source

A, B, C, D, E are spectrographs
F, G, H are imagers
I is a tracking image

Other files are defined on the page

Page 3 - @ b.lst – a list of all records from the b-CCD, ie: b spectrograph

Page 5 – The Geometric Parameters in the header of each" *.fit" files

Page 7 – A plot of the elevation history in data set 3d0535 and 3e0535

Data sets are named by the name of the first file in the data set

3d0535 means:
3rd day
d flight
05 hrs
35 min

GLO DATA file system:

Flight	*GLO#*	*DAY*	*Flight*	*hr*	*min*
STS-53	1	____	____	__	__
STS-63	2	____	a	__	__
STS-69	3	____	b	__	__
STS-74	4	____	c	__	__
STS-85	5	____	d	__	__
STS-85	5	____	e	__	__

Page 8 – TH (tangent height) of GLO-5, GLO-6 in file 3d_e0535.XLS.

Page 9 – Hyperspectral images of $O_2(0,0)$

Page 10 – Spectra and Hyperspectral images

Page 13 – Plot of geometric data showing top and bottom of the slit (corrected Altitude)

Page 14 – Hyperspectral images of 5 emissions

File name	*GLO 6*	
60H5_1	6	OH(5,1)
60I6300	6	OI(6300)
6O2_0_0	6	O2(0,0)
6OI5577	6	OI(5577)
6Na5892	6	Na(5892)

Page 15 – as above for GLO 5

50H5_1	5	OH(5,1)

Page 16 – Constant altitude plots. The TH of 59 km was selected since that elevation was common to both instruments.
Note the shift in maxima

Page 17 – 21

These plots show the relative position of the two traces @ 59kmTH for both instruments. The top plot shows the original position of the data in time. The bottom plot shows a shifted GLO-6 curve to match the GLO 5 curve. The time shift is noted.

They are in order of time delay between when the signature showed in the GLO-6 FOV pointing ahead and GLO-5 pointing behind shuttle track.

The difference in the latitude, longitude file was 6.7 min.

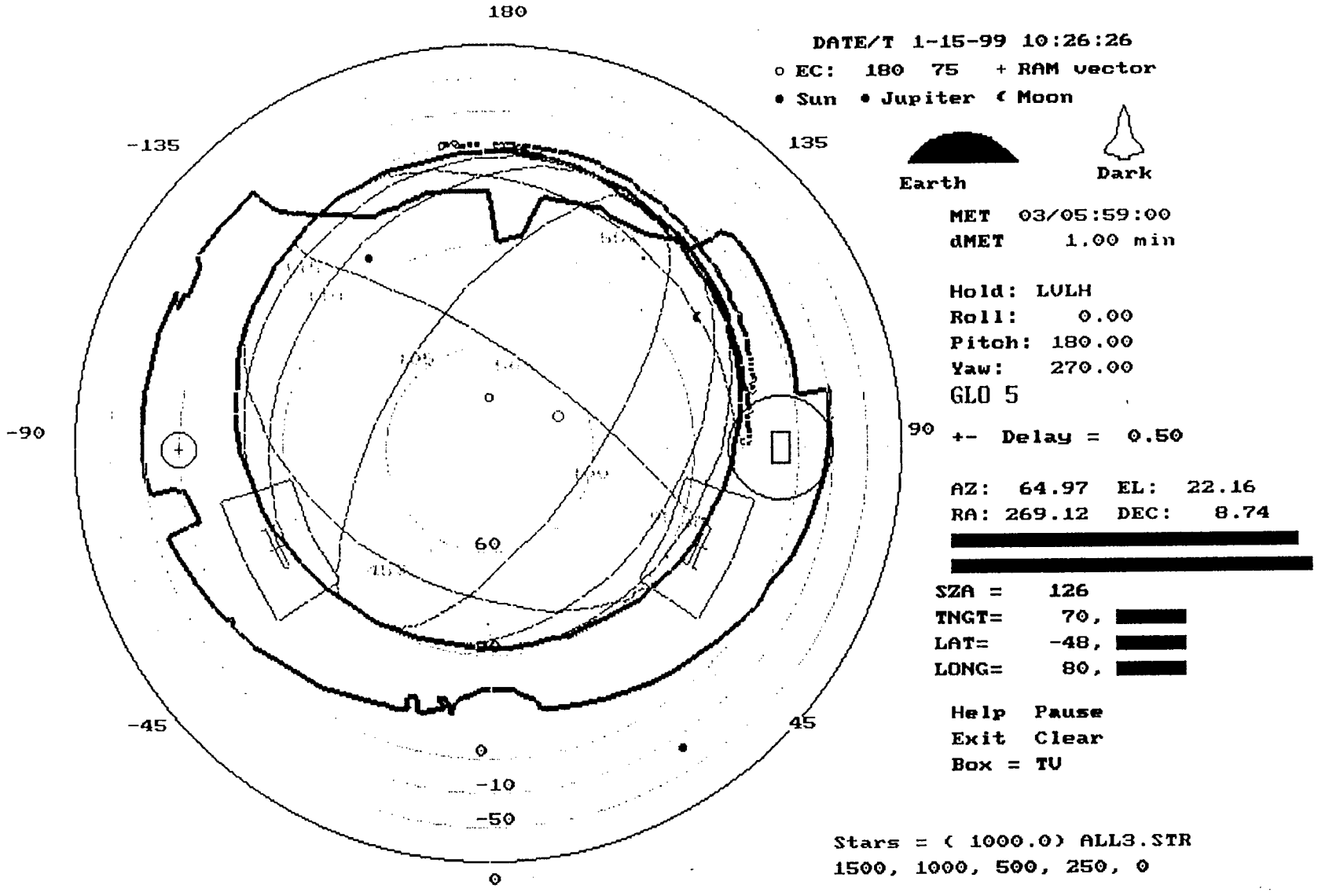
180
-135
135
-90
90
-45
45
0
60
30
-10
-50
0
GLO AZ/EL Grid
DATE/T 1-15-99 10:26:26
o EC: 180 75 + RAM vector
• Sun • Jupiter ☾ Moon
Earth
Dark
MET 03/05:59:00
dMET 1.00 min
Hold: LVLH
Roll: 0.00
Pitch: 180.00
Yaw: 270.00
GLO 5
+- Delay = 0.50
AZ: 64.97 EL: 22.16
RA: 269.12 DEC: 8.74
SZA = 126
TNGT= 70,
LAT= -48,
LONG= 80,
Help Pause
Exit Clear
Box = TV
Stars = (1000.0) ALL3.STR
1500, 1000, 500, 250, 0

This is a reference list of the files in this Directory with some comments that apply to all data sets
The File is dir.xls
Directory of E:\3d0535

.	<DIR>		01-10-99	7:52a	.	
..	<DIR>		01-10-99	7:52a	..	
3053530F	FIT	17,280	1/10/99	7:45a	3053530F.FIT	
3053530G	FIT	17,280	1/10/99	7:45a	3053530G.FIT	
3053530A	FIT	63,360	1/10/99	7:45a	3053530A.FIT	
3053530C	FIT	63,360	1/10/99	7:45a	3053530C.FIT	
3053530B	FIT	63,360	1/10/99	7:45a	3053530B.FIT	
3053530D	FIT	63,360	1/10/99	7:45a	3053530D.FIT	
3053530E	FIT	63,360	1/10/99	7:45a	3053530E.FIT	
3053556F	FIT	17,280	1/10/99	7:45a	3053556F.FIT	
3053556G	FIT	17,280	1/10/99	7:45a	3053556G.FIT	
3053556A	FIT	63,360	1/10/99	7:45a	3053556A.FIT	
3053556C	FIT	63,360	1/10/99	7:45a	3053556C.FIT	
3060603A	FIT	63,360	1/10/99	7:47a	3060603A.FIT	
3060603C	FIT	63,360	1/10/99	7:47a	3060603C.FIT	
3060603D	FIT	63,360	1/10/99	7:47a	3060603D.FIT	
3060603E	FIT	63,360	1/10/99	7:47a	3060603E.FIT	
3060618G	FIT	17,280	1/10/99	7:47a	3060618G.FIT	
3060618F	FIT	17,280	1/10/99	7:47a	3060618F.FIT	
3060618A	FIT	63,360	1/10/99	7:47a	3060618A.FIT	
3060618B	FIT	63,360	1/10/99	7:47a	3060618B.FIT	
3060618D	FIT	63,360	1/10/99	7:47a	3060618D.FIT	
3060618E	FIT	63,360	1/10/99	7:47a	3060618E.FIT	
3054306B		63,360	1/10/99	7:46a	3054306B	File Directory, All Files

864 file(s) 43,634,534 bytes
2 dir(s) 509,362,176 bytes free

3D_E0535	XLS	279,552	01-14-99	7:36a	3d_e0535.xls	XL worksheets for geometric data
A	LST	7,145	1/12/99	10:19p	a.lst	
B	LST	7,435	1/12/99	10:19p	b.lst	
C	LST	7,087	1/12/99	10:19p	c.lst	
D	LST	7,377	1/12/99	10:19p	d.lst	
E	LST	7,493	1/12/99	10:19p	e.lst	
F	LST	7,145	1/12/99	10:19p	f.lst	
G	LST	6,333	1/12/99	10:19p	g.lst	
H	LST	144	1/12/99	10:19p	h.lst	
I	LST	144	1/12/99	10:19p	i.lst	Lists of data images from each detector in GLO instrument
UCAT	MAP	1,396	1/8/99	3:02p	ucat.map	Ancillary data from JSC giving flight geometric information
GETMET	OUT	27,464	1/8/99	1:35p	GETMET.OUT	A file of MET times and exposure times prepared to request UCAT data
MAKEHDF	LST	23,083	1/11/99	3:55a	MAKEHDR.LST	Header or each spectral image in data set usualy merged with UCAT data
DIR	TXT	0	1/14/99	7:54a	dir.txt	File DIR.
B	XLS	29,696	1/14/99	7:51a	b.xls	b.lst in XL format
O2_0_1HY	FIT	46,080	1/12/99	10:38a	O2_0_1HY.FIT	
BG0_1HY	FIT	46,080	1/12/99	10:38a	GBO_1.FIT	
BG_REST	FIT	46,080	1/12/99	10:38a	BG_REST.FIT	
O2_0_0HY	FIT	46,080	1/12/99	10:38a	O2_0_0HY.FIT	
OH6_2HY	FIT	46,080	1/12/99	10:38a	OH6_2HY.FIT	
OH5_1HY	FIT	46,080	1/12/99	10:38a	OH5_1HY.FIT	
BG8_3HY	FIT	46,080	1/12/99	10:38a	BG8_3HY.FIT	
OH8_3HY	FIT	46,080	1/12/99	10:38a	OH8_3HY.FIT	
OI6300HY	FIT	46,080	1/12/99	10:38a	OI6300HY.FIT	Hyperspectral Images

C. RE

Volume in drive E has no label
Volume Serial Number is 4254-0301
Directory of E:\3d0535

3053530B FIT	63,360	1/10/99 7:45a	3053530B.
3053556B FIT	63,360	1/10/99 7:45a	3053556B.
3053557B FIT	63,360	1/10/99 7:45a	3053557B.
3053612B FIT	63,360	1/10/99 7:45a	3053612B.
3053626B FIT	63,360	1/10/99 7:45a	3053626B.
3053641B FIT	63,360	1/10/99 7:45a	3053641B.
3053703B FIT	63,360	1/10/99 7:45a	3053703B.
3053711B FIT	63,360	1/10/99 7:45a	3053711B.
3053726B FIT	63,360	1/10/99 7:45a	3053726B.
3053741B FIT	63,360	1/10/99 7:45a	3053741B.
3053802B FIT	63,360	1/10/99 7:45a	3053802B.
3053810B FIT	63,360	1/10/99 7:45a	3053810B.
3053840B FIT	63,360	1/10/99 7:45a	3053840B.
3053902B FIT	63,360	1/10/99 7:46a	3053902B.
3053909B FIT	63,360	1/10/99 7:46a	3053909B.
3053924B FIT	63,360	1/10/99 7:46a	3053924B.
3053939B FIT	63,360	1/10/99 7:46a	3053939B.
3054001B FIT	63,360	1/10/99 7:46a	3054001B.
3054011B FIT	63,360	1/10/99 7:46a	3054011B.
3054026B FIT	63,360	1/10/99 7:46a	3054026B.
3054028B FIT	63,360	1/10/99 7:46a	3054028B.
3054100B FIT	63,360	1/10/99 7:46a	3054100B.
3054108B FIT	63,360	1/10/99 7:46a	3054108B.
3054123B FIT	63,360	1/10/99 7:46a	3054123B.
3054137B FIT	63,360	1/10/99 7:46a	3054137B.
3054159B FIT	63,360	1/10/99 7:46a	3054159B.
3054207B FIT	63,360	1/10/99 7:46a	3054207B.
3054222B FIT	63,360	1/10/99 7:46a	3054222B.
3054237B FIT	63,360	1/10/99 7:46a	3054237B.
3054258B FIT	63,360	1/10/99 7:46a	3054258B.
3054306B FIT	63,360	1/10/99 7:46a	3054306B.
3054321B FIT	63,360	1/10/99 7:46a	3054321B.
3054336B FIT	63,360	1/10/99 7:46a	3054336B.
3054358B FIT	63,360	1/10/99 7:46a	3054358B.
3054405B FIT	63,360	1/10/99 7:46a	3054405B.
3054420B FIT	63,360	1/10/99 7:46a	3054420B.
3054435B FIT	63,360	1/10/99 7:46a	3054435B.
3054457B FIT	63,360	1/10/99 7:46a	3054457B.
3054507B FIT	63,360	1/10/99 7:46a	3054507B.
3054522B FIT	63,360	1/10/99 7:46a	3054522B.
3054534B FIT	63,360	1/10/99 7:46a	3054534B.
3054556B FIT	63,360	1/10/99 7:46a	3054556B.
3054604B FIT	63,360	1/10/99 7:46a	3054604B.
3054618B FIT	63,360	1/10/99 7:46a	3054618B.
3054633B FIT	63,360	1/10/99 7:46a	3054633B.
3054656B FIT	63,360	1/10/99 7:46a	3054656B.
3054703B FIT	63,360	1/10/99 7:46a	3054703B.
3054718B FIT	63,360	1/10/99 7:46a	3054718B.
3054733B FIT	63,360	1/10/99 7:46a	3054733B.
3054756B FIT	63,360	1/10/99 7:46a	3054756B.
3054802B FIT	63,360	1/10/99 7:46a	3054802B.
3054817B FIT	63,360	1/10/99 7:46a	3054817B.
3054832B FIT	63,360	1/10/99 7:46a	3054832B.
3054856B FIT	63,360	1/10/99 7:46a	3054856B.
3054901B FIT	63,360	1/10/99 7:46a	3054901B.
3054916B FIT	63,360	1/10/99 7:46a	3054916B.
3054931B FIT	63,360	1/10/99 7:46a	3054931B.
3054956B FIT	63,360	1/10/99 7:46a	3054956B.
3055003B FIT	63,360	1/10/99 7:46a	3055003B.
3055018B FIT	63,360	1/10/99 7:46a	3055018B.
3055030B FIT	63,360	1/10/99 7:46a	3055030B.
3055056B FIT	63,360	1/10/99 7:46a	3055056B.
3055100B FIT	63,360	1/10/99 7:46a	3055100B.

3055115B FIT	63,360	1/10/99 7:46a	3055115B.
3055129B FIT	63,360	1/10/99 7:46a	3055129B.
3055156B FIT	63,360	1/10/99 7:46a	3055156B.
3055159B FIT	63,360	1/10/99 7:46a	3055159B.
3055214B FIT	63,360	1/10/99 7:46a	3055214B.
3055229B FIT	63,360	1/10/99 7:46a	3055229B.
3055256B FIT	63,360	1/10/99 7:46a	3055256B.
3055258B FIT	63,360	1/10/99 7:46a	3055258B.
3055313B FIT	63,360	1/10/99 7:46a	3055313B.
3055328B FIT	63,360	1/10/99 7:46a	3055328B.
3055356B FIT	63,360	1/10/99 7:46a	3055356B.
3055358B FIT	63,360	1/10/99 7:46a	3055358B.
3055413B FIT	63,360	1/10/99 7:46a	3055413B.
3055428B FIT	63,360	1/10/99 7:46a	3055428B.
3055456B FIT	63,360	1/10/99 7:46a	3055456B.
3055500B FIT	63,360	1/10/99 7:46a	3055500B.
3055514B FIT	63,360	1/10/99 7:46a	3055514B.
3055527B FIT	63,360	1/10/99 7:46a	3055527B.
3055541B FIT	63,360	1/10/99 7:46a	3055541B.
3055603B FIT	63,360	1/10/99 7:46a	3055603B.
3055611B FIT	63,360	1/10/99 7:46a	3055611B.
3055625B FIT	63,360	1/10/99 7:46a	3055625B.
3055640B FIT	63,360	1/10/99 7:46a	3055640B.
3055702B FIT	63,360	1/10/99 7:46a	3055702B.
3055710B FIT	63,360	1/10/99 7:46a	3055710B.
3055725B FIT	63,360	1/10/99 7:46a	3055725B.
3055740B FIT	63,360	1/10/99 7:46a	3055740B.
3055801B FIT	63,360	1/10/99 7:46a	3055801B.
3055809B FIT	63,360	1/10/99 7:46a	3055809B.
3055824B FIT	63,360	1/10/99 7:46a	3055824B.
3055839B FIT	63,360	1/10/99 7:46a	3055839B.
3055901B FIT	63,360	1/10/99 7:46a	3055901B.
3055908B FIT	63,360	1/10/99 7:46a	3055908B.
3055923B FIT	63,360	1/10/99 7:46a	3055923B.
3055938B FIT	63,360	1/10/99 7:46a	3055938B.
3060002B FIT	63,360	1/10/99 7:46a	3060002B.
3060010B FIT	63,360	1/10/99 7:47a	3060010B.
3060022B FIT	63,360	1/10/99 7:47a	3060022B.
3060037B FIT	63,360	1/10/99 7:47a	3060037B.
3060059B FIT	63,360	1/10/99 7:47a	3060059B.
3060107B FIT	63,360	1/10/99 7:47a	3060107B.
3060122B FIT	63,360	1/10/99 7:47a	3060122B.
3060136B FIT	63,360	1/10/99 7:47a	3060136B.
3060158B FIT	63,360	1/10/99 7:47a	3060158B.
3060206B FIT	63,360	1/10/99 7:47a	3060206B.
3060221B FIT	63,360	1/10/99 7:47a	3060221B.
3060236B FIT	63,360	1/10/99 7:47a	3060236B.
3060258B FIT	63,360	1/10/99 7:47a	3060258B.
3060305B FIT	63,360	1/10/99 7:47a	3060305B.
3060320B FIT	63,360	1/10/99 7:47a	3060320B.
3060335B FIT	63,360	1/10/99 7:47a	3060335B.
3060357B FIT	63,360	1/10/99 7:47a	3060357B.
3060405B FIT	63,360	1/10/99 7:47a	3060405B.
3060419B FIT	63,360	1/10/99 7:47a	3060419B.
3060434B FIT	63,360	1/10/99 7:47a	3060434B.
3060458B FIT	63,360	1/10/99 7:47a	3060458B.
3060506B FIT	63,360	1/10/99 7:47a	3060506B.
3060518B FIT	63,360	1/10/99 7:47a	3060518B.
3060533B FIT	63,360	1/10/99 7:47a	3060533B.
3060556B FIT	63,360	1/10/99 7:47a	3060556B.
3060603B FIT	63,360	1/10/99 7:47a	3060603B.
3060618B FIT	63,360	1/10/99 7:47a	3060618B.

125 file(s) 7,920,000 bytes
0 dir(s) 508,788,736 bytes free

Geometric Parameters

Makeset List for set 3d0539

Xeas		MET	L	MET D	H	M	S	HV on Exp	HV	AZ	EL	AZ pot	EL pot	Sun	Orbiter Olong	Olat	Oalt	OSZA	OSHt	Oltime	LOSt	LOSp	LOS_AZ	Target Point Parameters Tlong	Tlat	Talt	TSHt	Tmg	TSZA	TSHt	CF	A/	Bs	SatBot	SatTop	Pixel Data Sine	Cosine	LOSheta
37.633	44.333	3053732	B	3	5	37	38	11.5	12	1	-65	22	-65	22	8	1	353.5	-23	300.2	120	113	19.787	73.85	329.64	473.43	10.7	-28.5	38.2	13.8	1857	135	-39.1	6	1	0	3 410	67 421	43 709	41 235	44 000
37.833	44.533	3053744	B	3	5	37	50	12	14.8	1	-65	22	-65	22	8	1	354	-23.0	300.3	121	114	19.803	73.83	329.7	473.29	10.9	-29.1	38	13.6	1858	136	-39.6	6	1	0	3 207	67 253	44 213	41 766	45 160
38.083	44.783	3053759	B	3	5	38	5	12	14.6	1	-65	22	-65	22	8	1	354.5	-24.4	300.5	121	114	19.867	73.88	329.78	473.08	11.6	-29.9	39.5	13.5	1854	136	-40.1	6	1	0	4 886	66 334	42 112	39 418	42 260
38.317	45.017	3053823	B	3	5	38	19	12	14.6	1	-65	22	-65	22	8	1	355.1	-25.2	300.6	122	115	19.906	73.97	329.86	472.92	12.2	-30.5	42.8	13.4	1843	137	-40.2	6	1	0	6 596	71 208	38 402	33 642	37 040
38.567	45.267	3053838	B	3	5	38	34	12	14.6	1	-65	22	-65	22	8	1	355.7	-26	300.8	123	115	19.952	73.95	329.9	472.67	13	-31.2	42.3	13.5	1846	138	-40.9	6	1	0	7 647	70 819	37 928	34 843	38 200
38.800	45.500	3053842	B	3	5	38	48	12	14.6	1	-65	22	-65	22	8	1	356.2	-26.7	301	123	116	19.992	74.08	329.97	472.47	13.6	-31.8	46.8	13.5	1830	138	-40.9	6	1	0	12 716	75 341	29 817	27 082	30 660
39.050	45.750	3053857	B	3	5	39	3	12	14.6	1	-65	22	-65	22	8	1	356.9	-27.5	301.2	124	117	20.038	74.06	330	472.19	14.4	-32.5	46	13.6	1834	138	-41.6	6	1	0	11 471	74 689	31 658	28 887	31 820
39.300	46.000	3053923	B	3	5	39	18	12	14.6	1	-65	22	-65	22	8	1	357.5	-28.3	301.4	125	117	20.088	74.12	330.05	471.9	15.1	-33.2	46.3	13.6	1828	139	-41.9	6	1	0	14 100	77 042	27 491	25 049	28 340
39.533	46.233	3053926	B	3	5	39	32	12	14.6	1	-65	22	-65	22	8	1	358.1	-29	301.5	125	118	20.128	74.24	330.1	471.65	15.7	-33.7	52.2	13.6	1813	139	-42	6	1	0	18 114	80 608	20 755	18 083	21 380
39.783	46.483	3053941	B	3	5	39	47	12	14.6	1	-65	22	-65	22	8	1	358.8	-29.8	301.7	126	118	20.176	74.21	330.12	471.32	16.6	-34.4	51.4	13.7	1818	140	-42.6	6	1	0	17 182	80 232	22 278	19 608	23 120
40.017	46.717	3053955	B	3	5	40	1	12	14.6	1	-65	22	-65	22	8	1	359.4	-30.5	301.9	128	119	20.219	74.35	330.17	471.05	17.2	-35	56.1	13.7	1800	140	-42.6	6	1	0	22 174	84 668	13 982	11 600	15 400
40.267	46.967	3054023	B	3	5	40	16	12	14.6	1	-65	22	-65	22	8	1	0	-31.3	302.1	127	-19	20.269	74.31	330.18	470.67	18.1	-35.6	54.8	13.7	1805	141	-43.2	6	1	0	20 891	83 559	18 537	14 368	17 120
40.517	47.217	3054025	B	3	5	40	31	12	14.6	1	-65	22	-65	22	8	1	0.7	-32.1	302.3	127	-20	20.32	74.37	330.22	470.32	19	-36.3	57	13.6	1798	141	-43.5	6	1	0	22 947	85 818	12 893	10 647	13 840
40.750	47.450	3054039	B	3	5	40	45	12	14.6	1	-65	22	-65	22	8	1	1.4	-32.8	302.5	128	-21	20.365	74.5	330.26	469.99	19.6	-36.8	61.1	13.8	1784	141	-43.5	6	1	0	27 301	89 683	5 638	3 378	6 300
41.000	47.700	3054054	B	3	5	41	0	12	14.6	1	-65	22	-65	22	8	1	2.1	-33.5	302.7	128	-21	20.418	74.46	330.27	469.57	20.6	-37.5	60.1	13.9	1788	142	-44.1	6	1	0	28 091	89 057	7 673	5 604	8 620
41.250	47.950	3054109	B	3	5	41	15	12	14.6	1	-65	22	-65	22	8	1	2.8	-34.3	302.9	129	-22	20.468	74.56	330.31	469.19	21.4	-38	63.2	13.9	1777	142	-44.2	6	1	0	29 543	92 121	1 969	0 172	2 820
41.483	48.183	3054131	B	3	5	41	29	12	14.6	1	-65	22	-65	22	8	1	3.5	-35	303.1	130	-22	20.519	74.57	330.31	468.76	22.3	-38.6	63.7	14	1776	143	-44.6	6	1	0	29 810	92 794	1 425	-0 404	2 240
41.733	48.433	3054136	B	3	5	41	44	12	14.6	1	-65	22	-65	22	8	1	4.3	-35.7	303.3	130	-23	20.574	74.64	330.34	468.31	23.1	-39.2	66	14	1769	143	-44.8	6	1	0	32 070	94 808	-2 213	-4 363	-1 820
41.967	48.667	3054152	B	3	5	41	58	12	14.6	1	-65	22	-65	22	8	1	4.9	-36.4	303.5	131	-23	20.624	74.77	330.36	467.88	23.9	-39.7	70.2	14	1754	143	-44.8	6	1	0	36 650	96 854	9 975	+11 939	9 180
42.200	48.900	3054210	B	3	5	42	12	21	12	1	-65	22	-65	22	8	1	5.7	-37.1	303.7	131	-24	20.678	74.78	330.36	467.41	24.8	-40.2	70.7	14.1	1752	144	-45	6	1	0	37 206	96 773	-11 033	-12 592	-9 940
42.500	49.200	3054231	B	3	5	42	30	11.5	12	1	-65	22	-65	22	8	1	6.7	-38	303.9	132	-24	20.747	74.8	330.38	466.78	26	-40.9	71.6	14.2	1749	144	-45.4	6	1	0	38 051	100 945	-12 606	-13 867	-11 100
42.700	49.400	3054236	B	3	5	42	42	12	14.6	1	-65	22	-65	22	8	1	7.3	-38.5	304.1	132	-25	20.792	74.82	330.35	466.36	26.8	-41.3	72.1	14.3	1748	144	-45	6	1	0	38 317	101 608	-13 148	-14 461	-12 260
42.950	49.650	3054251	B	3	5	42	57	12	14.6	1	-65	22	-65	22	8	1	8.1	-39.3	304.2	132	-25	20.853	74.89	330.36	465.79	27.8	-41.8	74.3	14.3	1740	145	-45.6	6	1	0	40 731	103 734	-17 283	-18 464	-16 120
43.200	49.900	3054306	B	3	5	43	12	12	14.6	1	-65	22	-65	22	8	1	8.9	-39.9	304.4	133	-26	20.911	74.95	330.35	465.22	28.7	-42.3	76.4	14.4	1733	145	-45.9	6	1	0	42 713	105 991	-20 915	-22 116	-19 600
43.433	50.133	3054328	B	3	5	43	26	12	14.6	1	-65	22	-65	22	8	1	9.8	-40.6	304.6	133	-26	20.97	74.97	330.33	464.63	29.7	-42.8	77	14.5	1731	145	-46.2	6	1	0	43 275	106 899	-21 971	-22 960	-20 960
43.683	50.383	3054335	B	3	5	43	41	12	14.6	1	-65	22	-65	22	8	1	10.7	-41.3	304.8	134	-26	21.035	75.04	330.33	464	30.8	-43.3	79.3	14.5	1723	145	-46.2	6	1	0	45 772	108 013	-26 116	-26 968	-25 020
43.917	50.617	3054349	B	3	5	43	55	12	14.6	1	-65	22	-65	22	8	1	11.5	-41.9	305	134	-27	21.092	75.17	330.33	463.45	31.6	-43.7	83.3	14.5	1709	145	-46.3	6	1	0	49 942	112 698	-33 345	-34 328	-32 560
44.167	50.867	3054404	B	3	5	44	10	12	14.6	1	-65	22	-65	22	8	1	12.4	-42.6	305.2	135	-27	21.159	75.12	330.29	462.71	32.8	-44.2	82	14.7	1714	146	-46.5	6	1	0	48 296	112 055	-30 800	-31 485	-29 660
44.417	51.117	3054418	B	3	5	44	25	12	14.6	1	-65	22	-65	22	8	1	13.3	-43.3	305.3	135	-28	21.224	75.19	330.27	462.04	33.9	-44.8	84.2	14.8	1708	146	-46.5	6	1	0	50 443	114 328	-34 928	-35 518	-33 720
44.650	51.350	3054433	B	3	5	44	39	12	14.6	1	-65	22	-65	22	8	1	14.2	-43.9	305.5	135	-28	21.289	75.21	330.25	461.33	35	-45	84.8	14.9	1704	146	-46.7	6	1	0	50 990	115 220	-35 982	-36 319	-34 680
44.900	51.600	3054446	B	3	5	44	54	12	14.6	1	-65	22	-65	22	8	1	15.3	-44.6	305.7	136	-28	21.361	75.28	330.22	460.56	36.1	-45.5	86.9	14.9	1696	146	-46.7	6	1	0	53 455	117 363	-40 122	-40 046	-38 940
45.133	51.833	3054502	B	3	5	45	8	12	14.6	1	-65	22	-65	22	8	1	16.2	-45.1	305.8	136	-29	21.425	75.4	330.19	459.85	37	-45.8	90.5	15	1683	146	-46.6	6	1	0	56 962	120 838	-46 815	-46 987	-45 900
45.383	52.083	3054525	B	3	5	45	23	12	14.6	1	-65	22	-65	22	8	1	17.2	-45.8	306	136	-29	21.5	75.29	330.18	459.04	38.5	-46.2	87.5	15	1694	146	-46.6	6	1	0	54 104	118 375	-41 188	-40 663	-39 920
45.633	52.333	3054532	B	3	5	45	38	12	14.6	1	-65	22	-65	22	8	1	18.2	-46.4	306.2	137	-29	21.571	75.28	330.18	458.27	39.7	-46.8	87.3	14.9	1695	147	-47	6	1	0	54 254	118 144	-40 701	-39 882	-38 940
45.867	52.567	3054546	B	3	5	45	52	12	14.6	1	-65	22	-65	22	8	1	19.3	-47	306.3	137	-30	21.645	75.23	330.17	457.47	41	-46.9	85.8	14.9	1701	147	-47.2	6	1	0	52 686	118 762	-37 630	-36 760	-36 040
46.117	52.817	3054601	B	3	5	46	7	12	14.6	1	-65	22	-65	22	8	1	20.4	-47.8	306.5	137	-30	21.724	75.23	330.17	456.58	42.3	-47.3	85.9	14.9	1701	147	-47.3	6	1	0	52 872	118 969	-37 656	-36 576	-36 040
46.367	53.067	3054623	B	3	5	46	22	12	14.6	1	-65	22	-65	22	8	1	21.5	-48.1	306.6	138	-30	21.801	75.24	330.17	455.74	43.5	-47.6	86.2	14.8	1700	147	-47.3	6	1	0	53 483	117 142	-38 183	-38 975	-36 620
46.600	53.300	3054630	B	3	5	46	36	12	14.6	1	-65	22	-65	22	8	1	22.6	-48.7	306.8	138	-30	21.879	75.18	330.17	454.85	44.9	-47.9	84.6	14.8	1708	147	-47.4	6	1	0	51 935	116 878	-35 125	-33 461	-33 140
46.850	53.550	3054645	B	3	5	46	51	12	14.6	1	-65	22	-65	22	8	1	23.7	-49.2	306.9	138	-31	21.959	75.2	330.17	453.96	46.2	-48.1	85.2	14.8	1704	147	-47.4	6	1	0	52 664	116 472	-36 186	-34 460	-34 300
47.067	53.767	3054702	B	3	5	47	4	12	12	1	-65	22	-65	22	8	1	24.8	-49.7	307	138	-31	22.035	75.21	330.17	453.08	47.4	-48.4	85.4	14.8	1704	147	-47.3	6	1	0	52 767	116 575	-36 179	-34 661	-34 480
47.383	54.083	3054723	B	3	5	47	23	11.5	12	1	-65	22	-65	22	8	1	26.4	-50.4	307.2	139	-31	22.146	75.2	330.17	451.81	49.2	-48.7	85.2	14.7	1704	147	-47.3	6	1	0	53 200	116 548	-36 205	-33 698	-34 300
47.583	54.283	3054729	B	3	5	47	35	12	14.6	1	-65	22	-65	22	8	1	27.4	-50.8	307.3	139	-31	22.215	75.16	330.17	451.01	50.3	-48.8	84.1	14.7	1709	147	-47.3	6	1	0	51 868	115 461	-33 848	-31 571	-31 980
47.817	54.517	3054743	B	3	5	47	49	12	14.6	1	-65	22	-65	22	8	1	28.6	-51.3	307.4	139	-31	22.302	75.11	330.16	449.99	51.7	-49	82.4	14.7	1715	147	-47.3	6	1	0	50 288	114 084	-30 576	-28 093	-29 080
48.067	54.767	3054758	B	3	5	48	4	12	14.6	1	-65	22	-65	22	8	1	30	-51.9	307.5	139	-32	22.397	75.11	330.16	448.88	53.2	-49.2	82.5	14.7	1715	148	-47.2	6	1	0	50 391	114 187	-30 589	-28 069	-29 080
48.317	55.017	3054823	B	3	5	48	19	12	14.6	1	-65	22	-65	22	8	1	31.3	-52.2	307.6	139	-32	22.487	75.13	330.16	447.81	54.5	-49.4	83	14.7	1713	148	-47	6	1	0	51 063	114 785	-31 630	-28 879	-30 240
48.550	55.250	3054827	B	3	5	48	33	12	14.6	1	-65	22	-65	22	8	1	32.6	-52.7	307.7	139	-32	22.58	75.07	330.14	446.7	56	-49.5	81.4	14.7	1719	148	-46.9	6	1	0	49 459	113 404	-28 558	-25 604	-26 160
49.033	55.733	3054842	B	3	5	49	2	12	14.6	1	-65	22	-65	22	8	1	35.4	-53.5	307.9	139	-32	22.771	75.04	330.13	444.4	58.8	-49.7	80.2	14.7	1723	148	-46.6	6	1	0	48 525	112 618	-26 527	-22 924	-25 020
49.283	55.983	3054923	B	3	5	49	17	12	14.6	1	-65	22	-65	22	8	1	36.9	-53.9	308	139	-32	22.875	75.02	330.13	443.14	60.3	-49.7	79.6	14.7	1725	148	-46.4	6	1	0	48 058	112 224	-25 511	-21 587	-23 660
49.767	56.467	3054926	B	3	5	49	46	12	14.5	1	-65	22	-65	22	8	1	39.8	-54.6	308.1	139	-32	23.077	74.99	330.11	440.66	63.1	-49.8	78.5	14.8	1729	145	-48	6	1	0	46 765	111 530	-23 487	-18 295	-22 120
50.017	56.717	3054941	B	3	5	50	1	12	14.4	1	-65	22	-65	22	8	1	41.3	-54.9	308.2	139	-32	23.18	74.98	330.1	439.4	64.5	-49.8	78.3	14.7	1729	145	-45.7	6	1	0	47.118	111.434	-23 480	-18 728	-21 540
50.250	56.950	3054955	B	3	5	50	15	12	14.4	1	-65	22	-65	22	8	1	42.8	-55.2	308.2	139	-32	23.285	74.93	330.08	438.08	66	-49.8	76.6	14.8	1735	144	-45.5	6	1	0	45.165	110 134	-20 392	+15 483	-18 640
50.483	57.183	3055031	B	3	5	50	29	12	14.4	1	-65	22	-65	22	8	1	44.3	-55.6	308.2	139	-32	23.391	74.99	330.07	436.77	67.3	-49.8	78.6	14.8	1728	144	-45	6	1	0	47.176	111.883	-23 994	-18 301	-22 120
50.967	57.667	3055038	B	3	5	50	58	12	14.4	1	-65	22	-65	22	8	1	47.5	-56	308.3	139	-32	23.609	74.95	330.05	434.06	70.2	-49.6	77.1	14.8	1733	143	-44.9	6	1	0	45 844	110 738	-21 435	-16 262	-19 600
51.217	57.917	3055053	B	3	5	51	13	12	14.4	1	-65	22	-65	22	8	1	49	-56.2	308.3	139	-32	23.719	74.95	330.04	432.65	71.5	-49.5	77	14.8	1733	143	-44.2	6	1	0	45 844	110 738	-21.435	-16 062	-19 600

Geometric Parameters

NOTES:

Makeset List for set 360535

Xsec	MET	L	D	H	M	S	HV on Exp	HV	AZ	EL	AZ pot	EL pot	Sum	Orbital Glong	Glat	Glat	OSZA	OSIII	Glimb	LOSt	LOSp	LOS_AZ	Target Point Parameters Tlong	Tlat	Talt	Tilt	Ting	TSZA	TSIII	CF	A/	Bs	0.000 SatBot	0.000 Sat Top	Fixed Data Skew	Coplan	LOSdelta
35 617	3053530	B	3	5	36	37	11 5	12	1	65	22 2	65	22.2	8	1	349	-16 4	298 9	115	-8	19 459	75 07	208 8	354.24	347 6	41 5	72	12 8	1719	110	-11 5	6	1	0	44 676	100 505	-27 893	-23 874	-28 700
35 817	3053556	B	3	5	36	49	12	14 7	1	65	22 2	65	22 2	8	1	349 5	-17	299	115	-8	19.492	75.13	208.73	354 03	348	-2 3	78 6	12 8	1713	111	-12	6	1	0	46 475	102 108	-30 406	-26 773	-30 240
36 050	3053597	B	3	5	36	3	12	15	1	65	22 2	65	22.2	8	1	350	+17 8	299 1	116	+9	19.577	75 08	208 65	353 6	348.4	-3	72 2	12 8	1719	111	-12 8	6	1	0	44 883	100 712	-27 419	-23 867	-27 340
36 300	3053612	B	3	5	36	18	12	14.7	1	66	22 2	65	22 2	8	1	350.5	+18 6	299 3	117	+9	19.568	75 2	208 55	353 5	348.9	-3 9	75 7	12 7	1705	112	-13 3	6	1	0	49 283	104 211	-34 654	+30 277	-34 300
36 550	3053626	B	3	5	36	33	12	14 7	1	66	22 2	65	22 2	8	1	351.1	+19.5	299 5	117	-10	19 61	75 15	208 48	353 20	349.4	-4.7	74 2	12 7	1711	113	-14 2	6	1	0	47 783	102 925	-31 582	+28 969	-31 400
36 800	3053641	B	3	5	36	48	12	15	1	65	22 2	65	22 2	8	1	351 8	+20.3	299 8	118	-11	19 649	75.04	208 42	352 98	349 9	-5.4	71	12 7	1723	114	-15	6	1	0	44 495	100 024	-25 429	+20 662	-25 020
37 050	3053703	B	3	5	37	3	12	14 7	1	66	22 2	65	22 2	8	1	352.2	+21.1	299 8	119	-11	19 691	74 98	208 37	352 7	350.3	-6 2	69 2	12 8	1730	114	-15 8	6	1	0	42 483	98 670	-21 848	+16 887	-21 340
37 280	3053711	B	3	5	37	17	12	14 7	1	65	22 2	65	22 2	8	1	352.7	+21 9	299 9	119	-12	19 731	74 96	208 3	352 42	350.8	-6 9	69 2	12 9	1730	115	-16 5	6	1	0	42 356	98 976	-21 859	+16 662	-21 340
37 530	3053726	B	3	5	37	32	12	15	1	65	22 2	65	22 2	8	1	353.3	+22.8	300 1	120	-13	19 771	74 92	208 25	352 14	351.3	-7 7	67 4	12 9	1737	116	-17 3	6	1	0	40 586	97 413	-18 279	+12 854	-18 000
37 780	3053741	B	3	5	37	47	12	14.7	1	65	22 2	65	22 2	8	1	353.8	+23.5	300 3	121	-13	19 815	74 83	208 31	351 94	351.8	-8 4	64 8	12 9	1747	116	-18 2	6	1	0	37 943	95 077	-13 151	-7 181	-12 840
38 030	3053802	B	3	5	38	2	12	14.7	1	65	22 2	65	22 2	8	1	354.4	+24 2	300 4	121	-14	19.858	74 75	208 37	351 75	352.3	-9 1	62 5	12 9	1755	117	-19	6	1	0	36 689	93 135	-9 039	-3 089	-8 200
38 267	3053810	B	3	5	38	16	12	15 1	1	65	22 2	65	22 2	8	1	355	+25	300 6	122	-15	19.898	74 73	208 42	351 54	352 8	-9 9	61 7	12 9	1758	118	-19 8	6	1	0	35 038	92 572	-7 519	-1 174	-7 040
38 767	3053840	B	3	5	38	46	12	14 7	1	65	22 2	65	22 2	8	1	356 2	-26 6	301	123	-16	19 986	74 65	208 59	351.13	353 9	-11 4	59 5	13	1787	119	-21 4	6	1	0	32 605	90 874	-2 931	3 667	-2 400
39 017	3053902	B	3	5	39	1	12	15	1	65	22 2	65	22 2	8	1	356 8	-27 4	301 2	124	-17	20 033	74 74	208 64	350 87	354 4	-12 3	62 3	13 1	1757	120	-22	6	1	0	35 485	93 862	-8 117	-1 214	7 820
39 267	3053909	B	3	5	39	16	12	14 7	1	65	22 2	65	22 2	8	1	357 4	-28.2	301 4	124	-17	20.08	74 72	208.71	350 61	355	-13.1	61 8	13 1	1759	121	-22 8	6	1	0	35 112	93 556	-7 112	0 088	-6 480
39 517	3053924	B	3	5	39	31	12	14 7	1	65	22 2	65	22.2	8	1	358	-29	301 5	125	-18	20 125	74 69	208 78	350 36	355 5	-13 8	61	13 2	1762	121	-23 5	6	1	0	34 112	93 095	-5 579	1 764	-4 720
39 750	3053939	B	3	5	39	45	12	15	1	65	22 2	65	22 2	8	1	358 7	-29.7	301.7	126	-18	20.17	74.74	208 84	350 08	358 1	-14 6	62 4	13 2	1757	122	-24 1	6	1	0	35 771	94 586	-6 184	-0 497	-7 620
40 000	3054001	B	3	5	40	0	12	14 7	1	65	22 2	65	22.2	8	1	359 3	-30 5	301 9	126	-19	20.218	74 71	208 92	349 82	358 6	-15.4	61 6	13 3	1760	123	-24 9	6	1	0	34 875	94 228	-6 684	1 363	-5 660
40 238	3054011	B	3	5	40	14	2 2	12	1	65	22 2	65	22 2	8	1	360	+31 2	302 1	127	-19	20.263	74 75	208 96	349 5	357 2	-16 1	62 9	13 4	1756	124	-25 5	6	1	0	36 011	95 667	-8 754	-0 712	-8 200
40 550	3054026	B	3	5	40	33	11 5	12	1	65	22 2	65	22 2	8	1	0 8	+32 2	302 4	127	-20	20.327	74 75	209 04	349 08	357.9	-17.1	63 1	13 5	1758	124	-26 4	6	1	0	36 000	95 183	-8 785	-0 544	-8 200
40 750	3054038	B	3	5	40	45	12	14.7	1	65	22 2	65	22 2	8	1	1.4	+32.8	302 5	128	-21	20.365	74.67	209.1	348 83	358.4	-17 7	60 8	13 6	1764	125	-27 1	6	1	0	33 635	94 440	-4 683	3 939	-3 500
40 980	3054100	B	3	5	40	59	12	14.7	1	65	22 2	65	22 2	8	1	2	+33 5	302 7	128	-21	20.415	74 72	209 15	348 48	358.9	-18.5	62 3	13 6	1759	126	-27 7	6	1	0	36 297	95 930	-7 289	1 498	-6 400
41 230	3054108	B	3	5	41	14	12	15 1	1	65	22 2	65	22 2	8	1	2.7	+34 2	302 9	129	-22	20.465	74.7	209 22	348 16	359.5	-19.2	61 9	13 7	1761	126	-28 4	6	1	0	34 691	95 830	-6 285	2 605	-5 300
41 480	3054123	B	3	5	41	29	12	14.7	1	65	22 2	65	22 2	8	1	3.5	-35	303 1	130	-22	20.519	74.81	209.25	347 7	0.2	-20.1	65 5	13 7	1748	127	-28 8	6	1	0	38 647	99 356	-13 013	-3 795	-11 660
41 730	3054137	B	3	5	41	44	12	14.7	1	65	22 2	65	22 2	8	1	4.3	+35.7	303 3	130	-23	20.574	74 81	209 31	347 28	0.6	-20 9	65 7	13 8	1748	128	-29 6	6	1	0	38 643	99 766	-13 040	-3 798	-11 660
41 980	3054149	B	3	5	41	59	12	15	1	65	22 2	65	22 2	8	1	5	+36 4	303 5	131	-23	20.627	74 81	209 35	346 85	1.4	-21 8	65 5	13 9	1749	128	-30 2	6	1	0	38 330	99 922	-12 952	-3 059	-11 660
42 230	3054207	B	3	5	42	14	12	14 7	1	65	22 2	65	22 2	8	1	5.8	+37 2	303 7	131	-24	20.685	74 81	209 4	346 38	2	-22 4	65 8	14	1749	129	-30 9	6	1	0	38 306	100 333	-12 579	-3 260	-11 660
42 480	3054222	B	3	5	42	28	12	14 7	1	65	22 2	65	22 2	8	1	6.5	-37 9	303 9	132	-24	20.74	74 87	209 43	345 98	2.7	-23 1	67 8	14	1742	130	-31 4	6	1	0	40 535	102 313	-16 212	-6 665	-15 180
42 717	3054237	B	3	5	42	43	12	15	1	65	22 2	65	22 2	8	1	7.3	+38 6	304 1	132	-25	20.796	74 87	209 48	345 44	3.3	-23 8	67 8	14 1	1742	130	-32	6	1	0	40 512	102 722	-16 239	-6 301	-15 180
42 967	3054256	B	3	5	42	58	12	14 7	1	65	22 2	65	22 2	8	1	8.2	+39 3	304 3	133	-25	20.858	74 88	209 51	344 91	4	-24 6	68 4	14 2	1741	131	-32 7	6	1	0	40 777	103 384	-16 781	-7 069	-15 740
43 217	3054306	B	3	5	43	13	12	14 7	1	65	22 2	65	22 2	8	1	9	-40	304 5	133	-26	20.915	74 89	209 55	344 38	4.6	-25 3	68 8	14 3	1740	132	-33 3	6	1	0	41 042	104 044	-17 323	-7 461	-16 320
43 450	3054321	B	3	5	43	27	12	15	1	65	22 2	65	22 2	8	1	9.8	+40 7	304 6	133	-26	20.974	74 86	209 57	343 83	5.3	-26.1	71	14 4	1732	132	-33 8	6	1	0	43 217	108 359	-21 458	+11 443	-20 360
43 700	3054336	B	3	5	43	42	12	14.7	1	65	22 2	65	22 2	8	1	10.7	+41.4	304 8	134	-26	21.039	74 87	209 61	343 24	6	-26 9	71 6	14 5	1730	133	-34 4	6	1	0	43 769	107 268	-22 913	-12 215	-20 980
43 950	3054358	B	3	5	43	57	12	14.7	1	65	22 2	65	22 2	8	1	11.6	-42	305	134	-27	21.1	74.89	209 64	342 65	6.7	-27 6	72 3	14 6	1728	134	-35	6	1	0	44 320	108 172	-23 589	-13 179	-22 120
44 200	3054405	B	3	5	44	12	12	15	1	65	22 2	65	22 2	8	1	12.5	+42 7	305 2	135	-27	21.166	75.13	209 65	341 98	7.4	-28.4	73.7	14 6	1713	134	-35 4	6	1	0	48 807	112 105	-31 314	+21 211	-30 240
44 450	3054420	B	3	5	44	27	12	14.7	1	65	22 2	65	22 2	8	1	13.4	+43 3	305 4	135	-28	21.232	75 15	209 66	341 34	8.1	-28.1	77 5	14 7	1710	135	-35 9	6	1	0	49 639	113 248	-32 884	+22 376	-31 400
44 680	3054435	B	3	5	44	41	12	14.7	1	65	22 2	65	22 2	8	1	14.4	+44	305 5	135	-28	21.298	75 23	209 68	340 67	8.9	-29 9	80	14 8	1701	135	-36 3	6	1	0	52 084	115 780	-37 525	-27 004	-36 040
44 980	3054457	B	3	5	44	59	12	15	1	65	22 2	65	22 2	8	1	15.6	+44.8	305 7	136	-28	21.364	75 21	209 71	339 81	9.8	-30.7	79 5	14 9	1704	136	-37 1	6	1	0	51 187	115 427	-36 008	+25 656	-34 860
45 167	3054507	B	3	5	45	10	2 2	12	1	65	22 2	65	22 2	8	1	16 3	+45 2	305 9	136	-29	21.434	75 2	209 71	339 27	10.3	-31.2	79 4	15	1705	137	-37 5	6	1	0	50 895	115 584	-35 521	+25 101	-34 300
45 480	3054522	B	3	5	45	29	11 4	12	1	65	22 2	65	22 2	8	1	17.6	+46	306 1	137	-29	21.526	75.28	209 66	338 22	11.3	-32.1	81 9	14 9	1696	137	-38 1	6	1	0	53 869	117 797	-40 174	+29 586	-38 940
45 683	3054534	B	3	5	45	41	12	14.7	1	65	22 2	65	22 2	8	1	18.5	+46.5	306 2	137	-29	21.591	75.18	209 66	337 54	11.9	-32.6	79	14 9	1707	138	-38 7	6	1	0	50 865	115 208	-34 532	+23 774	-33 140
45 917	3054556	B	3	5	45	55	12	15	1	65	22 2	65	22 2	8	1	19.5	+47.1	306 4	137	-30	21.659	75.19	209 63	336 76	12.7	-33.2	79.7	14 8	1708	138	-39 1	6	1	0	51 581	115 464	-35 072	+24.749	-33 720
46 167	3054604	B	3	5	46	10	12	14.7	1	65	22 2	65	22 2	8	1	20 6	+47.7	306 5	137	-30	21.74	75.16	209 62	335 85	13.5	-33 8	78 8	14 8	1709	139	-39 7	6	1	0	50 834	114 830	-35 543	+22 892	-31 980
46 417	3054618	B	3	5	46	25	12	14 7	1	65	22 2	65	22 2	8	1	21 7	+48 2	306 7	138	-30	21.816	75.12	209 6	334 98	14.3	-34.4	77 8	14 8	1713	139	-40 2	6	1	0	49 605	114 051	-31 512	+20 735	-29 660
46 667	3054633	B	3	5	46	40	12	15 1	1	65	22 2	65	22 2	8	1	22 9	-48 8	306 8	138	-30	21 9	75.21	209 57	334 02	15 1	-35 2	80 6	14 7	1704	140	-40 8	6	1	0	52 786	118 173	-36 153	+25 786	-34 660
46 917	3054656	B	3	5	46	55	12	14.7	1	65	22 2	65	22 2	8	1	24 1	-49 4	306 9	138	-31	21.988	75.16	209 57	333 05	16	-35 8	79 5	14 7	1709	140	-41 2	6	1	0	51 474	115 047	-33 595	+23 435	-31 980
47.150	3054703	B	3	5	47	9	12	14.7	1	65	22 2	65	22 2	8	1	25 2	-49 9	307 1	138	-31	22.063	75.08	209 57	332 18	16 8	-36 3	77 1	14 7	1718	141	-41 7	6	1	0	49 123	113 031	-28 983	+18 454	-27 340
47 400	3054718	B	3	5	47	24	12	15	1	65	22 2	65	22 2	8	1	26 6	-50 4	307 2	139	-31	22.152	75.17	209 54	331 11	17 7	-37	80	14 6	1708	141	-42	6	1	0	52 284	115 407	-34 149	+23 889	-32 480
47 650	3054733	B	3	5	47	39	12	14.7	1	65	22 2	65	22 2	8	1	27.7	-50 9	307 3	139	-31	22.236	75.14	209 64	330 12	18 5	-37 6	78 3	14 6	1711	142	-42 5	6	1	0	51 547	114 771	-32 819	+22 308	-30 820
47 900	3054756	B	3	5	47	54	12	14.7	1	65	22 2	65	22 2	8	1	29 1	-51 4	307 4	139	-31	22.331	75 13	209 53	329 02	19 5	-38 2	79	14 6	1713	142	-43	6	1	0	51 063	114 361	-31 804	+21 547	-30 240
48.150	3054802	B	3	5	48	9	12	15	1	65	22 2	65	22 2	8	1	30 4	+51 9	307 5	139	-32	22.427	75.11	209 52	327 89	20 5	-38 8	78 8	14 8	1715	142	-43 4	6	1	0	50 618	113 940	-30 589	+20 595	-29 060
48 400	3054817	B	3	5	48	24	12	14 7	1	65	22 2	65	22 2	8	1	31 7	+52 4	307 6	139	-32	22.518	75.1	209 52	326 6	21 4	-39 3	78 4	14 8	1716	143	-43 8	6	1	0	50 437	113 846	-30 088	+20 027	-29 300
48 638	3054832	B	3	5	48	38	12	14 7	1	65	22 2	65	22 2	8	1	33 1	+52 8	307 7	139	-32	22 611	75.13	209 5	325 68	22 3	-39 9	79 4	14 8	1713	143	-44	6	1	0	51 381	114 691	-31 644	+21 759	-30 240
48.888	3054846	B	3	5	48	53	12	15	1	65	22.2	65	22 2	8	1	34.5	+53.2	307.8	139	-32	22.713	75.12	209 5	324.47	23.3	-40.4	79 2	14.8	1714	144	-44.5	6	1	0	51 213	114 547	-31 143	+21.190	-29 660

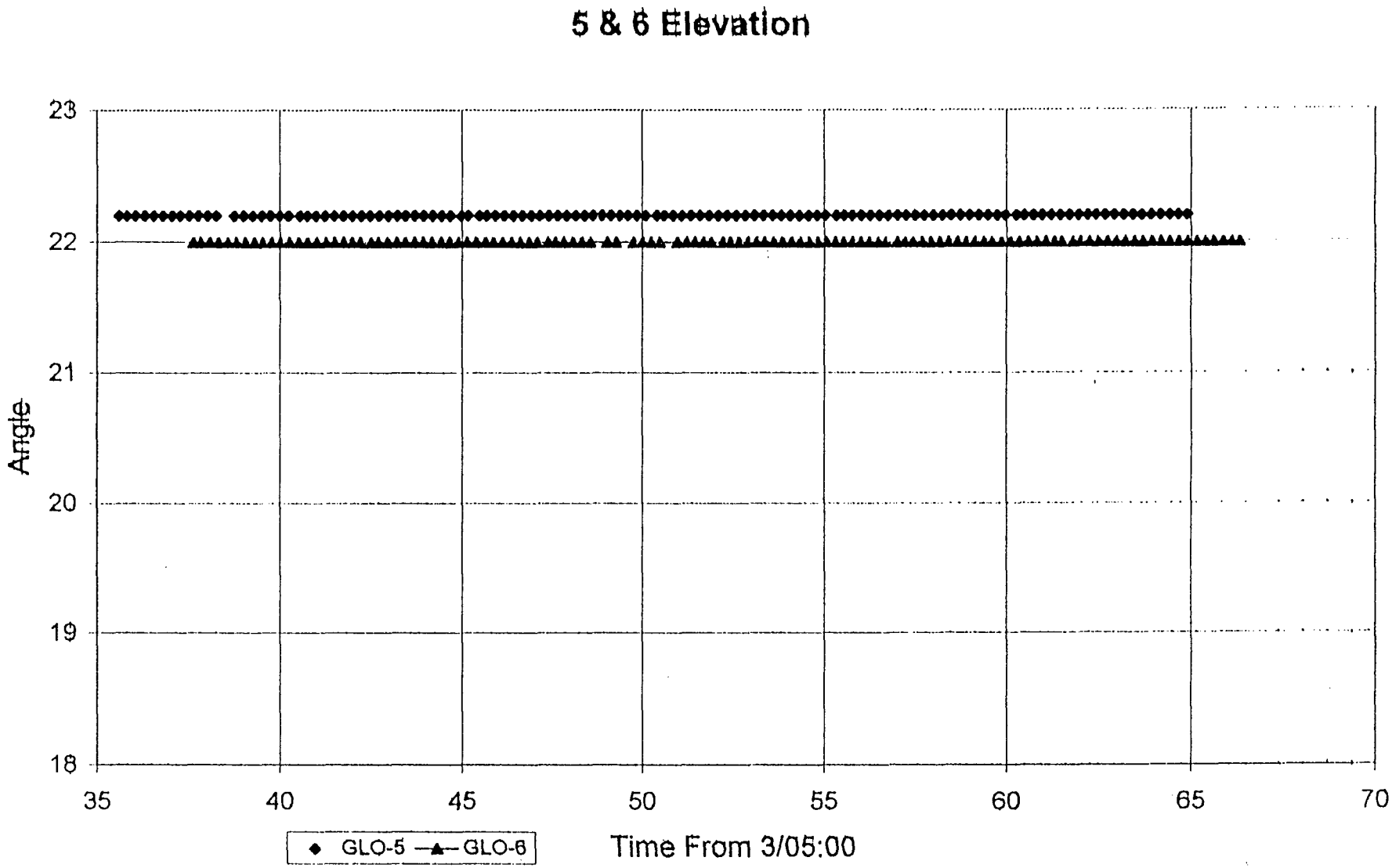
5 & 6 Elevation
23
22
21
20
19
18
Angle
35
40
45
50
55
60
65
70
GLO-5
GLO-6
Time From 3/05:00

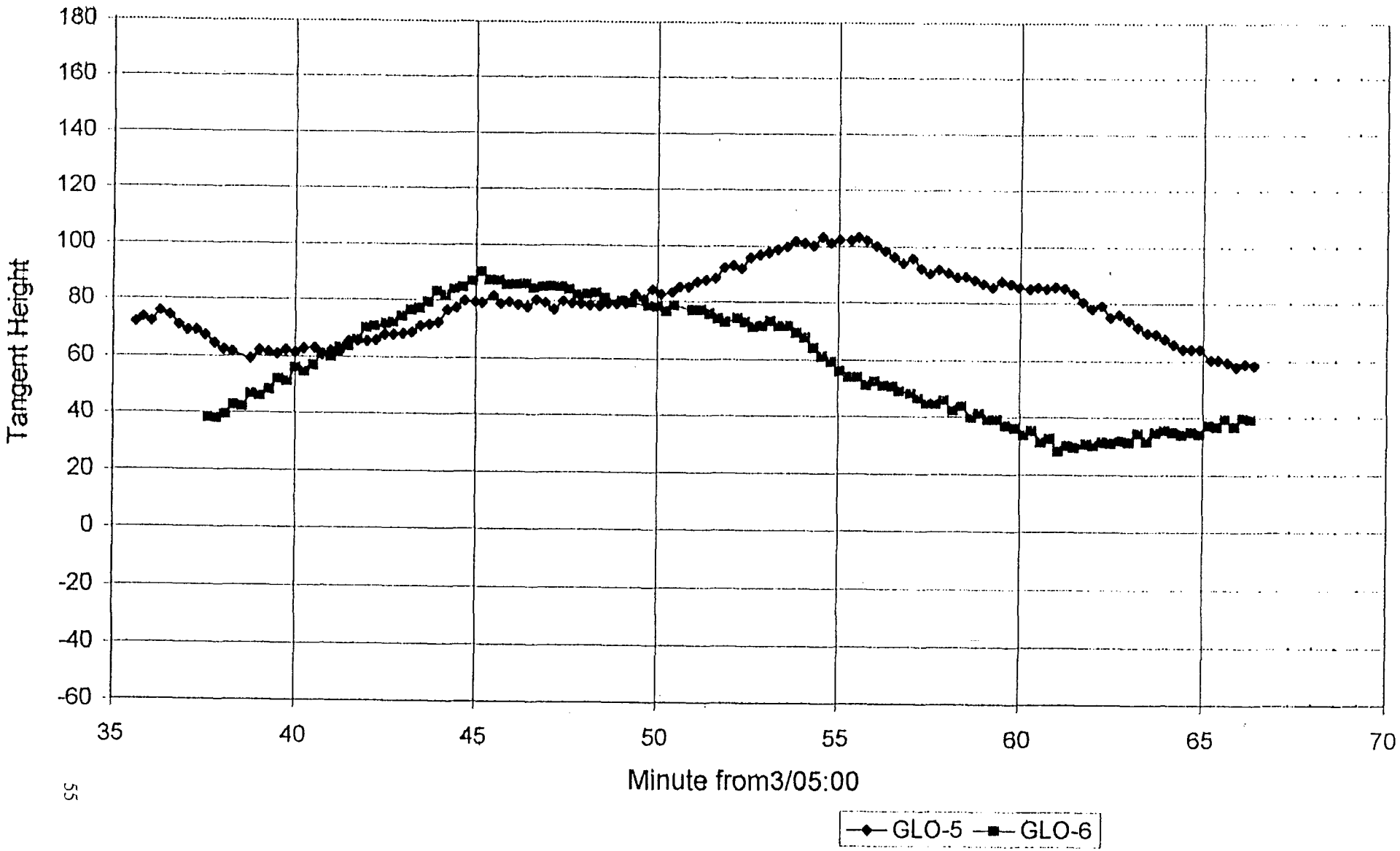
Geometric Data; Set 3d_e0535
Tangent Height
180
160
140
120
100
80
60
40
20
0
-20
-40
-60
35
40
45
50
55
60
65
70
Minute from3/05:00
GLO-5
GLO-6

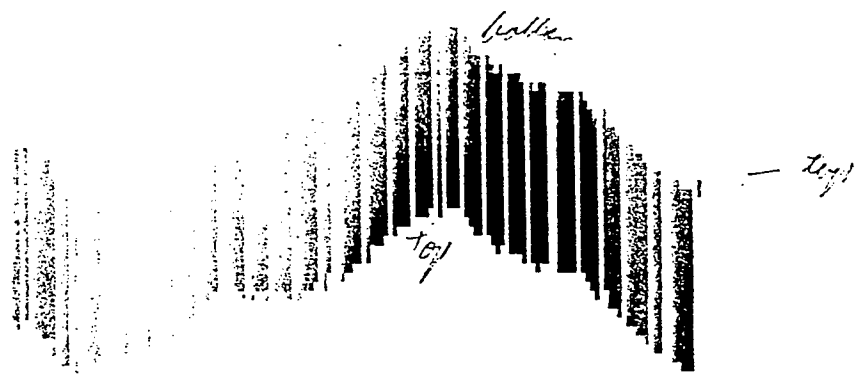

I5 (lst -1) (3D0535): (-10000)-(90000)

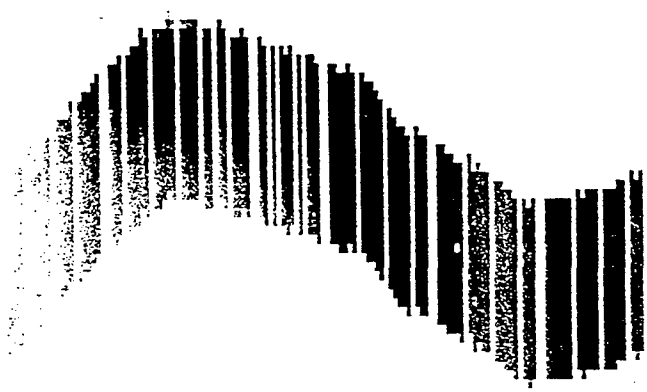

I6 (lst -1) (3E0535): (-10000)-(90000)

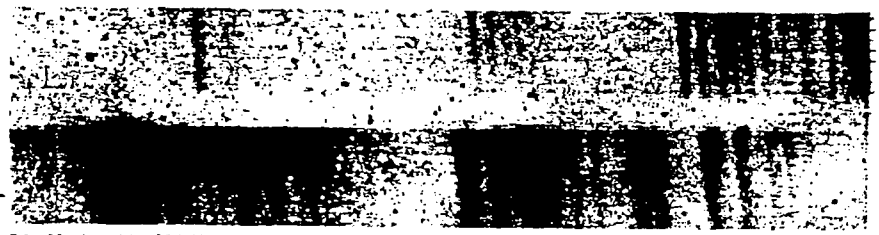

I4 (lst -1) (3055400B): (367)-(786)

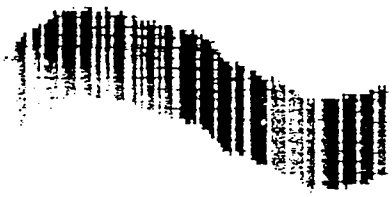

I2 (lst -1) (02_0_0HY): (0)-(80000)

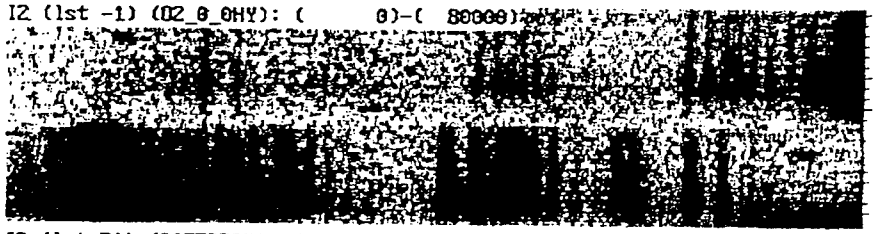

I3 (lst 71) (3055358B): (235)-(388)

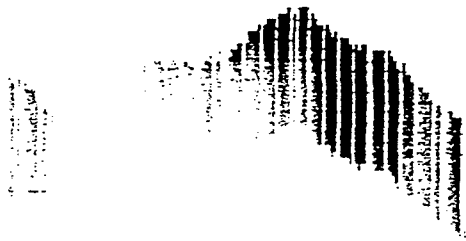

I1 (lst -1) (02_0_0HY): (0)-(80000)

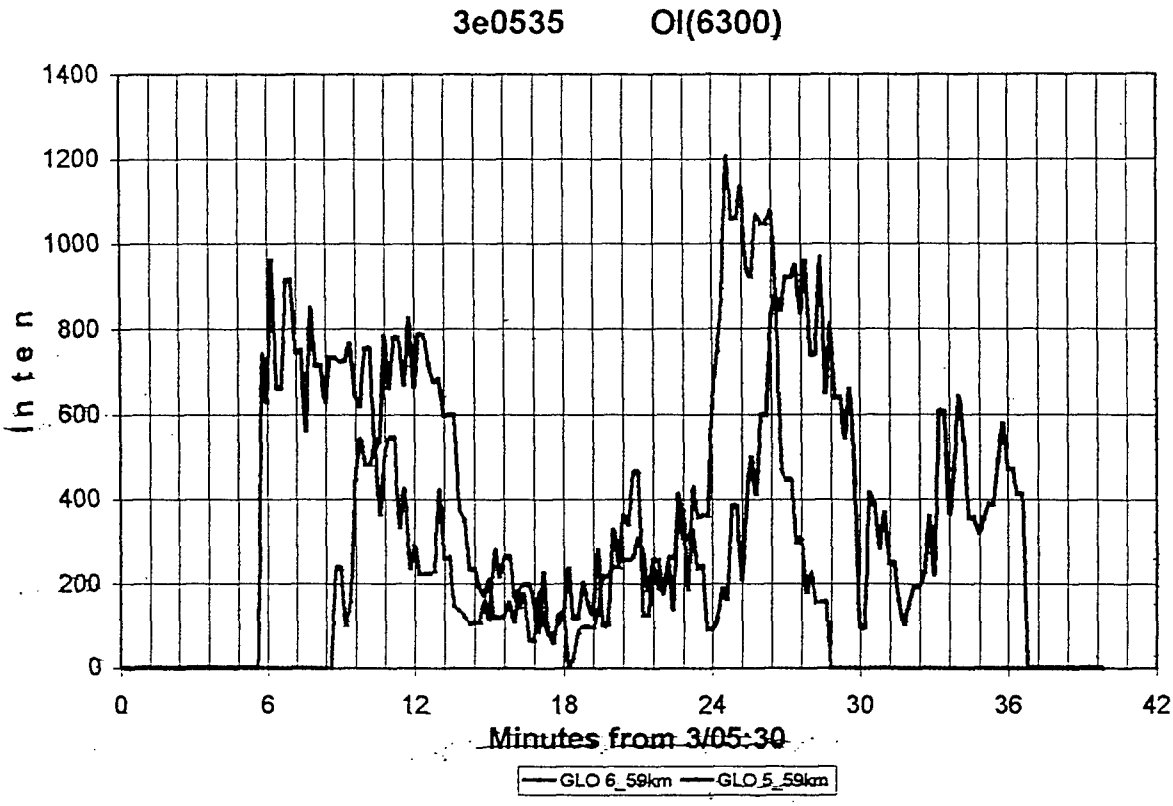
3e0535 OI(6300)
1400
1200
1000
800
600
400
200
0
Inten
0
6
12
18
24
30
36
42
Minutes from 3/05:30
GLO 6_59km
GLO 5_59km

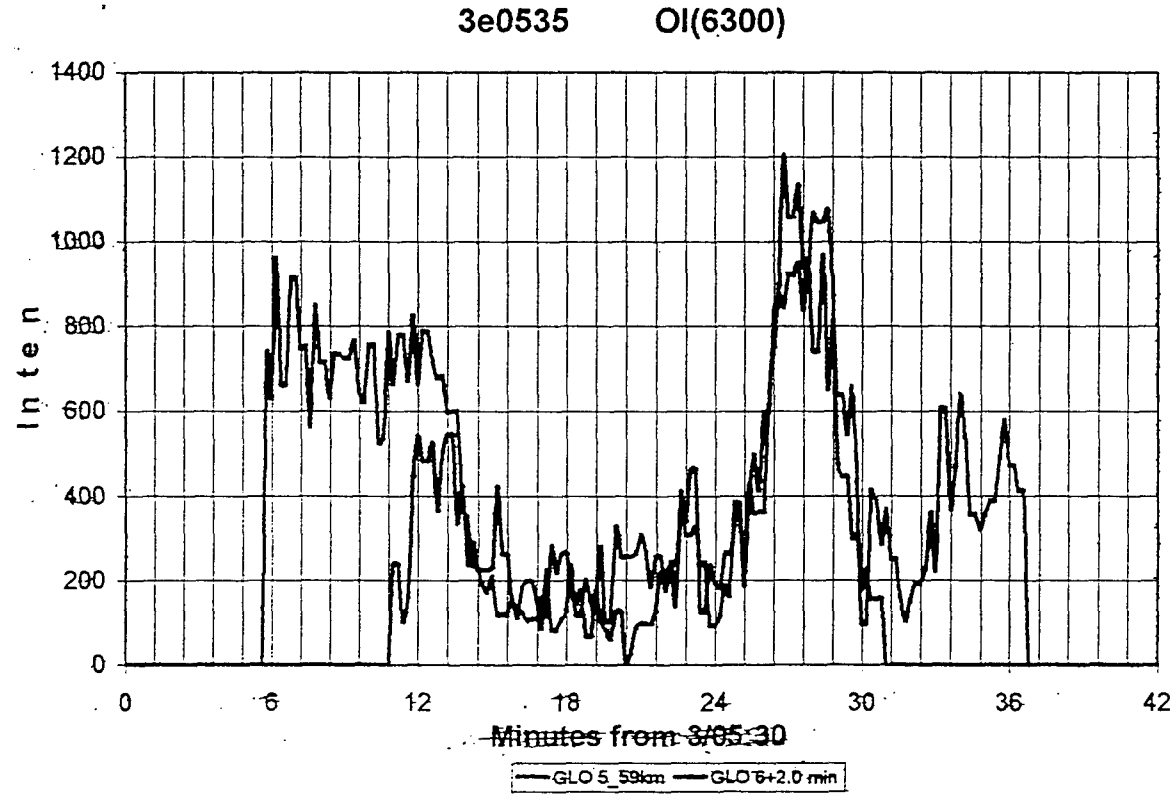
3e0535 OI(6300)
1400
1200
1000
800
600
400
200
0
Inten
0
6
12
18
24
30
36
42
Minutes from 3/05:30
GLO 5_59km
GLO 6+2.0 min

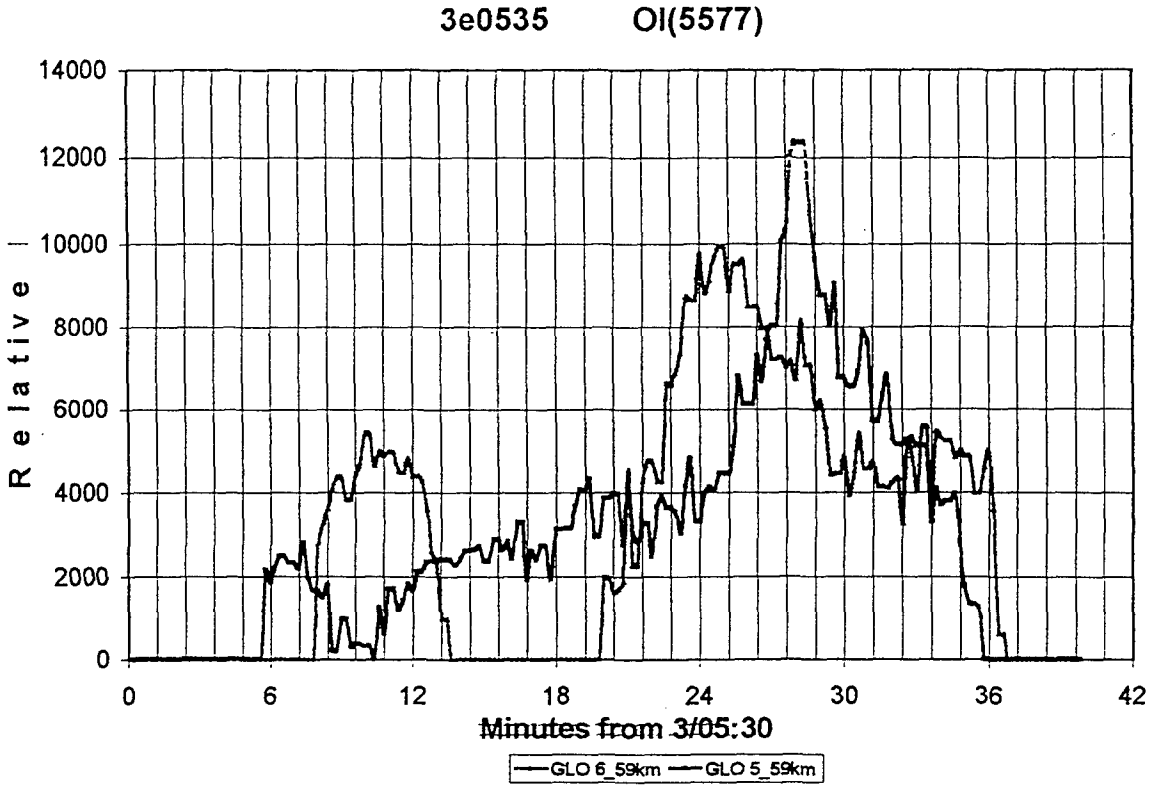
3e0535 OI(5577)
Relative I
14000
12000
10000
8000
6000
4000
2000
0
0
6
12
18
24
30
36
42
Minutes from 3/05:30
GLO 6_59km
GLO 5_59km

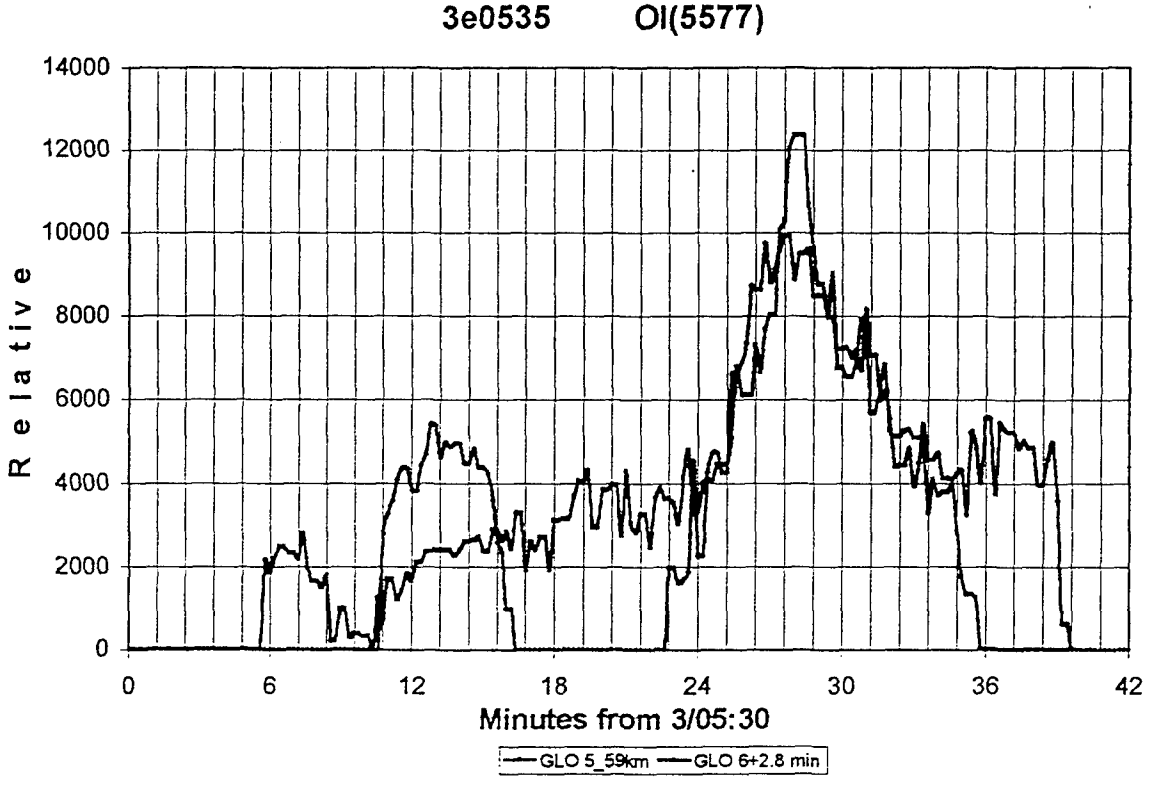
3e0535 OI(5577)
Relative
14000
12000
10000
8000
6000
4000
2000
0
0
6
12
18
24
30
36
42
Minutes from 3/05:30
GLO 5_59km
GLO 6+2.8 min

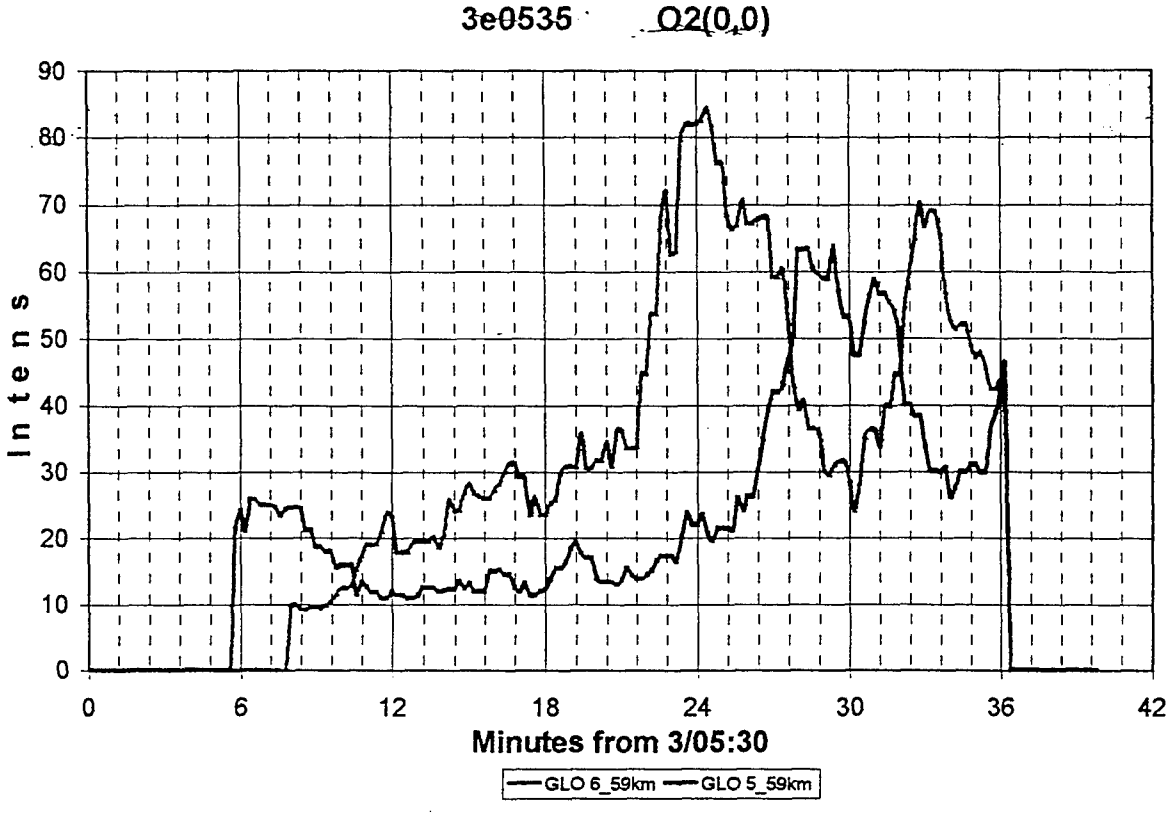
3e0535 O2(0,0)
Intens
Minutes from 3/05:30
GLO 6_59km
GLO 5_59km

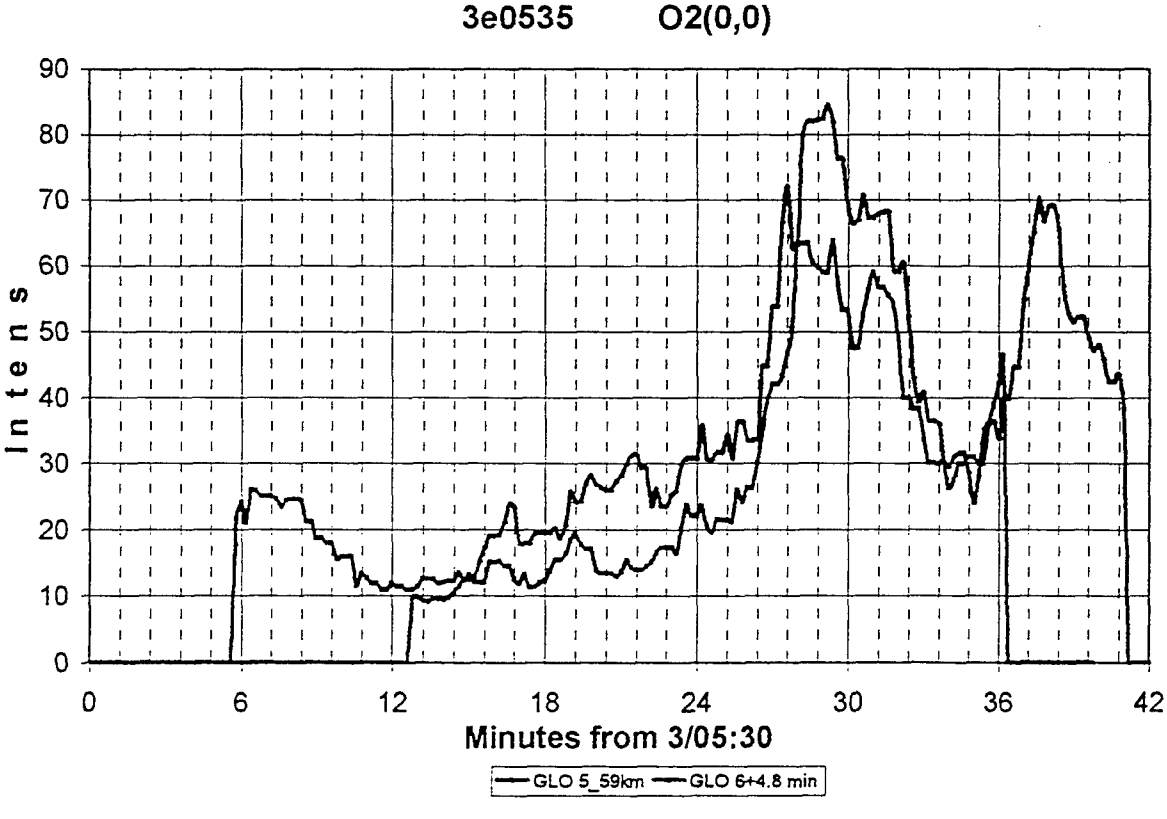
3e0535 O2(0,0)
Intens
Minutes from 3/05:30
GLO 5_59km
GLO 6+4.8 min

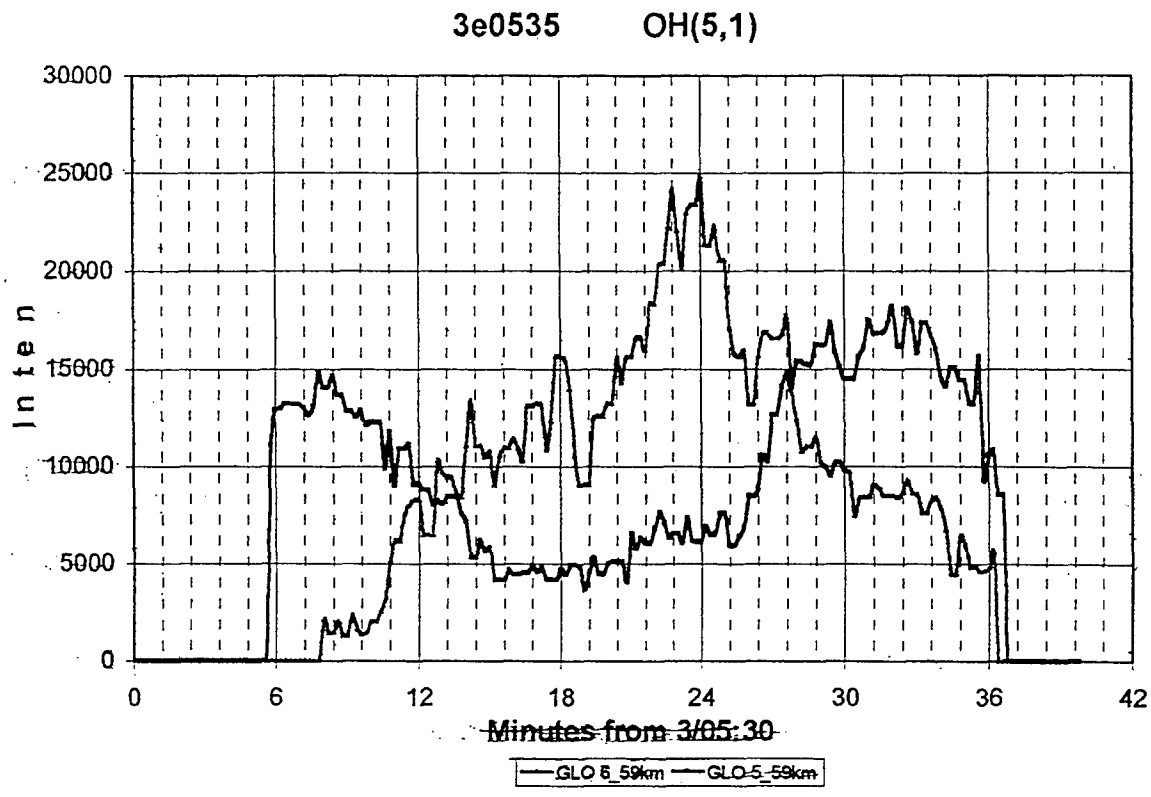
3e0535 OH(5,1)
30000
25000
20000
15000
10000
5000
0
Inten
0
6
12
18
24
30
36
42
Minutes from 3/05:30
GLO 6_59km
GLO 5_59km

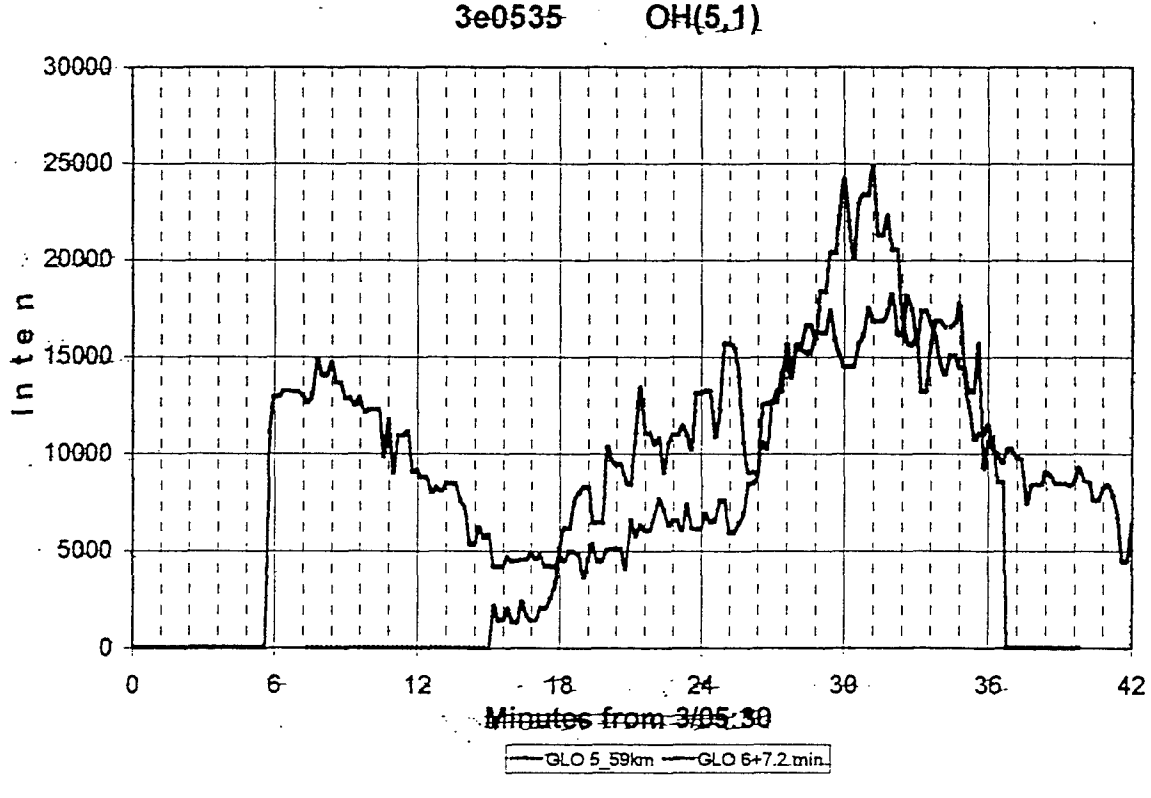
3e0535 OH(5,1)
30000
25000
20000
15000
10000
5000
0
Inten
0
6
12
18
24
30
36
42
Minutes from 3/05:30
GLO 5_59km
GLO 6+7.2 min

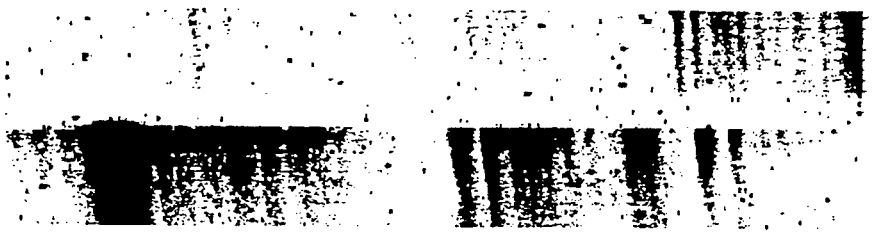

I4 (lst -1) (3055400B): (367)-(786)

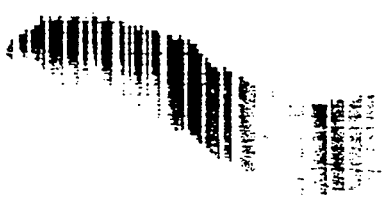

I2 (lst -1) (02_0_0HY): (0)-(80000)

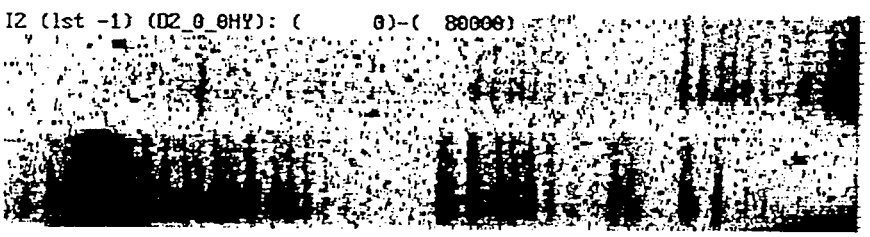

I3 (lst 71) (3055358B): (235)-(380)

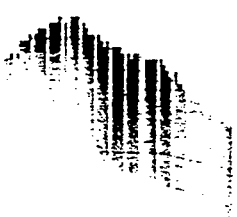

I1 (lst -1) (02_0_0HY): (0)-(80000)

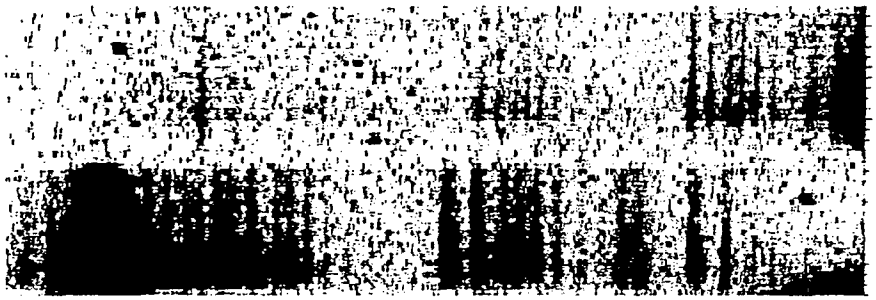

I3 (1st 71) (3055358B): (235)-(300)

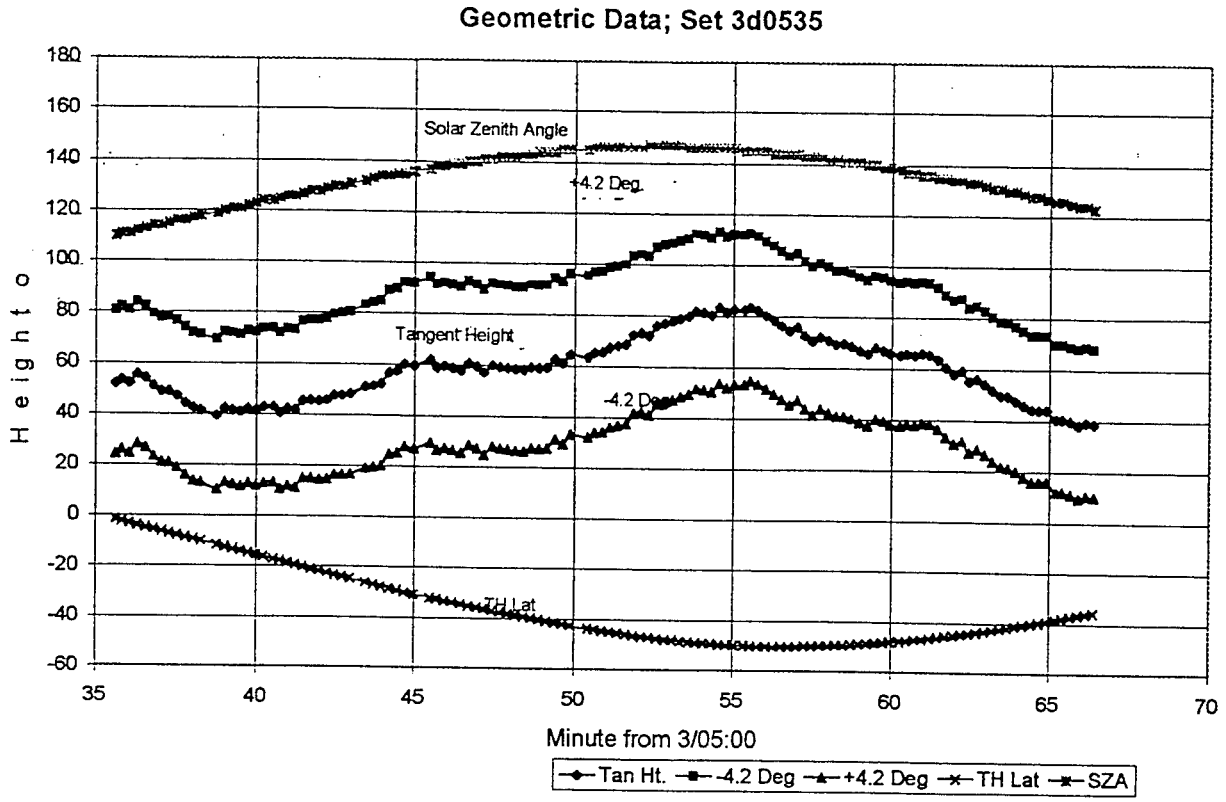
Geometric Data; Set 3d0535
Solar Zenith Angle
+4.2 Deg.
Tangent Height
-4.2 Deg.
TH Lat
Height o
Minute from 3/05:00
Tan Ht.
-4.2 Deg
+4.2 Deg
TH Lat
SZA

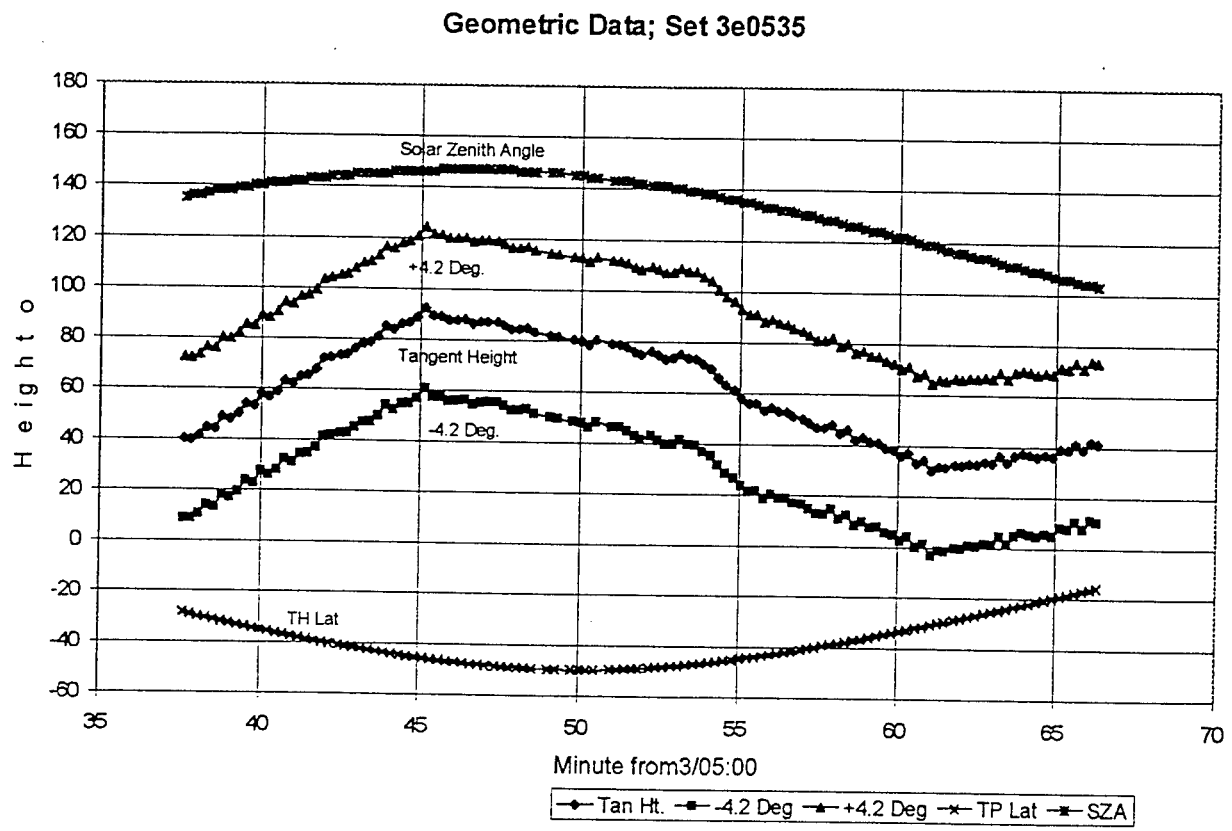
Geometric Data; Set 3e0535
Solar Zenith Angle
+4.2 Deg.
Tangent Height
-4.2 Deg.
TH Lat
Height o
Minute from3/05:00
Tan Ht.
-4.2 Deg
+4.2 Deg
TP Lat
SZA

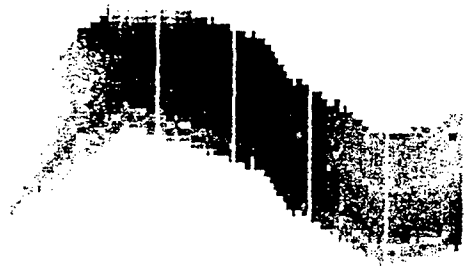

I6 (lst -1) (60H5_1): (0)-(28000)

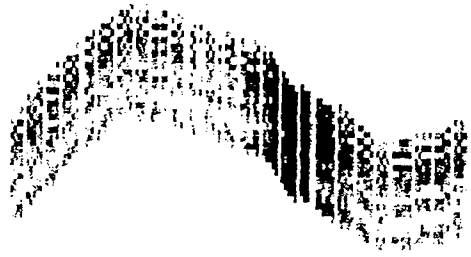

I5 (lst -1) (60I6300): (0)-(1000)

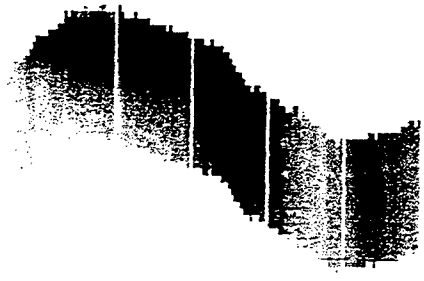

I4 (lst -1) (602_0_0): (3000)-(100000)

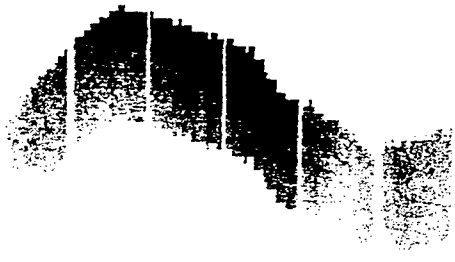

I3 (lst -1) (60I_5577): (0)-(15000)

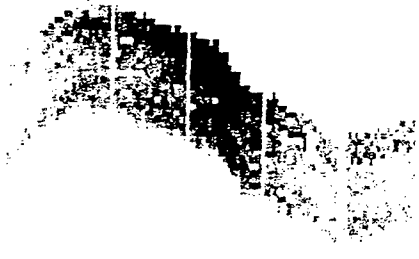

I4 (lst -1) (6NA_5892): (0)-(5000)

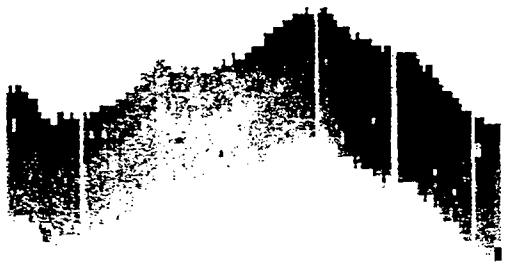

I3 (lst -1) (SOHS_1): (2000)-(18000)

I2 (lst -1) (SOI6300): (0)-(900)

I1 (lst -1) (SO2_0_0): (1000)-(90000)

I1 (lst -1) (SOI_5577): (0)-(9000)

I2 (lst -1) (SNA_5892): (500)-(1000)

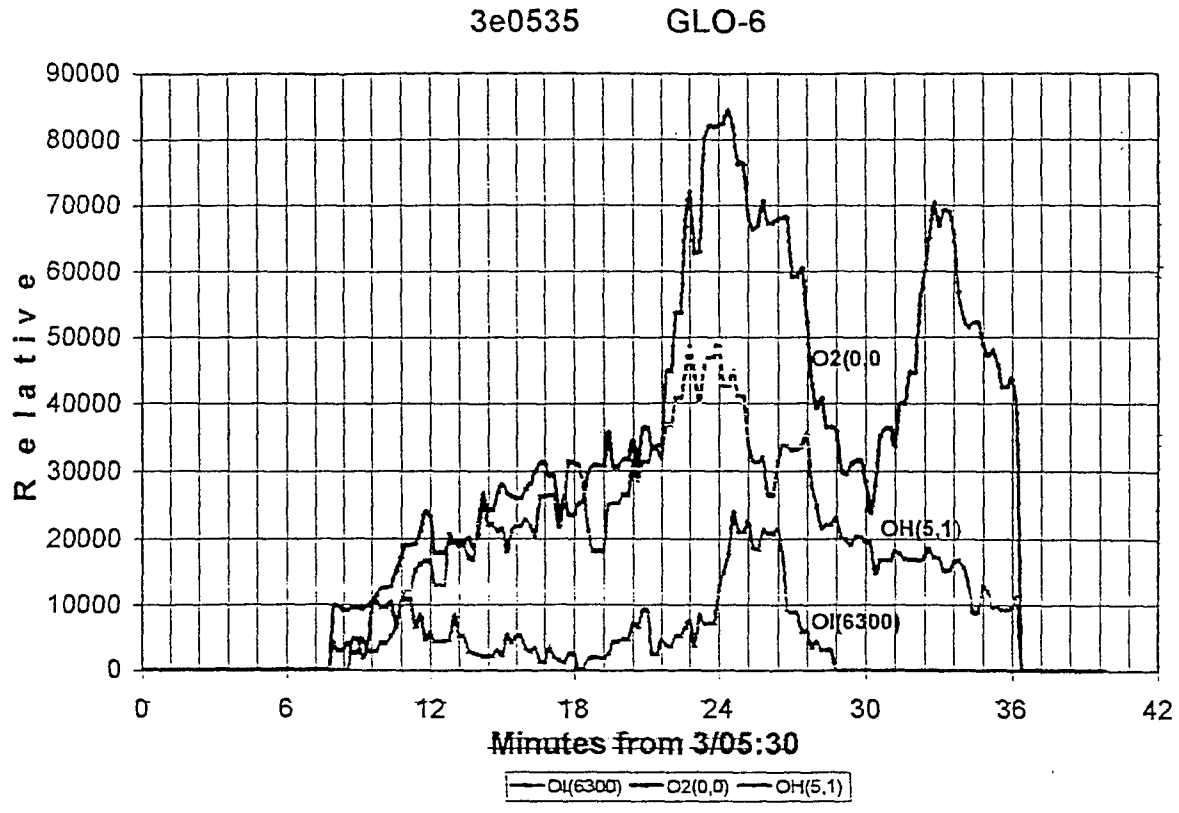
3e0535 GLO-6
Relative
90000
80000
70000
60000
50000
40000
30000
20000
10000
0
0
6
12
18
24
30
36
42
O2(0,0
OH(5,1)
OI(6300)
Minutes from 3/05:30
OI(6300) O2(0,0) OH(5,1)

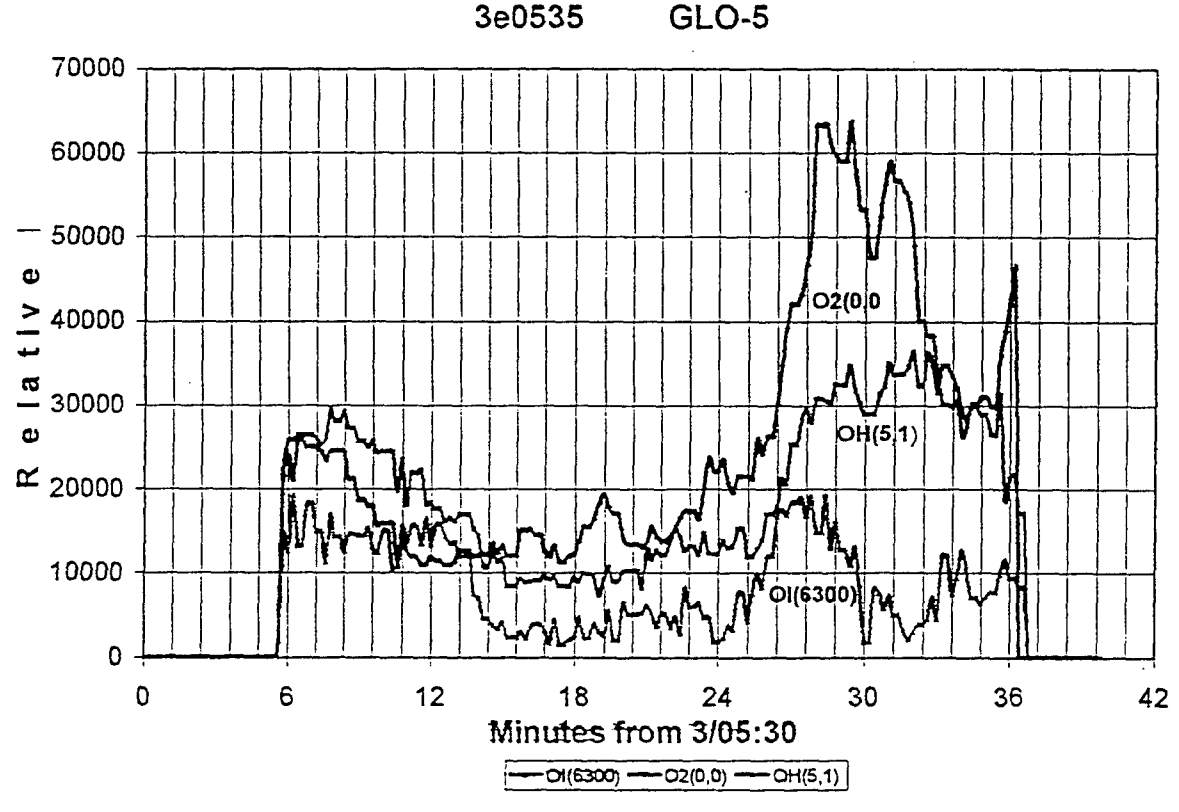
3e0535 GLO-5
Relative
70000
60000
50000
40000
30000
20000
10000
0
0
6
12
18
24
30
36
42
O2(0,0
OH(5,1)
OI(6300)
Minutes from 3/05:30
OI(6300) O2(0,0) OH(5,1)

Vanguard Research, Inc.

www.vriffx.com
10400 Eaton Place, Suite 450
Fairfax, VA 22030-2201
Phone (703) 934-6300
Fax (703) 273-9398

20000314023

May 4, 2000
00-0292

Defense Technical Information Center
8725 John J. Kingman Road
Suite 0944
Ft. Belvoir, VA 22060-6218

Subject: Final Report – Replacement Page, SF298

Reference: Contract No. DASG60-98-M-0073

Dear Sir or Madam:

Please find enclosed two copies of a replacement page for SF298 for the final report. Please replace this page in your copies of the final report.

Should you have any questions, do not hesitate to contact me at (703) 934-6300.

Sincerely,

Debra A. Spear
Contracts Administrator

Enclosure as stated

AQM00-06-1531